The Dissertation Committee for Leqian Liu Certifies that this is the
approved version of the following dissertation:

# Engineering *Yarrowia lipolytica* for High Lipid Production

**Committee:**

_____

Hal S. Alper, Supervisor

_____

Dean Appling

_____

Lydia Contreras

_____

Vishwanath Iyer

_____

Marvin Whiteley

**Engineering *Yarrowia lipolytica* for High Lipid Production**

**by**

**Leqian Liu, B.S.;B.S.**

**Dissertation**

Presented to the Faculty of the Graduate School of

The University of Texas at Austin

in Partial Fulfillment

of the Requirements

for the Degree of

**Doctor of Philosophy**

**The University of Texas at Austin**
**December 2014**

# Dedication

To Wenzong Li
You are always there.

## Acknowledgement

I would like to first thank my advisor, Dr. Hal Alper. His support, guidance and advice are the major reasons of the accomplishments and successes of the studies described herein. His tolerance over my ignorance and his passion over my very limited progresses kept me going forward with my research. His insights and suggestions guided the projects towards the unexpected but fruitful directions. He also put his trust in me to explore new research fields.  I can't thank him enough for all his helps and advices through these five years.

I would also want to thank the members of my committee, who have all given thoughtful advices and suggestions. The suggestions from Dr. Whiteley opened the possibility of my omics based study in this work. The lessons from Dr. Iyer in human genetics gave me a clear overview of the methods for genotyping and their applications. The discussions with Dr. Contreras and Dr. Appling helped to guide my research directions. Their availability for my committee meetings and discussions made my life much easier.

Many other people I worked with while studying my PhD helped me on this project with their expertise and efforts. I could not accomplish all these without their help. I would like to first thank the people I worked with in Alper group: Dr. John Blazeck for his guidance, training and collaboration on engineering *Yarrowia lipolytica*, we struggled but we made it; Andrew Hill for his collaboration on lipid accumulation work and lots of interesting conversations; Dr. Eric Young for all the late night talks, discussions and fun

# Engineering *Yarrowia lipolytica* for High Lipid Production

by

Leqian Liu, Ph.D.

The University of Texas at Austin, 2014

SUPERVISOR: Hal S. Alper

Among potential value-added fuels and chemicals, fatty acid-based chemicals are important due to their wide use in industrial processes and in daily life. Fatty acids produced from microbial systems could provide a sustainable supply to replace the current costly and unsustainable process using plant oil or animal fat. The oleaginous yeast *Yarrowia lipolytica* naturally possesses moderate lipid production capacity and grows on different kinds of biomass and organic waste. However, fatty acid production from native, un-engineered strains is not economically viable. Therefore, this work develops strategies inspired from synthetic biology and metabolic engineering to expand the engineering potential of *Y. lipolytica* — helping to establish this organism as a premier platform for industrial-level, high lipid production as well as providing a platform for uncovering novel understanding of lipogenesis.

To do so, first, novel synthetic promoters and high expression plasmid were necessary to achieve the ability to tune gene expression levels inside the cell. We developed a hybrid promoter engineering strategy to create a promoter library exhibiting a range of more than 400-fold in terms of mRNA levels as well as engineered plasmids with regulated centromeric function to achieve a 2.7 fold expression range. Next, a rational and evolutionary metabolic engineering approach was coupled with genomic and transcriptomic studies to both engineer and understand underlying lipogenesis in this organism. Through the engineering efforts, we successfully increased the lipid production titer to over 40 g/L in bioreactor as well as identified novel lipogenic enhancers and mechanisms. In addition, we identified and characterized a mutant mga2 protein with superior lipogenesis enhancing capacity, which can regulate fatty acid desaturation and carbon flux inside the cells. Collectively, these studies have facilitated the utilization of *Y. lipolytica* as an industrially relevant microbial lipid production platform and supplied novel understanding of its lipogenesis process. The methods and concepts developed here can also be adapted to other oleaginous microbes and serve as a template for enabling value-added chemical production in other nonconventional organism.

# Table of Contents

# List of Tables

# List of Figures

# Chapter 1: Introduction and Background

## 1.1 Value-added chemical production in yeast

Fungal systems possess an extensive track record in biotechnological applications such as ethanol fermentation and enzyme production (1-2). Although metabolic engineering endeavors over the past 20 years have focused primarily on diverse chemical production in *Escherichia coli* (3-6), this organism is not always an ideal fermentation host since it demonstrates relatively low stress tolerance (7), limited post-translational modifications, difficulty in expressing complex enzymes such as P450s (2), and a lack of subcellular compartments. In contrast, yeasts often lack these inherent flaws and possess favorable attributes such as larger cell sizes (thus simplifying separation), lower growth temperatures, higher pH and by-product tolerances (8), and immunity to phage contamination. Collectively, these advantageous traits encourage the use of yeasts for industrial-scale chemical and fuel production.

Contemporary metabolic engineering relies on bypassing native feedback inhibition, constructing heterologous pathways and general optimization and rewiring of metabolic flux. This approach has developed fungal platforms for the production of new chemicals such as alcohols, sugar derivatives, organic acid, fats, terpenes, aromatics and polyketides (9). This dissertation demonstrates a reproducible methodology used to develop a nonconventional yeast, *Yarrowia lipolytica*, into a premier value-added chemical (lipid) production platform. In particular, this feat is accomplished through expanding the control over gene expression (Chapters 2 and 3), rational and evolutionary

metabolic engineering (Chapters 4 and 5) as well as probing novel regulators of metabolism (Chapter 6). Chapter 7 provides a brief review of major findings and future study recommendations and Chapter 8 contains comprehensive description of materials and methods.

Figure 1.1 Metabolic map for value-added chemical production in yeast
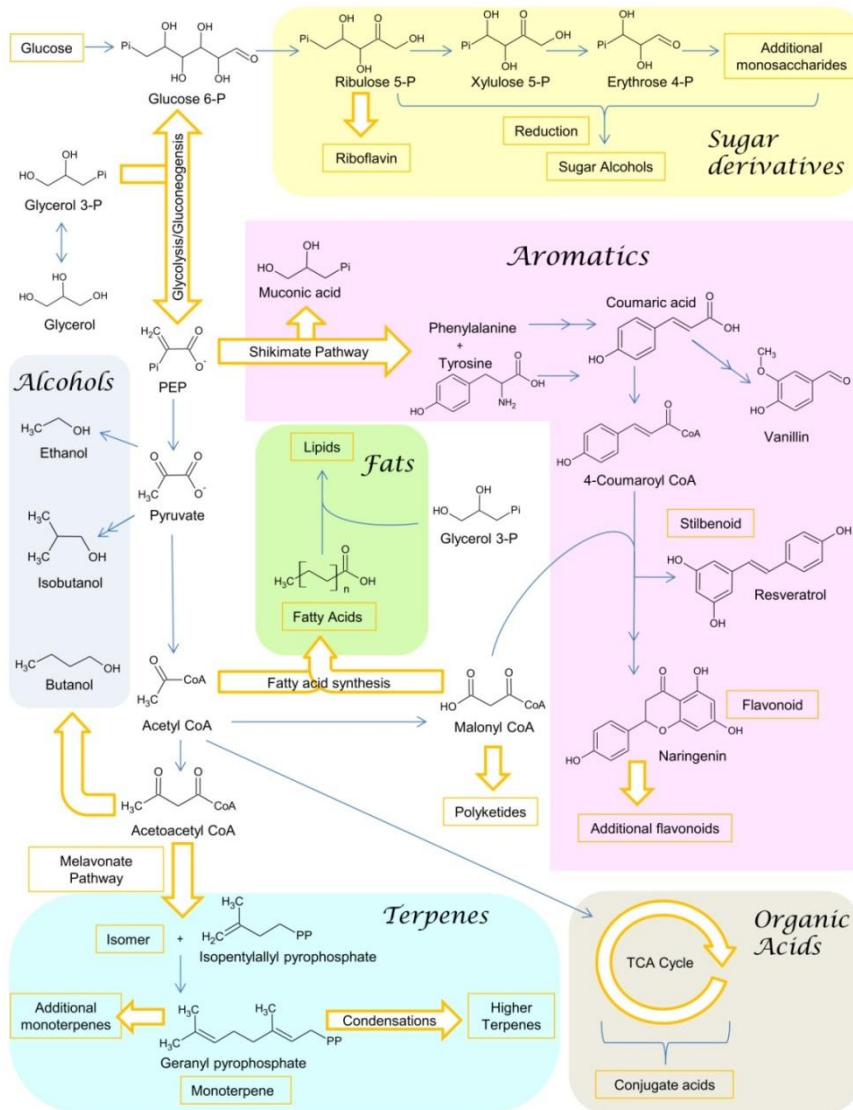


Examples of value-added chemicals produced in yeast production systems showing with simplified biosynthesis pathways.

## 1.2 Metabolic engineering for microbial production

The goal of metabolic engineering is to rewire metabolic flux inside cells toward desired phenotype, typically using recombinant DNA technology. Since native microorganisms often inefficiently produce value added chemicals or consume different types of feedstock like lignocellulose, metabolic engineering can be used to enhance these capabilities or even create novel functions. This methodology has enabled the microbial production of various value-added chemicals such as short chain alcohols (10), fatty acids (11), terpenoids (12), opioids (13) and artemisinic acid precursors (14). There are two basic requirements to successfully apply metabolic engineering for value-added chemical production: (1) the ability to manipulate gene expressions and (2) a basic understanding of the biosynthesis process. There are still numerous challenges associated with both requirements currently, especially when working with non-model organisms or poorly understood biosynthetic pathways.

## 1.2.1 Promoter and plasmid engineering for gene expression

Manipulation of cellular gene expression can be achieved by using genetic toolboxes, which can be used to facilitate engineering efforts. Genetic engineering techniques such as genomic integrations, gene-knockouts, and gene-knockdowns as well as engineering of genetic components such as plasmids, promoters, and terminators enable control over gene expression. Specifically in this work, we used promoter and

plasmid engineering to develop effective means for manipulating gene expression in *Y. lipolytica*.

Promoter engineering is an efficient means to tune gene expression since endogenous promoters do not fully sample the complete continuum of transcriptional control (15). Synthetic control of gene expression is critical for metabolic engineering efforts since precise control of key pathway enzymes (heterologous or native) can help maximize product formation. To this end, several studies have developed techniques for engineering promoters for desired expression characteristics. For instance, mutagenesis-based promoter engineering has been used to create a library of mutants that could be screened for those with desirable expression levels (16). Recently, a hybrid-promoter engineering strategy was developed which paired multiple UAS sequences from one native promoter with a different core promoter (17). Moreover, novel design of synthetic yeast promoters has also been accomplished by tuning promoter sequences to alter nucleosome architecture (18). These methods enabled the creation of different promoters with a wide range of strength and properties. However, most of these promoters were developed for model organisms such as *S. cerevisiae*. In order to unleash the microbial production potential of non-conventional yeasts like *Y. lipolytica*, such tools need to be developed for use in those organisms. In the work presented in Chapter 2, a hybrid promoter engineering strategy was developed and implemented in *Y. lipolytica* to greatly expand the ability for tuning gene expression in this yeast.

In addition to engineering of promoters, altering plasmid design can function as a convenient means for tuning expression. In *S. cerevisiae*, plasmid-based control of gene

expression is achieved by using varieties of plasmids such as centromeric (CEN) plasmids (low copy), 2-micron plasmids (high copy), and autonomously replicating sequence (ARS) plasmids (high copy) (19-21) that possess different properties. However, in *Y. lipolytica*, there is only CEN plasmid available. In the work presented in Chapter 3, an alternative route to enable plasmid level gene expression control in *Y. lipolytica* was enabled through developing a high expressing plasmid by repressing centromeric function. This tuning ability on plasmid added another level of control over gene expression in this yeast.

**1.2.2 Rational and evolutionary metabolic engineering**

Rational metabolic engineering refers to such engineering efforts which select enzymes, transporters, or regulatory proteins as targets for genetic manipulation based on available information regarding the pathways, enzymes, and regulation associated with generating the product of interest. Rational metabolic engineering has been fairly successful in various applications including the production of antimalarial drug precursor artemisinic acid (14), the industrially versatile commodity chemical phenol (22), and medically essential opioids (13). Common strategies used in rational metabolic engineering include by-product elimination, precursor enrichment, rerouting metabolic pathways and cofactor optimization (5). These approaches have been very efficient when utilized to enable the production of various chemicals in different microbial hosts (23-26). By engineering the precursor biosynthesis pathways, riboflavin production was significantly improved in *Ashbya gossypii* (27). In addition, optimization of co-factor

supply and precursor production enabled α-santalene overproduction in *S. cerevisiae* (28). Furthermore, inhibition of hydrocarbon accumulation in cyanobacteria has led to improved production of fatty alcohols in these organisms (29). Chapter 4 describes our efforts to utilize rational metabolic engineering techniques to systematically engineer *Y. lipolytica* for high lipid production, which achieved a genetic background capable of at a titer of over 25 g/L.

Although rational metabolic engineering has demonstrated successful in numerous applications, manipulating only rational targets can be less successful than predicted or even demonstrate detrimental effects. This arises due to an incomplete understanding of the complex global metabolic network, which prevents the anticipation of every consequence of a genetic modification. Evolutionary metabolic engineering, often associated with multiple cycles of random genetic perturbation and selection, can be very effective in overcoming this challenge by identifying phenotypically advantageous variants (30-32). This approach has been successfully implemented to rapidly provide strains with complex desired phenotypes such as improved galactose and xylose catabolism in *S. cerevisiae* (30, 33), increased isobutanol, succinate, and L-tyrosine production in *E. coli* (31, 34-35), as well as riboflavin production in *Candida famata* (36). If a working selection method accompanied with techniques for screening and/or enrichment has been developed, evolutionary engineering can provide a powerful complimentary method to rational metabolic engineering. In the work presented in Chapter 5, an evolutionary metabolic engineering strategy was developed and successful implemented which further increased lipid production in *Y. lipolytica*. This provided a

strain able to achieve a lipid titer of over 40 g/L, which represents a 60% improvement

over the strain generated using rational metabolic engineering alone, without sacrificing

productivity or yield. Moreover, implementing inverse metabolic engineering with strains

developed using evolutionary metabolic engineering to identify the genetic basis for the

differing phenotypes provided novel understandings as well as additional engineering

targets. This can be achieved by using next generation sequencing to resolve strain

differences that arise from evolutionary engineering.

## 1.2.3 Next generation sequencing analysis in metabolic engineering

Analysis of evolutionary engineering efforts through next generation sequencing

(NGS) can reveal the detailed genomic and transcriptomic information within these

strains. This can then be utilized to identify beneficial mutations and identify novel

underlying cellular mechanisms. The rapid advances in next generation sequencing

technology has greatly enhanced genomic approaches, providing new potential for

evolutionary engineering and inverse metabolic engineering successes (37). NGS usually

refers to non-Sanger-based high-throughput DNA sequencing technologies including

Illumina sequencing, Roche 454 sequencing, SOLiD sequencing, etc. Millions or billions

of DNA strands can be sequenced in parallel, substantially improving sequencing

throughput and minimizing the need for fragment-cloning methods that are often

necessary for sequencing genomes using Sanger sequencing (38). Illumina sequencing is

the most popular sequencing technique used for omic studies such as whole genome

sequencing (WGS) and RNA-Seq. Utilization of both of these techniques can be very

informative in the application of metabolic engineering for microbial production of value-added chemicals.

WGS provides access to the information coded in the genome of a microorganism, which enhances our understanding of the organism, enabling metabolic engineering endeavors. This information is commonly used for genome mining to identify novel enzymes and pathways. Additionally, this can probe genotype-phenotype linkage to identify changes at the genome level present in strains demonstrating a superior phenotype, which can be used for identifying targets for inverse metabolic engineering. A recent WGS study revealed the enriched difference in cAMP pathway genes by comparing a model stain for modern industrial biotechnology, *S. cerevisiae* CEN.PK113-7D, with another strain S288C. Moreover, beneficial mutations have been identified through WGS approaches with improved galactose utilization as well as improving heat tolerance in *S. cerevisiae* (39-40). The work presented in Chapters 5 and 6 describes the implementation of WGS analysis to identify beneficial mutations, which arose from evolutionary engineering and random mutation, to enhancing understanding of lipogenesis in *Y. lipolytica*.

Although WGS reveals detailed genomic information, RNA-Seq experiments can analyze the cellular transcriptome which provides substantial information regarding to the cellular metabolic state. RNA-Seq is especially useful when working with non-conventional microorganisms since standard microarrays are not available for many of these organisms. More importantly, RNA-Seq supplies more information compared to

traditional methods such as alternative splicing (41), differential isoform expression (42), and promoter usage (43). It can also enable a more precise comparison of the expression level of different genes within samples in addition to the differential gene expression resulting from different samples/conditions. A recent study using RNA-Seq analysis to investigate host-strain dependency for xylose utilization in recombinant *S. cerevisiae* strains identified important transcription factors (44). Another study of *Hansenula polymorpha* transcriptome identified abundant and highly upregulated expression of 40% of the genome in methanol grown cells, and revealed alternative splicing events (45). Chapters 5 and 6 describe transcriptomic analysis employed to unveil relevant mechanisms present in high lipogenic strains.

## 1.3 *Yarrowia lipolytica* as a microbial production host for lipid production

Recently, there has been a surge in the types of microbially-derived oleochemicals produced (46-48), including alkanes (46), alkenes (49-50), fatty alcohols (51), and fatty esters (25, 51) as well as polyunsaturated fatty acids (52). However, most of these efforts still suffer from low titers largely in part from the choice of the cellular host, typically *E. coli*. Alternatively, oleaginous organisms, such as the fungus *Y. lipolytica*, could serve as a more ideal host due to higher innate lipogenesis potential. *Y. lipolytica* is increasingly being recognized as promising hosts for the production of valuable compounds (53). It is a unique host for biochemical production and heterologous protein excretion on account of its abilities to accumulate high levels of lipids (54-56), overproduce organic acids (23-

24, 57-58), utilize hydrophobic and waste carbon sources (59-61), and secrete native and heterologous proteins at high levels (62-64). The availability of *Y. lipolytica*'s genome sequence (65-66) along with basic genetic tools such as transformation methods (67-69), gene knockouts (70), and both episomal (68, 71-73) and integrative expression cassettes (74-75) enable metabolic engineering approaches.

### 1.3.1 Lipid biosynthesis in *Y. lipolytica*

Lipid biosynthesis in *Y. lipolytica* starts from taking glucose into the cells followed by glycolysis pathway and TCA cycles. After that, accumulated citrate in mitochondria gets transported out into cytosol and then feed into fatty acid/lipid biosynthesis pathways (**Figure 1.2**). Lipid biosynthesis here is thought to be initiated by the activity of four enzymes - AMP deaminase (AMPD), ATP-citrate lyase (ACL), malic enzyme (MAE) and acetyl-CoA carboxylase (ACC) - that collaboratively divert carbon flux from central carbon metabolism towards fatty acid biosynthesis (56, 76). Previous efforts to increase lipid accumulation have shown promise in *Y. lipolytica*. Deletion of β-oxidation enzymes coupled with enhancing glycerol synthesis substantially increases *ex novo* lipid accumulation (56, 76), and deletion of the *pex10* peroxisomal biogenesis gene greatly increases eicosapentaenoic acid yield (24).  Although there is success from the previous engineering efforts, the resulted production is still below the ideal performances. The *de novo* lipid content in this organism has been limited to below around 60% by dry cell weight (23). Therefore, further action is required to develop *Y. lipolytica* for higher

lipid production. In the work presented in Chapters 4, 5 and 6, we successfully increased

the lipid production metrics in *Y. lipolytica*.

Figure 1.2 Simplified scheme of lipid metabolism in *Y. lipolytica*
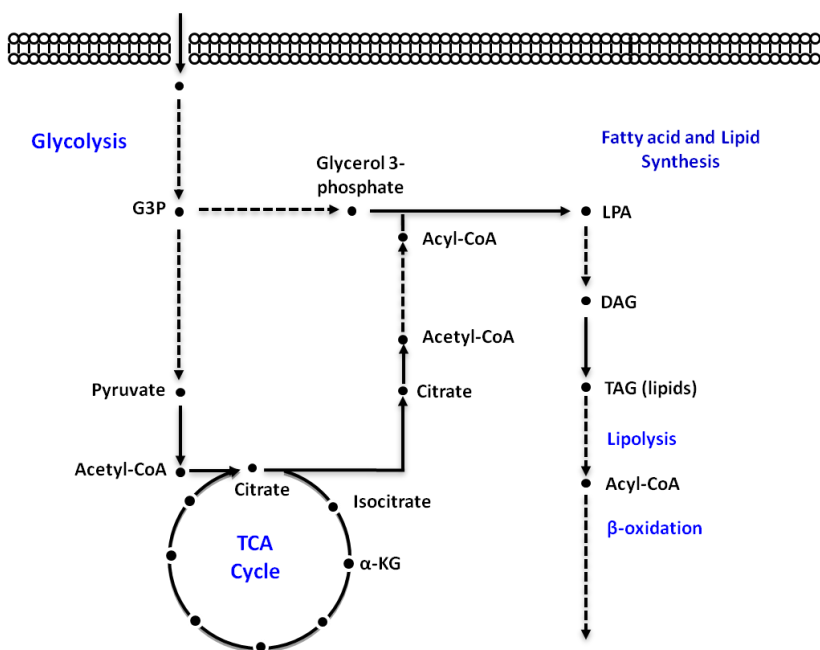


Simplified lipid metabolism in *Y. lipolytica* showing carbon flux through glycolysis, TCA cycles
and fatty acid and lipid biosynthesis.

## 1.3.2 Current challenges for high lipid production in *Y. lipolytica*

As a nonconventional oleaginous yeast, *Y. lipolytica* presents an exciting starting

point to be developed into a microbial lipid production host. However, the lack of control

over gene expression, the insufficient lipid production performance and the incomplete

understanding over its lipogenesis processes significantly hampered its industrial

potential. In the work, we first used promoter and plasmid engineering efforts to enable a

high level control over gene expression in *Y. lipolytica* (Chapters 2 and 3). Then we

employed rational and evolutionary metabolic engineering to develop *Y. lipolytica* into a high lipid production host and in the same time, we supplied novel understanding over lipogenesis process (Chapters 4 and 5). Lastly, we identified and analyzed a novel lipogenesis regulator, a mutant mga2 protein, which expand the limited knowledge of complex regulation of lipid production (Chapter 6).

# Chapter 2: Hybrid promoter engineering in *Yarrowia lipolytica*[1]

## 2.1 Chapter summary

The development of strong and tunable promoter elements is necessary to enable metabolic and pathway engineering applications for any host organism. In this chapter, we have expanded and generalized a hybrid promoter approach to produce libraries of high-expressing, tunable promoters in the nonconventional yeast, *Yarrowia lipolytica* to enable the gene expression manipulation in this yeast. These synthetic promoters are comprised of two modular components—the enhancer element and the core promoter element. By exploiting this basic promoter architecture, we have overcome native expression limitations and provided a strategy for both increasing native promoter capacity and producing libraries for tunable gene expression in a cellular system with ill-defined genetic tools.  In doing so, the work presented in this chapter has created the strongest promoters ever reported in *Y. lipolytica*. Furthermore, we have characterized these promoters at the single-cell level through the use of a developed fluorescence based assay as well as at the transcriptional and whole-cell level. The resulting promoter libraries exhibited a range of more than 400 fold in terms of mRNA levels, and the strongest promoters in this set had eight-fold higher fluorescence levels compared with typically used endogenous promoters. These results suggest that promoters in *Y. lipolytica* are enhancer limited and this limitation can be partially or fully alleviated

---

[1] Portion of this chapter has been published previously in AEM, 77(22), 7905-7914 with JB, LL, HR, HA designed and carried the experiments.

13

through the addition of tandem copies of upstream activation sequences (UAS). Finally, the results from this chapter illustrates that tandem copies of UAS regions can serve as synthetic transcriptional amplifiers that may be generically used to increase the expression level of promoters.

## 2.2 Introduction

Developing and establishing a comprehensive suite of promoter elements in organisms with poorly defined genetic tools is essential for enabling metabolic and pathway engineering applications. To this end, the oleaginous yeast *Yarrowia lipolytica* has received attention as a potential biofuels producing host, yet lacks genetic tools for tunable and high level gene expression. In other organisms, prior attempts of promoter engineering relied on modifying the expression range of endogenous promoters through point mutations. As an example, error-prone PCR of the native *Saccharomyces cerevisiae* TEF promoter yielded a library of mutant promoters with a nearly seventeen-fold range in relative expression strength (77). A similar approach in *E. coli* led to a nearly eighteen-fold range in relative expression strength based on the heterologous Pl-lambda promoter (16). An alternative strategy aimed at tuning intergenic regions in heterologous *Escherichia coli* operons enabled a seven-fold improvement in pathway throughput and was used to prevent the accumulation of a toxic intermediate (78). While successful, these methods and applications are quite limited by: (1) their reliance on a strong, well-defined starting core promoter and (2) the tendency of alterations to result in

expression levels lower than these baselines. These limitations present a challenge for creating a dynamic range of promoters with similar regulation in a novel organism without highly characterized strong promoter elements.

Beyond point mutations, the generation of hybrid promoters has been previously successful in significantly augmenting promoter architecture and function (79-81). Most of these approaches attempt to create synthetic hybrid promoters by fusing an upstream activating sequence (UAS) to a separate (often minimal) core promoter region. The result is a functional UAS-core promoter chimera. In this construct, the UAS regulatory site enhances gene expression by localizing trans-acting regulatory elements (transcription factors). As a result, this approach raises the possibility to uniquely engineer promoters as two independent, synthetic parts—activating regions and core regions. In this chapter, we present a generalizable approach of hybrid promoter engineering for the construction of both very high-strength promoters and tunable promoter libraries in the non-conventional, oleaginous yeast host *Y. lipolytica*.

Although *Y. lipolytica* is a promising production host, many of the methods in this organism rely on ill-defined genetic elements (60) especially in the area of promoters. One of the strongest promoters in *Y. lipolytica*, the XPR2 promoter (pXPR2) has complex requirements for induction that hinders its industrial applications (82). Nevertheless, this promoter has been functionally analyzed to reveal a 105 base pair distal UAS fragment named UAS1B (83-84). Previously, between one to four tandem UAS1B copies were fused to a core minimal LEU2 promoter to create four increasingly strong hybrid chimera promoters, named hp1d through hp4d (82). As a result, the hp4d promoter has become a

commonly used tool for heterologous protein expression in *Y. lipolytica*. A further re-analysis of these four promoters revealed a linear increase of promoter strength as a function of number of tandem UAS1B elements which raises the possibility of further improvements.

Specifically, in this chapter, we describe the development of a generic, hybrid promoter approach for creating synthetic, tunable promoters. Furthermore, these results demonstrate that the activating regions and core regions can act as independent synthetic parts to create a hybrid promoter. In particular, we construct and characterize two libraries of synthetic hybrid promoters: a UAS1B-leum library in which between one and thirty two UAS1B elements are fused to the minimal LEU2 promoter region and an UAS1B$_{8/16}$-TEF library in which eight or sixteen tandem UAS1B elements are fused to varying sized TEF promoter regions. In doing so, this work creates the strongest characterized promoters in *Y. lipolytica* and the first ever reported capacity for tunable gene expression in this system. Moreover, this work establishes synthetic hybrid promoter construction as a generic approach for promoter engineering to expand and enhance the strength of engineered promoters in a manner not accessible through traditional promoter engineering applications.

## 2.3 Results

### 2.3.1 Characterization of endogenous promoters at the single-cell level

Prior studies of promoter strength in *Y. lipolytica* have relied on assaying whole cultures for protein expression level (using reporters such as β-galactosidase) (62, 82). It

is commonly known that these methods can mask potential bimodal "on/off" distributions within the population.  Thus, to avoid this complication, we sought to utilize a fluorescence-based assay using the *Y. lipolytica* plasmid pSl16-Cen1-1(227) (85).  All results generated in this chapter, except where indicated, employed derivatives of this replicative, ARS-CEN based plasmid. Since codon biases are known to limit translation in *Y. lipolytica* (86) and no fluorescent reporter protein has been previously used in *Y. lipolytica* to gauge promoter strength, we initially evaluated several available fluorescent reporter proteins. The TEF promoter was coupled to four different fluorescence genes including yECitrine, EGFP, hrGFP and mStrawberry and flow cytometry was performed to determine reporter functionality.  Of these variants, only hrGFP imparted detectable fluorescence (**Figure 2.1a**).  This gene, optimized for expression in mammalian cells, has the highest Codon Adaptation Index for *Y. lipolytica* of the four fluorescence genes (87), indicating the closest compatibility with codon usage frequencies for this organism.

As a result, the hrGFP reporter gene was used to evaluate the promoter strength of seven previously identified endogenous *Y. lipolytica* promoters—TEF, EXP, FBA, GPAT, GPD, YAT, and XPR2 (**Table 2.1**, **Figure 2.1b)** (62, 88-89).  Based on this analysis, the relative ordering of promoters strengths is EXP > TEF > GPD > GPAT > YAT > XPR2 > FBA.  The low mean fluorescence values of even the strongest of these native promoters, EXP and TEF, highlight that even strong endogenous promoters in *Y. lipolytica* may be too low for metabolic engineering purposes.  When each of these promoters was used in a plasmid-based construct, a bimodal fluorescence distribution was seen.  Based on prior reports to further improve the expression strength, a consensus four nucleotide "caca"

sequence 5' of the +1 ATG codon was included (86, 90-92); however, this inclusion was found to be detrimental to expression levels in most cases (data not shown). The differential regulation patterns and small dynamic range of these endogenous promoters require a novel approach to enable metabolic engineering applications in this organism.

Figure 2.1 Fluorescence based assay for endogenous promoter characterization

Figure 2.1a
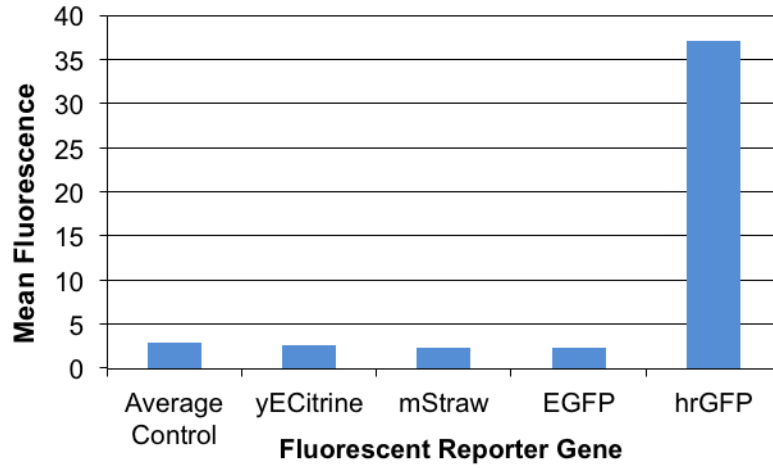


Figure 2.1b
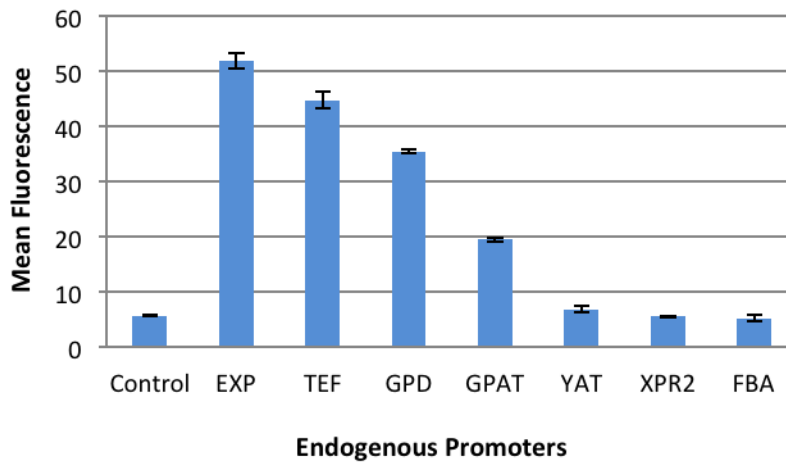
Figure 2.1 cont.

(**A**) The relative fluorescence levels of yECitrine, mStraw, EGFP and hrGFP driven by the TEF promoter in *Yarrowia lipolytica* were tested with flow cytometry and mean fluorescence from different fluorescent protein were presented for comparison.  These results indicate that hrGFP was the only functional fluorescent protein for this system.  (**B**)  Endogenous promoters including EXP, TEF, GPD, GPAT, YAT, XPR2, and FBA were used to drive the expression of hrGFP. The mean fluorescence data was collected with flow cytometry analysis for comparison. Error bars represent standard deviation from biological replicates.  The EXP and TEF promoters were identified as the strongest among this tested set.

Table 2.1 Promoter elements used in hybrid promoter engineering

| Promoter element name | Open reading frame regulated | YALI number | Basepair range | Reference number |
|---|---|---|---|---|
| EXP1 | Export protein | YALI0C12034p | -999 to -1 | (89) |
| GPAT | Glycerol-3-phosphate dehydrogenase | YALI0C00209p | -1130 to -1 | (89) |
| GPD | Glyceraldehyde-3-phosphate dehydrogenase | YALI0C06369p | -931 to -1 | (89) |
| TEF | Translation elongation factor EF-1α | YALI0C09141p | -406 to -1 | (89) |
| YAT1 | Ammonium transporter | YALI0E27203p | -775 to -1 | (89) |
| FBA | Fructose-bisphosphate aldolase | YALI0E26004p | -830 to +171 | (89) |
| XPR2 | Alkaline extracellular protease | YALI0E26719p | -947 to -1 | (82) |
| TEF(136) | Translation elongation factor EF-1α | YALI0C09141p | -136 to -1 | This chapter |
| TEF(203) | Translation elongation factor EF-1α | YALI0C09141p | -203 to -1 | This chapter |
| TEF(272) | Translation elongation factor EF-1α | YALI0C09141p | -272 to -1 | This chapter |
| TEF(504) | Translation elongation factor EF-1α | YALI0C09141p | -504 to -1 | This chapter |
| TEF(604) | Translation elongation factor EF-1α | YALI0C09141p | -604 to -1 | This chapter |
| TEF(804) | Translation elongation factor EF-1α | YALI0C09141p | -804 to -1 | This chapter |
| TEF(1004) | Translation elongation factor EF-1α | YALI0C09141p | -1004 to -1 | This chapter |
| Leum | β-isopropylmalate dehydrogenase | YALI0C00407p | -92 to +25 | (82) |
| UAS1B | Alkaline extracellular protease | YALI0E26719p | -805 to -701 | (82) |

## 2.3.2 Creating and characterizing a hybrid promoter series using the UAS1B element and minimal leucine core promoter

To bypass the limitations of endogenous promoters in *Y. lipolytica*, we evaluated the generalizable nature of hybrid promoters comprised of fused upstream activating sequences with a minimal core promoter. In prior work, a nearly perfect positive linear correlation was detected between the number of tandem UAS1B sequences and promoter outputs in the hp1d to hp4d promoter series (82). This observation led to our hypothesis

that these minimal core promoters and potentially other *Y. lipolytica* full-length, native promoters are enhancer limited.  To address this limitation, we created an expanded series of hybrid promoters by fusing between one and thirty two tandem UAS1B enhancer sequences to the leucine minimal promoter (Leum) to form promoters $UAS1B_1$-Leum through $UAS1B_{32}$-Leum (**Figure 2.2a**). The newly constructed UAS1B-Leum promoter series was tested with hrGFP based flow cytometry analysis.  The fluorescence data displayed several domains for correlation between output fluorescence and the number of upstream UAS elements.  Initially, an exponential increase in fluorescence was seen as UAS1B sequence count increased from one to eight.  This trend became linear through nineteen tandem repeats (a total of 1995 bp of upstream activating sequences upstream of the core promoter).  Finally, the output fluorescence seemed to be saturated through 32 tandem UAS1B repeats (**Figure 2.2b**).  This data strongly conformed to a Hill Cooperative Binding model (correlation coefficient of 0.95) and exhibited a high Hill Constant (3.889) which indicates a strong amount of binding cooperativity of the enhancer elements (**Figure 2.2b**).  Specifically, this data was fit to the equation:

$$\text{Mean FL} = \text{min mean FL} + (\text{max mean FL - min mean FL}) \times a \times \frac{\#\,\text{of UAS}^{\text{Hill Coefficient}}}{c^{\text{Hill Coefficient}} + \#\,\text{of UAS}^{\text{Hill Coefficient}}}$$

 with the resulting coefficients of  a= 0.794, Hill Coefficient= 3.889, and c= 10.146.  As with the prior tests using endogenous promoters, these plasmid-based expression cassettes showed a bimodal distribution of fluorescence levels.  However, when these cassettes were integrated into the genome, these promoters gave a singular, high expression peak which indicates that the bimodal nature was conceivably due to episomal

22

expression issue related to this organism.  These integrative expression cassettes generated roughly two-fold higher fluorescence values than their corresponding replicative-based cassettes (data not shown).

### 2.3.3 Transcriptional analysis of the UAS1B-leum hybrid promoter series

A transcriptional analysis was performed to confirm that the observed effect in fluorescence was indeed manifested at the transcriptional level.  To do so, qRT-PCR analysis was employed using the hrGFP mRNA of select promoter constructs (Leum, UAS1B$_4$-Leum, UAS1B$_8$-Leum, UAS1B$_{16}$-Leum, UAS1B$_{24}$-Leum, and UAS1B$_{32}$-Leum) (**Figure 2.2c**).  Expression values were normalized to the mRNA level seen with only the minimal leucine promoter used to drive hrGFP.  Indeed, the increase in mean fluorescence levels was strongly correlated with the increase in relative mRNA levels. The relative mRNA levels increased and likewise plateaued for constructs with a high number of UAS1B repeats.  Moreover, these results demonstrate an extraordinary range of promoter strength in this series with more than a 400 fold dynamic range of transcript level between the minimal promoter and strongest promoters in this set.

### 2.3.4 Utility and stability of the UAS1B-leum hybrid promoter series

To ensure that the observed effect was independent of reporter gene, we sought to provide a further characterization of the UAS1B-Leum promoter series with a separate reporter gene, the β-galactosidase gene encoded by *E. coli* lacZ.  Select promoter constructs (including the endogenous TEF, EXP, and XPR2 promoters as well as hybrid UAS1B-leum constructs containing 1, 2, 3, 4, 6, 8, 12, 16, 20, 24, 28, and 32 UAS1B copies) were used to construct expression cassettes with lacZ in place of hrGFP.  β-

23

galactosidase assays were performed as described previously (93-94) with a maximum value of 1198 miller units generated by the UAS1B$_{28}$-leum construct (**Figure 2.2d**). Promoter strength increased with increasing UAS1B copy number up through 32 UAS1B repeats unlike in the hrGFP assay. However, the β-galactosidase assay results matched well with the hrGFP analysis and the data showed a strong positive statistical correlation ($r^2$=0.85). These results demonstrate that the UAS1B-leum hybrid promoter series developed here is a generic tool for obtaining tuned gene expression in *Y. lipolytica*.

These hybrid promoters rely on a high number of tandem repeats, thus, genetic stability was evaluated. To accomplish this, selected promoter constructs (with 12 or 16 repeated UAS1B elements) were tested on the basis of sequence fidelity after non-selective serial subculturing. These strains were subcultured for a total of 36 generations. After this process, cells were harvested and plasmids were isolated and sequenced to assess gene construct stability. In total, 20 separate plasmids containing the UAS1B$_{12}$-Leum and 20 containing the UAS1B$_{16}$-Leum promoters were evaluated. 17 out of 20 UAS1B$_{12}$-Leum and 20 out of 20 UAS1B$_{16}$-Leum were positively sequence and restriction enzyme digest confirmed after 36 doublings. Thus, these promoters are suitably stable in *Y. lipolytica* for long-term expression and use. Collectively, this data suggests that the expression output from hybrid promoters can be altered by changing the number of activating regions with a given core promoter region. Next, we sought to address the ability to alter the core promote region of this construct.

Figure 2.2 Developing and characterizing a UAS1B-Leum hybrid promoter set

Figure 2.2a
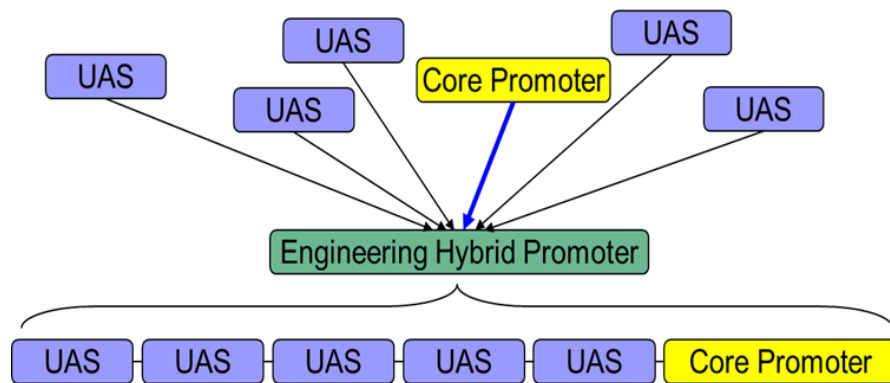


Figure 2.2b
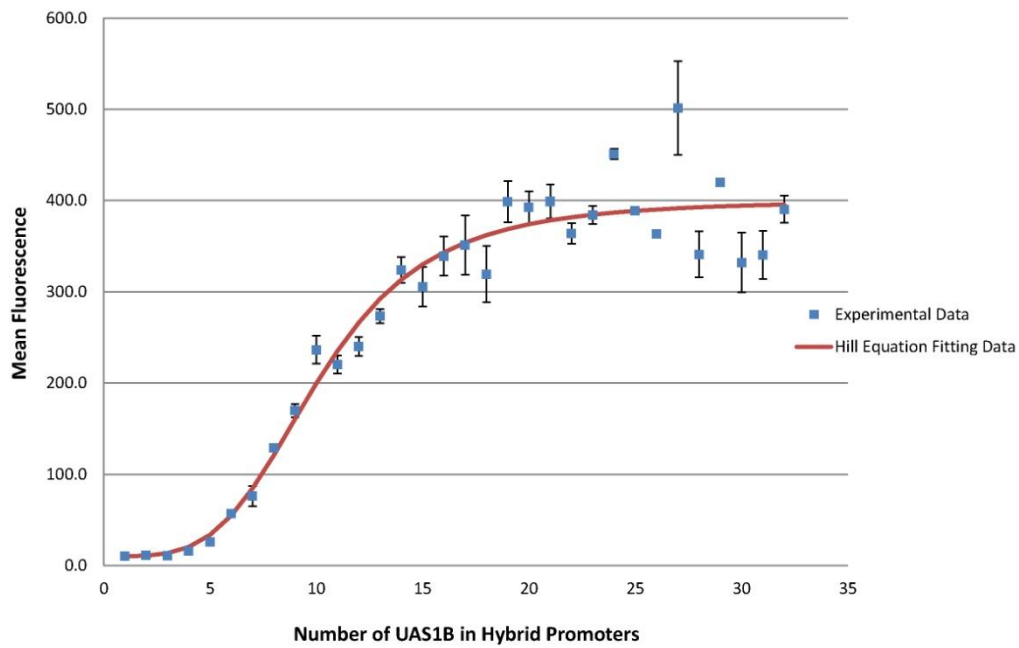
Figure 2.2 cont.

Figure 2.2c
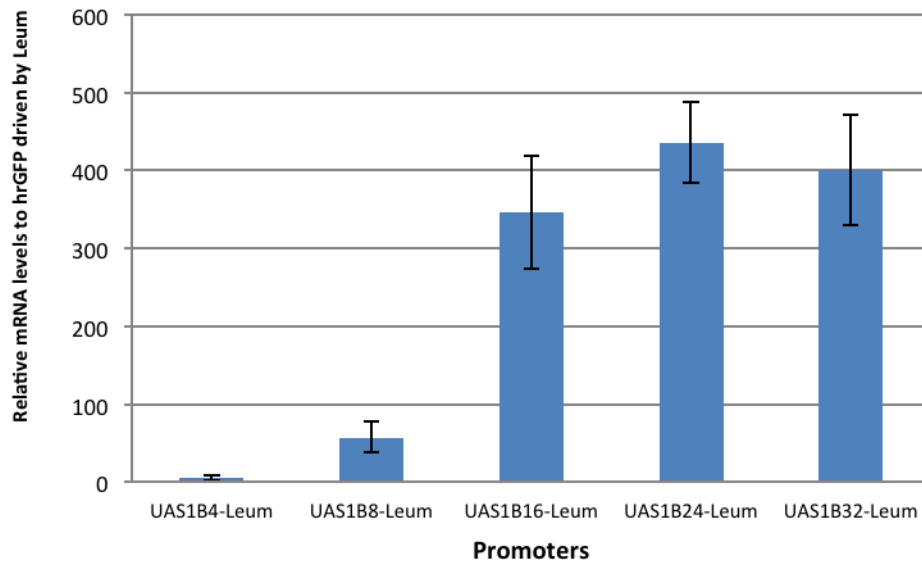
Figure 2.2 cont.

Figure 2.2d
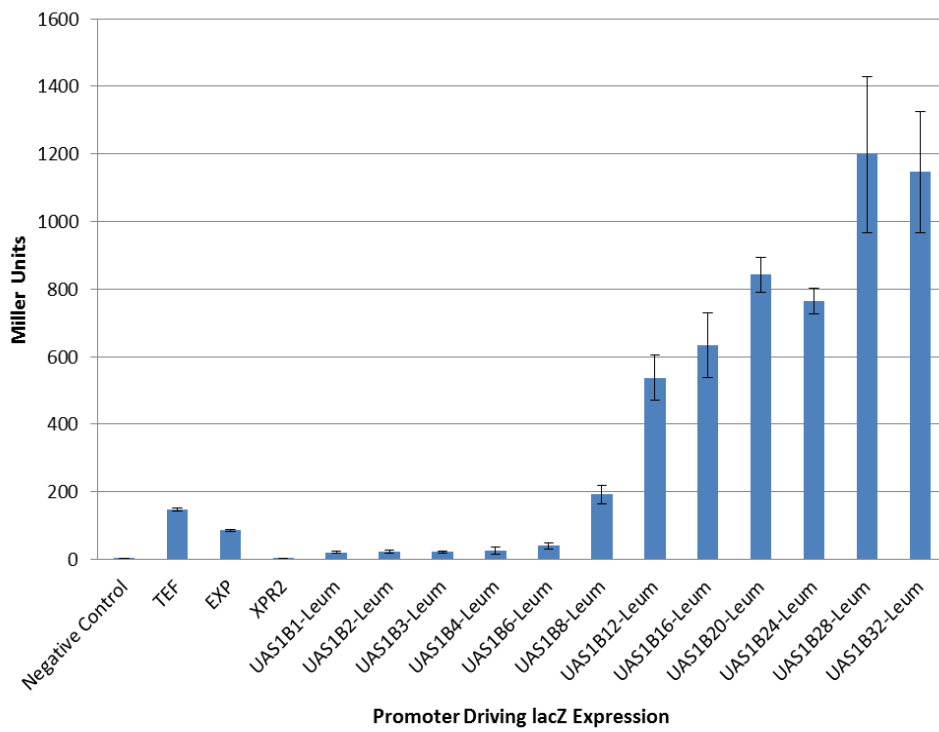
Figure 2.2 cont.

(A) A schematic diagram for UAS-enabled hybrid promoter engineering illustrates that these promoters were created from two distinct parts—the core promoter and upstream activation sequence (UAS) elements. By inserting tandem copies of UAS upstream to the core promoter, fine-tuned promoter sets with the strongest expression levels seen in *Y. lipolytica* were created. (**B**) The tandem insertion of 1 to 32 copies of UAS1B sequences upstream of a minimal LEU promoter enabled construction of the UAS1B$_1$-Leum to UAS1B$_{32}$-Leum promoters. Error bars represent standard deviation from biological triplicates. The relative promoter strengths of UAS1B-Leum promoters were fit to the Hill equation:

$$\text{Mean FL} = \text{min mean FL} + (\text{max mean FL - min mean FL}) \times a \times \frac{\text{\# of UAS}^{\text{Hill Coefficient}}}{c^{\text{Hill Coefficient}} + \text{\# of UAS}^{\text{Hill Coefficient}}}$$

resulting in a= 0.794, Hill Coefficient= 3.889, c= 10.146 and r$^2$= 0.9495 using Polymath Software (Willimantic, CT). (**C**) Transcriptional profiling of select promoter constructs was used to calculate mRNA levels relative to the minimal Leum promoter. Expression profiles matched fluorescence data. Error bars represent standard deviation from biological triplicates. (**D**) Endogenous and hybrid promoters were tested with a β-galactosidase reporter gene, yielding similar results to the hrGFP assay. Error bars represent standard deviation from biological triplicates.

**2.3.5 Generalizing the hybrid promoter approach by switching the core promoter region**

As discussed above, a hybrid promoter has two potential independent elements—activating regions and core promoter region. The data above suggests that tandem UAS elements may serve as movable, synthetic expression amplifiers for a given promoter. Next, we sought to test the hypothesis that even native promoters in *Y. lipolytica* are enhancer limited and can be strengthened by adding additional UAS elements. To do so, we constructed new hybrid promoters containing either eight tandem UAS1B sequences (UAS1B$_8$) or sixteen tandem UAS1B sequences (UAS1B$_{16}$) inserted 5' upstream of a series of different TEF-based core promoters. Specifically, we amplified eight different regions of the TEF promoter spanning 136 bp and 1004 bp upstream of the ATG starting site from PO1f (82) genomic DNA (**Table 2.1**). Included in this set is the consensus 404 bp TEF promoter for *Y. lipolytica* as well as lengthened and truncated versions of this promoter. These eight core TEF promoters and their corresponding UAS1B$_8$ and UAS1B$_{16}$ hybrid promoters were tested and compared with the Leum, UAS1B$_8$-Leum and UAS1B$_{16}$-Leum constructs.

This new series of hybrid promoters was assayed via hrGFP fluorescence by flow cytometry. In the absence of UAS elements, it can be seen that the fluorescence value decreases for truncated promoters below the consensus TEF size as expected. Moreover, the full length (and larger) TEF promoters have more strength than the minimal leucine promoter (**Figure 2.3a**). The UAS1B$_8$ and UAS1B$_{16}$ enhancer fragments in isolation do not confer any promoter activity (data not shown). When these enhancer fragments were

fused with the TEF promoter elements, a substantial increase in the net promoter strength was seen regardless of the TEF variant utilized. The enhancement provided by $UAS1B_8$ was roughly half the value obtained by using $UAS1B_{16}$. Moreover, these enhancements were seen for both more minimal and full length TEF promoter elements, even with the existence of naturally occurring UAS elements in the consensus and longer TEF promoters. Thus, this data suggests that even strong endogenous promoters like TEF are enhancer limited in *Y. lipolytica* and their expression capacity can be increased through additional UAS elements.

The amplification of expression imparted by the $UAS1B_8$ and $UAS1B_{16}$ enhancer elements was not even for all promoters. The fold increase of the constructs relative to the UAS-free TEF core promoters is plotted in (**Figure 2.3b**). In general, the largest improvement is obtained when the UAS elements are placed most closely 5' of a core promoter region. This fold improvement trend is rationalized in terms of a mechanism of proximity and localization of enhancer elements. However, it is interesting to note that the total promoter size (with 16 activating sequences and a core region) totals upwards of 3 kbp for many of these promoters—a region that is quite large for typical yeast constructs. In addition, many of these larger constructs were the best performing promoters. Specifically, nearly all of these promoters proved to be stronger than the corresponding $UAS1B_8$-Leum and $UAS1B_{16}$-Leum promoters, demonstrating the fitness of the TEF-based core promoter regions for strong hybrid promoter engineering. In this regard, this work demonstrates that tandem UAS elements serve to synthetically amplify the expression level imparted by the core promoter element chosen.

Figure 2.3 Expanding the hybrid promoter approach by altering the core promoter element

Figure 2.3a
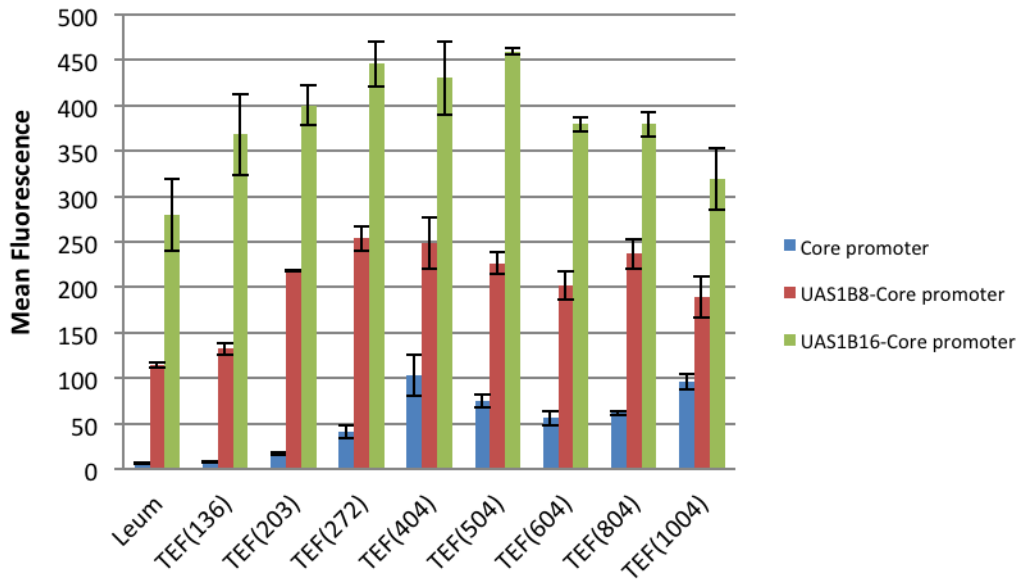


Figure 2.3b
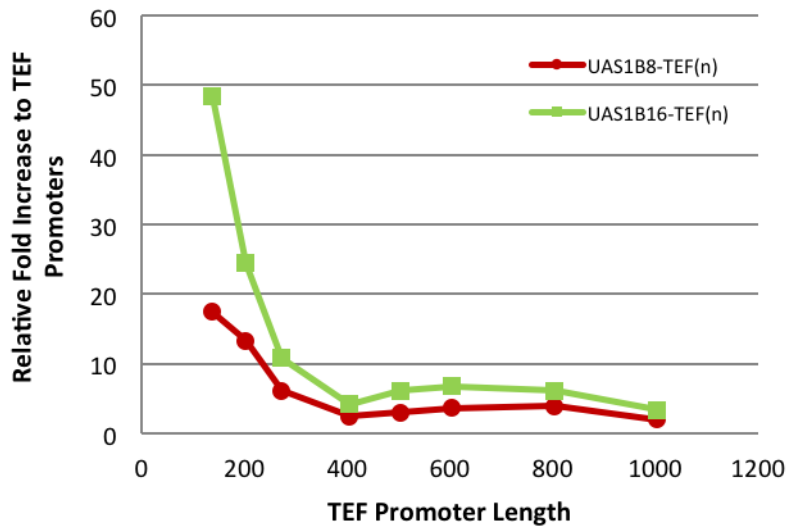
Figure 2.3 cont.

(**A**) The characterization of relative promoter strengths for the core TEF promoters (blue), UAS1B$_8$-TEF promoters (red) and UAS1B$_{16}$-TEF promoters (green) using flow cytometry. This data was compared with the UAS1B$_8$-Leum and UAS1B$_{16}$-Leum promoters. (**B**) The tuning ability of UAS1B$_8$ and UAS1B$_{16}$ decreases as a function of core promoter length.

## 2.4 Discussion and conclusion

The work presented in this chapter establishes a synthetic approach for tuning gene expression using a hybrid promoter approach. Moreover, this approach is unique in its capacity to up-regulate the expression of the baseline starting promoter unlike most traditional approaches that typically generate promoters of decreased expression. In doing so, this work created the strongest known promoters in the oleaginous yeast *Yarrowia lipolytica* and allows for fine-tuned gene expression in this organism. The general strategy developed in this chapter employing tandem UAS repeat elements could potentially be applied to other organisms and further generalized by using other UAS regions. Finally, these results have the biological implication that the expression capacity for promoters (at least in *Y. lipolytica*) is enhancer limited. In this regard, this approach expands the quantity and quality of parts available for systems biology research (95-96).

Using the hrGFP-enabled single-cell analysis, this work observed bimodal fluorescence distributions for all the data collected using plasmid based expression. These results strongly suggest an "on/off" switch mechanism resulting from the low copy CEN-based plasmid used in the study. It is interesting to note that this bimodal distribution was absent when using integrated expression cassette instead. As a result, this work highlights an important consideration for using plasmids in a *Y. lipolytica* system. Nevertheless, the hrGFP analysis allowed for a characterization of endogenous *Y. lipolytica* promoters and identified EXP and TEF as strong promoters among the set tested. Furthermore, this analysis led to the creation of several series of promoter elements capable of high-level expression.

The magnitude of these hybrid promoters can be seen by the relative mRNA range of more than 400 fold between the core promoter (Leum) and the maximum of UAS1B$_{24}$-Leum. The strongest UAS1B-Leum hybrid promoter exhibited a more than eight fold increase in promoter strength in terms of Miller units compared to the strong endogenous promoters tested in this chapter. It should be noted that the expression of the UAS1B$_4$-Leum reported here were substantially lower than previously reported. These comparisons are difficult due to the slight differences in restriction sites used to create these hybrid promoters, the use of rich media in prior reports, and the use of replicative plasmids here compared with integrated plasmids in other studies. Even with these difference and discrepancies, this work still presents up to a fourfold increase in performance compared with the best reported endogenous promoters or previously constructed hybrid promoters (82, 97). This illustrates that multiple tandem repeats of the UAS1B enhancer element activate transcription to levels far stronger than those previously described and that this enhancer activation can occur at regions more than 2000 nucleotides upstream of the start codon (for UAS1B$_{16-32}$-Leum).

The UAS1B$_8$ and UAS1B$_{16}$ elements were shown to behave as synthetic amplifiers when tested with various TEF-based promoters. In this regard, we demonstrated that the ability of a UAS1B element to amplify expression is independent of the core promoter element. However, the magnitude of this amplification was dependent on the core promoter used. Thus, both the choice of tandem enhancer element and core promoter element contribute to the collective strength of hybrid promoters. This observation raises the possibility of rationally designing hybrid promoters with specified

expression strength. The drastic increase in expression levels by both of the $UAS1B_8$ and $UAS1B_{16}$ elements across this series demonstrates that these genetic elements are portable, modular components that can generically alleviate native enhancer-limitation without disrupting endogenous regulation. The modularity of the UAS1B insert and the strength of the UAS1B-Leum and UAS1B-TEF series advocate the use of hybrid promoter engineering as generic approach towards building stronger, fine-tuned promoter libraries with interchangeable, modular components.

Collectively, these results give credence to the theory that *Y. lipolytica* promoters are enhancer-limited, and we have shown that this limitation can be effectively overcome through hybrid promoter engineering. Tandem UAS elements help bypass the enhancer limited nature of promoters by serving as transcriptional amplifiers. Cells containing the strong hybrid promoters developed in this chapter did not exhibit any growth defects. Therefore, transcription factor availability does not seem to be limiting for these cells as these promoters did not seem to deplete or starve cells of transcription factors. In this regard, transcription factor binding is posited to serve as a major rate limiting step for transcription at promoter sites with addition of upstream activating sites alleviating this limitation. Thus, it is possible for us to control transcriptional activity by indirectly modulating transcription factor localization or affinity through the choice of enhancer and core elements in a hybrid promoter.

The generic approach of hybrid promoter engineering described in this chapter is an important, generic synthetic biology tool enabling the construction of high-level and fine-tuned promoters with interchangeable promoter parts. This approach is one of the

first to rationally amplify the expression output of a given promoter element. By utilizing this approach, we have expanded the metabolic engineering toolbox in *Y. lipolytica* and developed several novel promoter series - UAS1B$_{1-32}$-Leum, UAS1B$_8$-TEF, and UAS1B$_{16}$-TEF. Heterologous protein expression requires strong promoters to obtain high protein expression level, while metabolic pathway engineering necessitates strictly controlled, fine-tuned promoters set to optimize pathways. The generic hybrid promoter approach described here accomplished both of these tasks. Moreover, these results demonstrate that the expression from *Y. lipolytica* native promoters is enhancer limited, which may be a generic phenomenon across other yeast organisms. Finally, given the results in this chapter, it is possible to conceive of novel combinations of upstream activation sequences with various promoter elements to achieve both fine-tuned expression and controlled regulation.

# Chapter 3: Increasing expression level and copy number of a *Yarrowia lipolytica* plasmid through regulated centromere function[2]

## 3.1 Chapter summary

Beyond the promoter engineering strategies described in Chapter 2, manipulating gene expression using different types of plasmids (centromeric, 2-micron, and autonomously replicating sequence) can expand expression levels and enables a quick characterization of combinations, both of which are highly desired for metabolic engineering applications. However, for the powerful potential industrial workhorse *Yarrowia lipolytica*, only a low-copy CEN plasmid is available. As presented in this chapter, we engineered the CEN plasmid from *Y. lipolytica* by fusing different promoters upstream of the centromeric region to regulate its function and expand its range. By doing this, we successfully improved the copy number and gene expression at plasmid level by 80% and enabled a dynamic range of nearly 2.7 fold. This improvement was seen to be independent from both the promoter and gene used in the expression cassette. These results present a better starting point for more potent plasmids in *Y. lipolytica*.

---

## 3.2 Introduction

The ability to tune gene expression is essential for the success of metabolic engineering efforts. To this end, previous work including endogenous promoter characterization (98), hybrid promoter engineering as described in Chapter 2, and multi-copy integration (99) have increased the capacity to engineer *Yarrowia lipolytica*. However, this tuning capacity has not been matched at the plasmid level, a convenience that would enable quick characterization of genetic constructs through a simple transformation and also a tool that can enable fundamental studies of replication and segregation (100).

In the widely used baker's yeast *Saccharomyces cerevisiae*, plasmid-based gene expression control is enabled by several varieties of plasmids including centromeric (CEN) plasmids (low copy), 2-micron plasmids (high copy), and autonomously replicating sequence (ARS) plasmids (high copy) (19-21). However, for the case of *Y. lipolytica*, a suitable 2-micron has not been identified and the CEN and ARS elements cannot be separated (68, 72, 85) leaving only low copy CEN-based plasmids. In *S. cerevisiae*, it has been reported that a CEN plasmid can be converted into an ARS-like plasmid by fusing a promoter upstream of the centromeric region leading to increase in copy number and gene expression (101). In the work presented in this chapter, we sought to invoke a similar strategy for a *Y. lipolytica* CEN plasmid to both increase copy number and expression level (**Figure 3.1a**).

## 3.3 Results

To accomplish this task, we first selected various endogenous promoters and synthetic variants (P-GPD, P-EXP, P-POT1, P-MET2, P-TEF and truncated P-TEF: P-TEF(272) and P-TEF(136) with 272 bp and 136 bp upstream of the ATG starting site  (98, 102-103) as well as two cell-cycle dependent promoters (P-CDC2 and P-YOX1) to regulate the centromere function in *Y. lipolytica* (all promoters were amplified with 50bp from the coding region). Previous studies in *S. cerevisiae* suggested CDC2 and YOX1 exhibit cell-cycle dependent expression patterns and express in G1-phase and mid G1 to early S phase respectively (104-106). Whereas the promoter fused to the CEN region was altered in each plasmid, each construct contained a strong hybrid promoter (P-UAS1B16-Leum) upstream of hrGFP, a green fluorescence protein. Through the use of flow cytometry, we found that altering the promoter upstream of the centromere region in *Y. lipolytica* leads to similar phenotype found in *S. cerevisiae*. As a result, it was possible to alter the expression level via regulated centromere function (**Figure 3.1b**). For the case of P-TEF(272), P-CDC2, P-POT1 and P-EXP based engineered plasmid, fluorescence was increased by at least 50% compared to the control plasmid construct and up to 80% for the case of P-TEF(272). Interestingly, the P-MET2 promoter upstream of the CEN region resulted in a decreased expression by 30%. Collectively, a nearly 2.7 fold dynamic range was achievable through this strategy.

Next, we replaced the hrGFP gene with a β-galactosidase reporter gene for two of the plasmids (containing the promoters P-POT1 and P-CDC2 upstream of CEN) to test the generalizability of this approach. Both plasmids showed a similar improvement of

roughly 50% in the β-galactosidase activity as seen with the hrGFP (**Figure 3.1c**). In addition, the increase in expression is preserved when a lower strength native promoter (P-EXP) is used to drive the expression of β-galactosidase, thus indicating that the approach is independent of reporter protein and promoter driving the expression cassette (**Figure 3.1d**).

To confirm that the increased protein expression level was the result of increases in plasmid copy number, we employed a relative copy number assay based on RT-PCR using a total genomic DNA extract (19, 107). The copy number in the augmented plasmids was found to be increased by roughly 80% compared to the initial plasmid construct (**Figure 3.1c**). Thus, these engineering efforts successfully increased the copy number as well as the expression level from *Y. lipolytica* plasmids.

One commonly observed feature of these *Y. lipolytica* plasmids is a bimodal distribution of fluorescence signal as mentioned in Chapter 2 (103). The improvement in expression seen in this chapter was the cumulative result of both an increase in the signal as well as a mild increase of the size of the positive subpopulation (**Figure 3.1e**). In an effort to further understand this bimodal phenotype, we separated the positive and negative subpopulations through cell sorting and cultivated the sorted populations. Whereas the positive population reverted back to the bimodal distribution, the negative population was unable to be grown in selective growth conditions. This data suggests a biased plasmid segregation occurs in *Y. lipolytica* CEN-based plasmids which can be attributed to the nature of the plasmid as well as the size (about 9.5kb).

Figure 3.1 Improving expression level and copy number of plasmid in *Yarrowia lipolytica* with regulated centromere function

Figure 3.1a
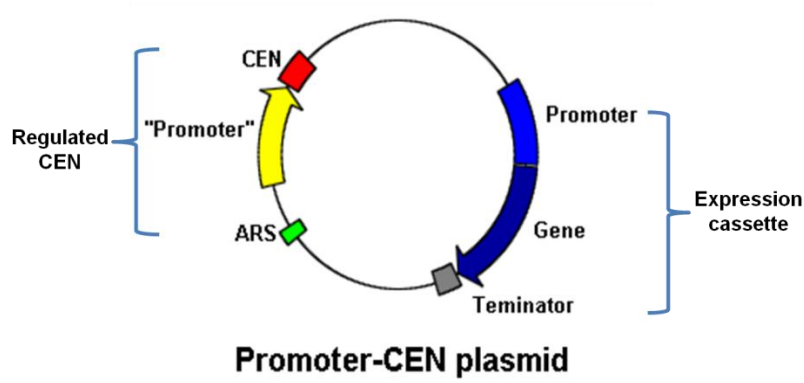


Figure 3.1b
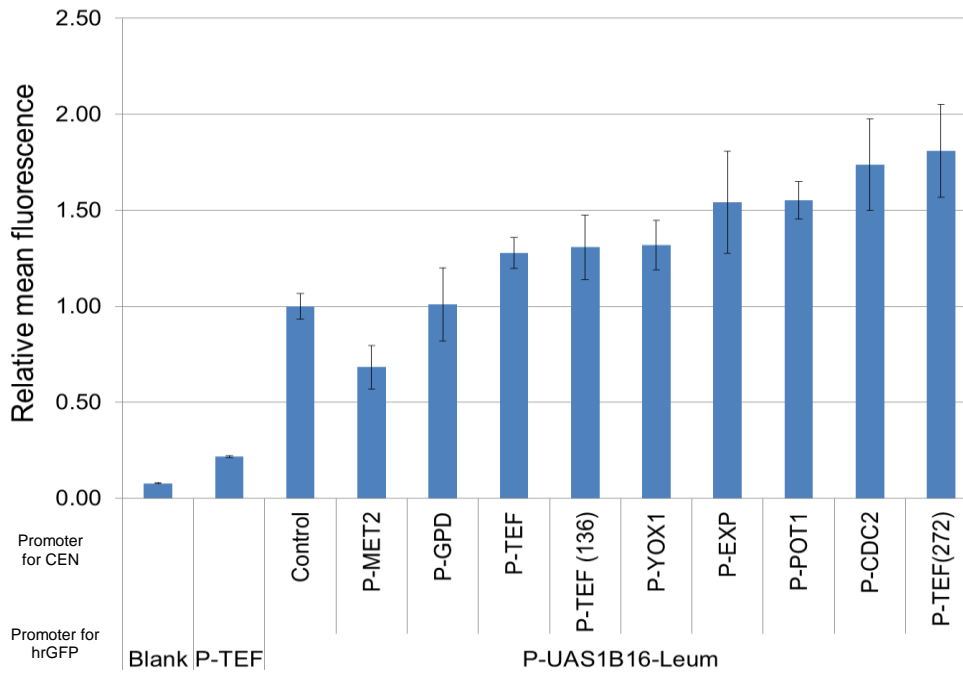
Figure 3.1 cont.

Figure 3.1c
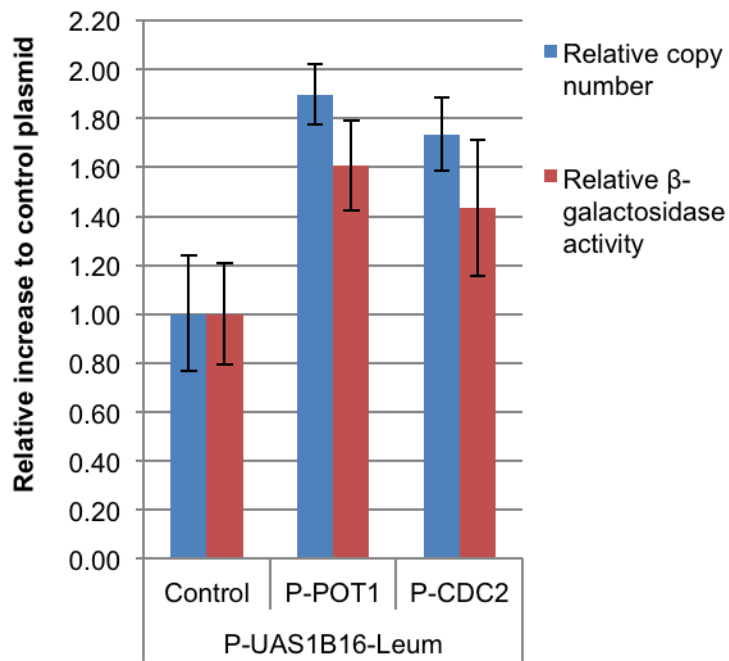
Figure 3.1 cont.

Figure 3.1d
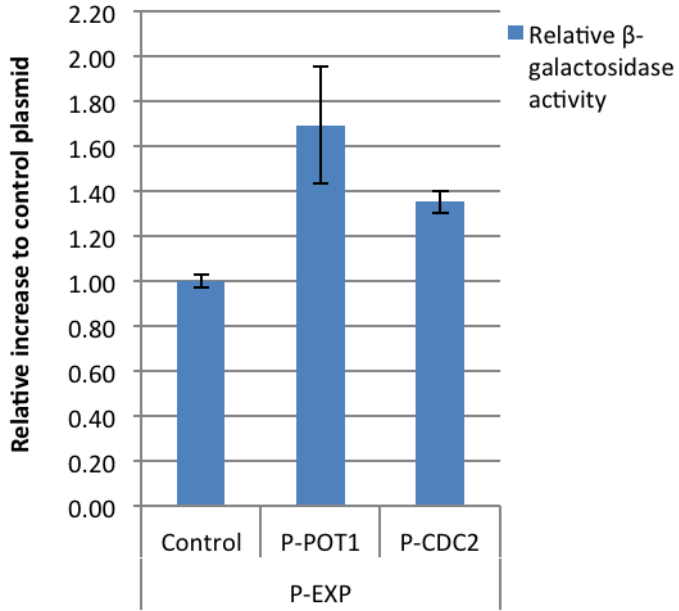


Figure 3.1e
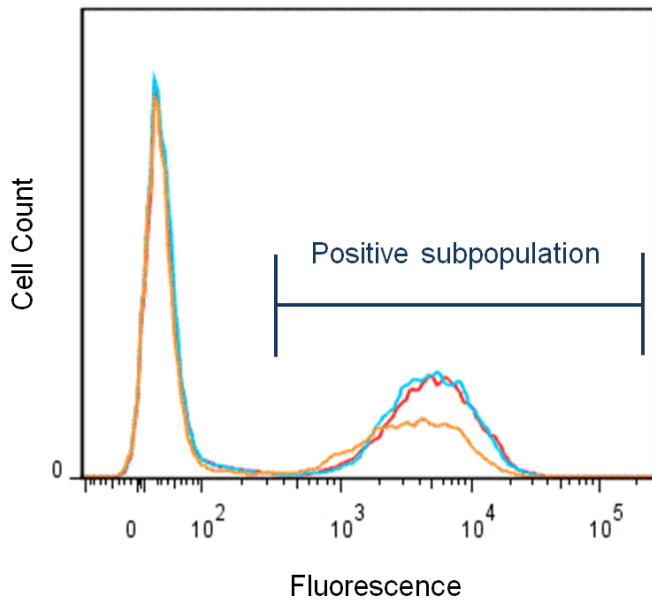
Figure 3.1 cont.

 (**A**) A schematic of the engineered plasmids with regulated centromere function. (**B**) Promoters, including P-MET2, P-GPD, P-TEF, P-TEF(136), P-YOX1, P-EXP, P-POT1, P-CDC2, P-TEF(272), were used to regulate centromere function.  Mean fluorescence data collected by flow cytometry analysis was used to compare expression at a time point of 48 h in minimal medium. (**C**) Relative plasmid copy number and β-galactosidase activity with P-POT1 and P-CDC2 based engineered plasmid and control plasmid with P-UAS1B16-Leum driving expression of β-galactosidase. The data was collected by RT-PCR and Gal-Screen™ β-Galactosidase Reporter Gene Assay System for Yeast or Mammalian Cells (life technologies) at a time point of 48 h in minimal medium. (**D**) Relative β-galactosidase activity with P-POT1 and P-CDC2 based engineered plasmids and control plasmid with promoter P-EXP driving expression of β-galactosidase. The data was collected by Gal-Screen™ β-Galactosidase Reporter Gene Assay System for Yeast or Mammalian Cells (life technologies) at a time point of 48 h in minimal medium. (**E**) Histogram of fluorescence signal showing the bimodal distribution with P-POT1 (blue), P-EXP (red) based engineered plasmids with the control plasmid (yellow). The data was collected by flow cytometry analysis to compare P-POT1, P-EXP based engineered plasmids with the control plasmid at a time point of 48h in minimal medium: P-POT1 based plasmid contains 46.1%, P-EXP based plasmid contains 46.2% and the control plasmid contains 36.6% positive subpopulations. The graph was made using FlowJo software (Tree Star Inc., Ashland, OR). In all graphs, error bars represent standard deviations from biological replicates.

**3.4 Discussion and conclusion**

From the data presented in this chapter, the improvements in expression and copy number at the plasmid level are highly dependent on the characteristics of the promoters repressing centromere function. Both of the strength and the expression pattern of the promoters affect the turning ability with the engineered plasmids. For instance, the decreased signal with promoter MET2 based plasmid could be resulted from the expression pattern of MET2 is not in favor of plasmid stability. The different expression levels exhibited with plasmids of constitutive promoter EXP, GPD and TEF series could be due to different strengths possessed by different promoters. Moreover, the increase of both positive population and mean fluorescence suggested a more stable plasmid behavior in the engineered plasmids. This stability could be a result of increased copy number inside the cells. The tuning ability achieved through this plasmid engineering strategy can largely facilitate the metabolic engineering and microbiological studies in *Y. lipolyitica*, since it supplies an opportunity to alter the gene expression level without changing genetic components such as promoter and terminator, thus, enables the preservation of native regulation pattern. In this chapter, we reported the improvement in expression level and copy number at the plasmid level in *Y. lipolytica* through altering its centromere function. These efforts resulted in over 80% improvement of plasmid copy number and expression and also enabled a dynamic range of nearly 2.7 fold. This improvement was seen to be independent of both the promoter and gene in the expression cassette. Although the improvement is significantly less comparing with other expression tuning strategies such as hybrid promoter engineering in this yeast (Chapter 2), the

method presented here can be applied in addition to the promoter engineering strategy to further increase the expression level. Specifically, with eight fold improvement in the term of fluorescence signal described in Chapter 2 and the 80% improvement described here, an over 14 fold total increment of gene expression on plasmid could be achieved.

# Chapter 4: Rational metabolic engineering *Yarrowia lipolytica* for high lipid production[3]

## 4.1 Chapter summary

Economic feasibility of biosynthetic fuel and chemical production hinges upon harnessing metabolism to achieve high titer and yield.  Once we gained the ability of manipulating gene expression in *Yarrowia lipolytica* as described in Chapters 2 and 3. We performed a thorough genotypic and phenotypic optimization of an oleaginous organism to create a strain with significant lipogenesis capability based on rational combinatorial metabolic engineering strategies described in this chapter. Specifically, we rewire *Y. lipolytica's* native metabolism for superior *de novo* lipogenesis by coupling combinatorial multiplexing of lipogenesis targets with phenotypic induction. We further complete direct conversion of lipid content into biodiesel. Tri-level metabolic control results in saturated cells containing upwards of 90% lipid content and titers exceeding 25 g/L lipids, a 60-fold improvement over parental strain and conditions.  Through this rewiring effort, we advance fundamental understanding of lipogenesis, demonstrate noncanonical environmental and intracellular stimuli, and uncouple lipogenesis from nitrogen starvation.  The high titers and carbon-source independent nature of this lipogenesis in *Y. lipolytica* in this chapter highlight the potential of this organism as a platform for efficient oleochemical production.

---

[3] Portion of this chapter has been published previously in Nature Comm 5:3131 with JB, LL, HA designed the experiments, JB, AH, LL, RK, JM, AP, PO carried the experiments and JB, HA wrote the manuscript.

## 4.2 Introduction

Microbial biosynthesis of fuels (such as ethanol and biodiesel) and industrial chemical precursors provides a renewable means to reduce dependence on petroleum feedstock (3, 5, 108-110). In particular, bio-based production of oils and lipids provides a unique platform for the sustainable production of biodiesel and other important oleochemicals (46, 110). Most efforts for developing such a platform involve either rewiring *E. coli* or cultivating cyanobacteria. These attempts suffer from low titers (less than 7 g/L) and variable lipid content (ranging between 10 and 87%), with the highest of these levels typically occurring in non-tractable, slow growing hosts cultivated in oil containing media (i.e., *ex novo* lipid incorporation instead of *de novo* lipogenesis) (51, 108, 110-114).

As an alternative, several groups have explored oleaginous organisms such as the fungus *Yarrowia lipolytica*, but total oil content and titers are still limited (23, 55, 57, 76, 115-116). Yet, the genetic tractability of *Y. lipolytica* (9, 65, 68, 70, 74, 102-103) coupled with its modest, innate *de novo* lipogenesis (~10-15% lipid content in wildtype (23, 55-56, 117-118)) make it a potential candidate as a platform organism for superior lipid production.

Lipid biosynthesis is primarily initiated by the activity of four enzymes - AMP Deaminase (AMPD), ATP-Citrate Lyase (ACL), Malic Enzyme (MAE) and Acetyl-CoA Carboxylase (ACC) - that cooperatively divert carbon flux from central carbon metabolism towards fatty acid precursors (56, 76). AMPD inhibits citric acid cycle flux to promote the accumulation of citrate, which is then cleaved into acetyl-CoA by ACL.

Fatty acid synthesis is further encouraged by carboxylation of acetyl-CoA to malonyl-CoA fatty acid building blocks by ACC and by an increased NADPH supply generated by MAE or the pentose phosphate pathway (56, 76, 119) (**Figure 4.1a**). Leucine biosynthetic capacity has also been implicated as an effector of lipogenic ability in oleaginous organisms (117, 120), and a putative acetyl-CoA generating leucine degradation pathway was recently identified through a comparative genomics analysis of non-oleaginous and oleaginous yeast strains (121). In this regard, *Y. lipolytica* also possesses homologs for every enzyme and enzymatic subunit necessary for acetyl-CoA generation through isoleucine degradation (>45% similarity to *Homo sapiens* enzymes) (66, 122). Previous efforts to increase lipid accumulation have shown promise in *Y. lipolytica*. In particular, deletion of β-oxidation enzymes coupled with enhancing glycerol synthesis substantially increased *ex novo* lipid accumulation (56, 76), and deletion of the *pex10* peroxisomal biogenesis gene greatly increased eicosapentaenoic acid yields (24). However, these studies have been limited by their breadth of metabolic control and their comprehensiveness of genotypic and phenotypic sampling towards complete redirection of metabolic flux towards lipid accumulation (23, 55, 76, 117). Moreover, *de novo* lipid content in this organism has been limited to below around 60% by dry cell weight (23).

In the work presented here, we undertake a large scale engineering effort - multiplexing genomic engineering of lipogenesis targets with phenotypic induction - and create a *Y. lipolytica* strain with significantly improved lipogenesis capability. Simultaneous perturbation of five lipogenic targets (affecting three disparate metabolic

pathways) results in lipid-saturated cells, culminating in the highest reported lipid content (~90%) and lipid titer (25.3 g/L). The latter milestone represents a more than 60-fold improvement over parental strain and conditions. Through this rewiring effort, we describe several non-canonical facets of lipogenesis, including that lipogenesis is dependent on absolute environmental carbon content, that rare odd-chain fatty acids pathways are naturally activated by high lipogenesis, that lipid accumulation phenotypes are dependent on leucine-mediated signaling, and that high lipogenesis can be un-coupled from nitrogen starvation and entails a reduction in citric acid cycling. We further demonstrate that these lipids can be easily converted into FAMEs (fatty acid methyl esters) suitable for biodiesel. This work demonstrates, and capitalizes upon, the lipogenic potential of *Y. lipolytica*, utilizing its amenable metabolism to realize high titers and carbon-source independent lipid accumulation.

## 4.3 Results

### 4.3.1 Combinatorial genomic rewiring for improved lipogenesis

In this work, we investigate a combinatorial, multiplexing of targets spanning fatty acid, lipid, and central metabolism through the overexpression of five lipogenesis enzymes in four genomic backgrounds marked by differential fatty acid catabolic capacity (**Table 4.1, Figure 4.1a**). Specifically, AMPDp, ACLp, and MAEp overexpression were investigated for their potential to increase acetyl-CoA and NADPH supply (ACCp overexpression has not been reported to significantly improve lipogenesis and was excluded (23)) and DGA1 and DGA2p (acyl-CoA:diacylglycerol

50

acyltransferases isozymes I and II) were included for their potential in catalyzing the ultimate step in triglyceride synthesis (123). These overexpression targets were multiplexed with deletions that served to reduce fatty acid catabolism by reducing one or both of β–oxidation (via *mfe1* deletion) (55, 76) and peroxisome biogenesis (via *pex10* deletion) (117, 124) (**Table 4.1**). We have previously demonstrated that restoration of a complete leucine biosynthetic pathway increased lipid accumulation more than alleviation of uracil auxotrophy in a PO1f base strain (117). Thus, we included the complementing of leucine and uracil biosynthetic capacity both singly and in tandem as targets for this multiplexing. Integrated expression cassettes were driven by our high strength synthetic UAS1B$_{16}$-TEF constitutive hybrid promoter developed in Chapter 2. Collectively, the combinatorial multiplexing of enzyme overexpressions, fatty-acid inhibition knockouts, and other biosynthetic pathways resulted in 57 distinct genotypes that were analyzed for lipogenesis capacity compared to the wild-type strain (**Figure 4.1b**). Initially, a Nile Red based fluorescence assay coupled with flow cytometry (125) was used to efficiently determine relative lipid content and assess critical genotype synergies. Across the resulting lipogenesis metabolic landscape, we observed a significant range in lipid accumulation that spanned a 74-fold improvement in fluorescence over unmodified *Y. lipolytica* PO1f (**Figure 4.1b**). Using fluorescence microscopy, it is evident that cells become larger and visibly more saturated with lipid content across the resulting lipogenic continuum in this landscape (**Figure 4.1c**).

Three dominant genetic targets exhibited cooperativity towards enhancing lipogenesis—*pex10* deletion, DGA1 or DGA2 overexpression, and restoration of a

complete leucine biosynthetic pathway (leucine$^+$ genotype) (**Figure 4.1b**). Each of these

targets independently improved Nile Red based fluorescence by more than threefold, and

DGA1 overexpression outperformed that of DGA2 (**Figure 4.1b**). Overexpression of

MAE and AMPD were positive effectors of lipogenesis, but offered no cooperative

advantage when combined into the *pex10* leucine$^+$ DGA1 overexpression background,

potentially by unbalancing metabolic flux towards lipid production through the

overproduction of fatty acid synthesis precursors (**Figure 4.1b**). Deletion of the *mfe1*

gene was not seen to alter total Nile Red based lipid fluorescence measurements, but its

removal reduces fatty acid degradation in carbon starvation conditions (76, 117).

Similarly, the uracil$^+$ genotype had minimal effect on fluorescence, but improved growth

rate and permitted cultivation in a pure minimal medium composition. Thus, the *pex10,*

*mfe1,* leucine$^+$, uracil$^+$, DGA1 overexpression genotype, the strain with the highest

lipogenesis potential in terms of fluorescence, was selected as our most advantageous

strain. We extracted and measured lipid content to confirm Nile Red-based flow

cytometry assessment of lipid content (**Figure 4.1d,e,f**). In small scale, test-tube

cultivations, the final engineered strain outperformed all others, yielding 6.00 g/L lipids

with 74% lipid content, a nearly 15-fold improvement over control (0.41 g/L lipid and

16.8% lipid content).

Figure 4.1 Combinatorial strain engineering for high lipid production in *Yarrowia lipolytica*

Figure 4.1a
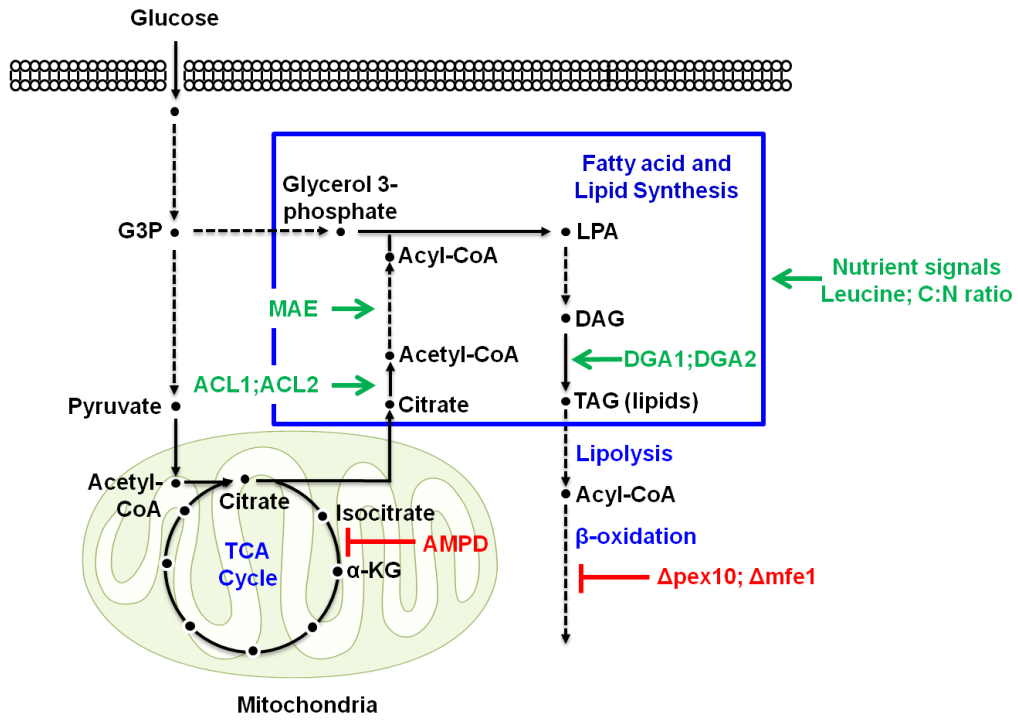
Figure 4.1 cont.

Figure 4.1b
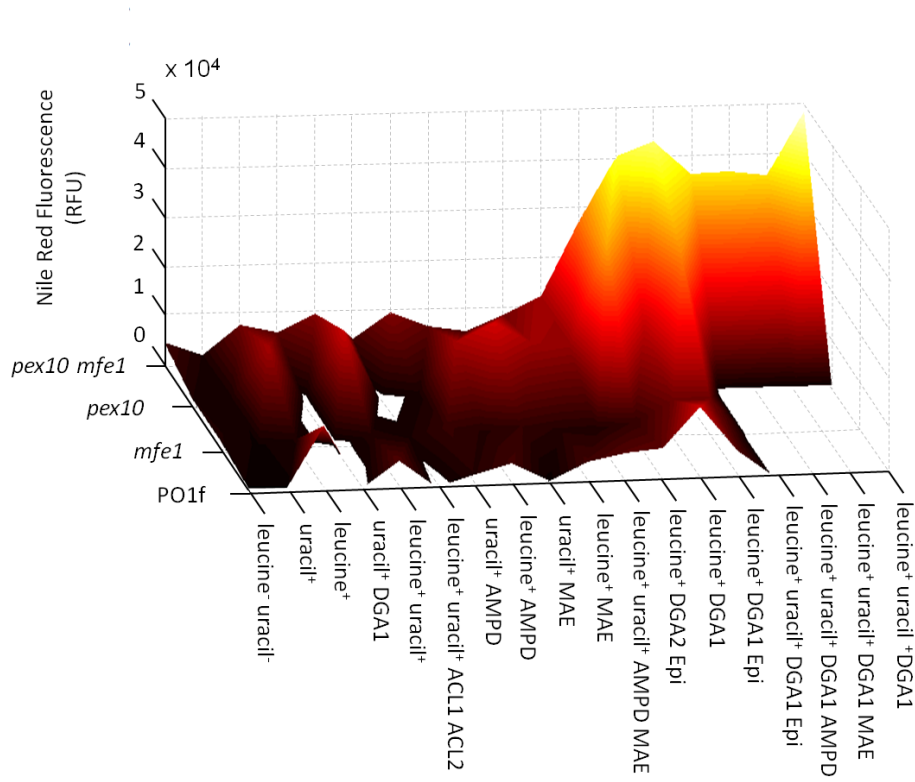


Figure 4.1c

Figure 4.1 cont.

Figure 4.1d
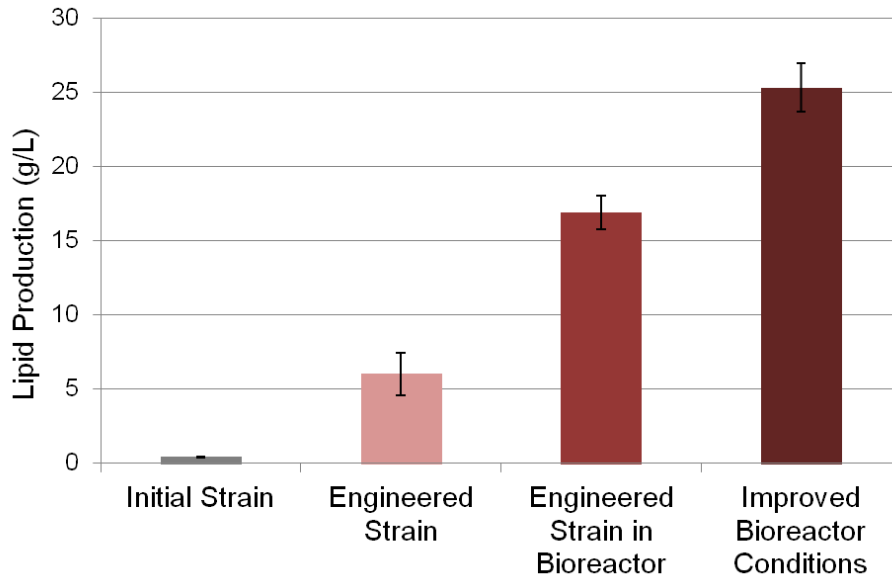


Figure 4.1e
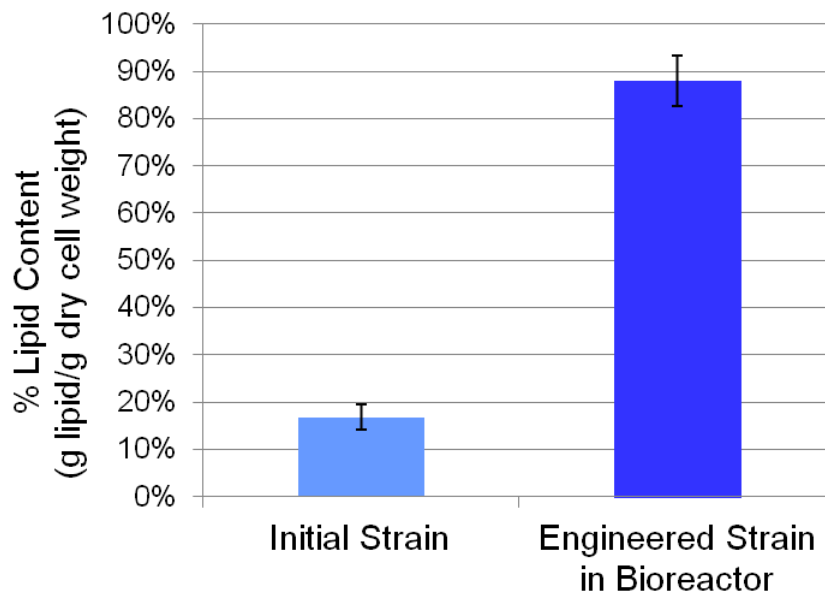
Figure 4.1 cont.

Figure 4.1f
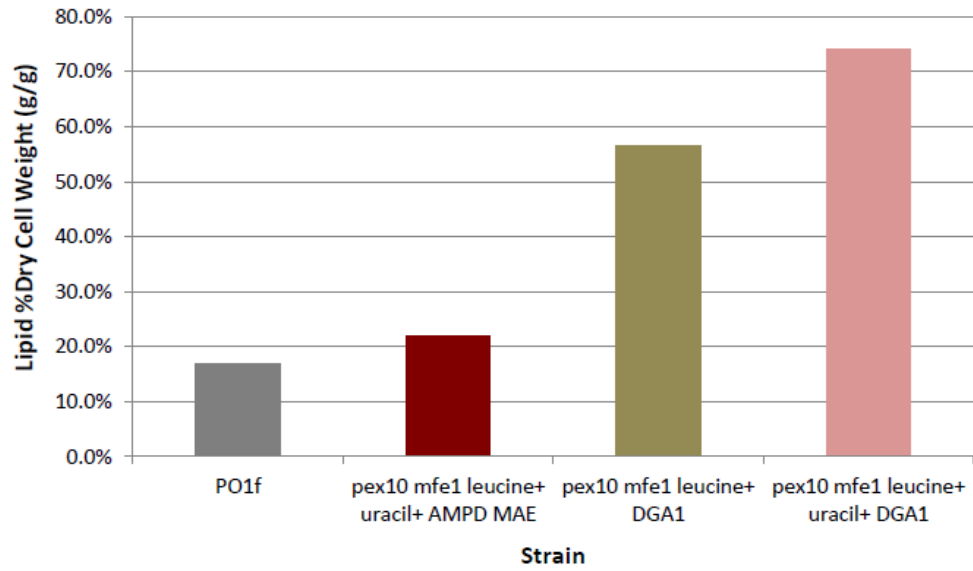
Figure 4.1 cont.

(**A**) A schematic illustrating the pathways rewired in *Y. lipolytica's* metabolism to drastically increase lipogenesis capacity. (**B**) Nile Red fluorescence analysis of the strains constructed in this chapter. Strain names include strain background (POlf, *pex10*, *mfe1*, *pex10 mfe1*), auxotrophies relieved (leucine$^+$ or uracil$^+$), and enzymes overexpressed. "Epi" denotes episomal overexpressions. Lipogenesis is induced as *pex10* deletion is coupled with leucine biosynthetic capacity and DGA1 overexpression – generally from front left to back right of the 3D contour heat map representation. Error bars represent the standard deviation of technical triplicates.(**C**) Fluorescence light microscopy images of six strains increasing in lipid content (white) from left (unmodified POlf) to right (*pex10 mfe1* leucine$^+$ DGA1). (**D, E**) Increases in lipid titer and lipid content realized by engineering POlf to create the *pex10 mfe1* leucine$^+$ uracil$^+$ DGA1 strain and then optimizing fermentation conditions in a bioreactor. Error bars represent standard deviations of technical triplicates. (**F**) Four strains were analyzed for percent lipid content (g lipids/g dry cell weight) after cultivation in 80 g/L glucose, 6.7 g/L Yeast Nitrogen Base w/o amino acids (1.365 g/L ammonium), and 0.79 g/L CSM supplement – POlf, *pex10 mfe1* leucine$^+$ uracil$^+$ AMPD MAE, *pex10 mfe1* leucine$^+$ DGA1, and *pex10 mfe1* leucine$^+$ uracil$^+$ DGA1. The *pex10 mfe1* leucine$^+$ uracil$^+$ DGA1 strain yielded the highest percentage lipid content (74%), a more than 4-fold improvement over PO1f control (16.8% lipid content).

Table 4.1 List of genes and enzymes for rational metabolic engineering for high lipid production

| Genomic backgrounds | |
|---|---|
| **Name** | **Genotype  and (*function of knockout*)** |
| POlf | MatA, leucine⁻, uracil⁻, no extracellular proteases |
| *pex10* | POlf-Δpex10 *(prevents peroxisome biogenesis)* |
| *mfe1* | POlf-Δmfe1 *(prevents β-oxidation)* |
| *pex10 mfe1* | POlf-Δpex10 Δmfe1 *(prevents peroxisome biogenesis and β-oxidation)* |
| **Enzymatic overexpressions** | |
| **Name** | **Function** |
| AMPD | Inhibits TCA cycle, increasing citric acid level |
| $ACL_{subunit}1$ | Cleaves citric acid to acetyl-CoA |
| $ACL_{subunit}2$ | Cleaves citric acid to acetyl-CoA |
| MAE | Increases NADPH cofactor supply |
| $DGA_{isozyme}1$ | Catalyzes lipid synthesis step |
| $DGA_{isozyme}2$ | Catalyzes lipid synthesis step |
| **Auxotrophic markers** | |
| **Name** | **Utilized for expression** |
| Leucine$^{+/-}$ | Episomally and chromosomally |
| Uracil$^{+/-}$ | Chromosomally |

AMPD = Adenosine monophosphate deaminase; ACL = ATP-Citrate Lyase; MAE = Malic Enzyme; DGA = acyl-CoA:diacylglycerol acyltransferases.  ACL is a heterodimeric protein so only dual overexpressions of the $ACL_{subunit}1$ and $ACL_{subunit}2$ were constructed and tested.

**4.3.2 Lipogenic induction through nutrient level optimization**

We next sought to understand the complex relationship between *de novo* lipid accumulation and nutrient levels. Previous studies generally accepted that lipogenesis capacity is highly dependent on the ratio of available carbon and nitrogen (C:N ratio) and that lipogenesis induction requires a nitrogen starvation mechanism (118, 126). However, no definitive, quantitative relationship between genotype and lipogenesis induction has been determined. Thus, we analyzed the effect of nitrogen starvation and carbon availability on lipogenesis for unmodified *Y. lipolytica* PO1f and eleven engineered strains spanning the lipogenesis landscape. Cultivation of these twelve strains in thirteen media formulations containing between 10 g/L and 160 g/L glucose and 0.055 g/L and 1.365 g/L ammonium revealed that absolute glucose level, rather than generally accepted C:N ratio, is crucial towards inducing lipid synthesis, and high lipid producers realized optimal accumulation in higher glucose media (**Figure 4.2**). In particular, unmodified *Y. lipolytica* PO1f and other low performing strains were most strongly induced by a lower carbon level (20 g/L glucose and 0.273 g/L ammonium), but responded poorly at similar C:N ratios with higher glucose and ammonium concentrations (**Figure 4.2a**). Moderate lipid accumulators were highly induced at intermediate glucose levels but again responded poorly at similar C:N ratios (**Figure 4.2b**). The highest accumulators, including the *pex10 mfe1* leucine[+] DGA1 overexpression genotype, were induced most intensely by higher levels of carbon and nitrogen (80 g/L glucose and 1.365 g/L ammonium) (**Figure 4.2c**). Thus, the current paradigm asserting the necessity of nitrogen starvation and that similar C:N ratios beget

59

similar induction irrespective of overall carbon and nitrogen levels is incorrect. Instead, a defined amount of carbon content ultimately controls lipid synthesis, and this favorable carbon level increases in strains capable of superior lipogenesis. Increasing carbon and nitrogen levels only improves lipogenesis to a certain extent, as lipid yield decreases when glucose levels are increased to 160 g/L (**Figure 4.2c**), and cultivation of various engineered strains in media containing 320 g/L glucose drastically reduced growth rate, most likely due to osmotic stress (127).

Figure 4.2 Genotypic dependency towards lipid induction phenotype with selected strains

Figure 4.2a
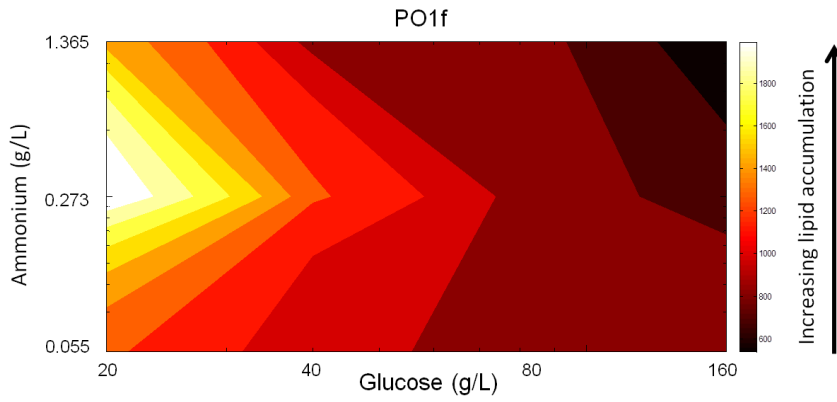


Figure 4.2b
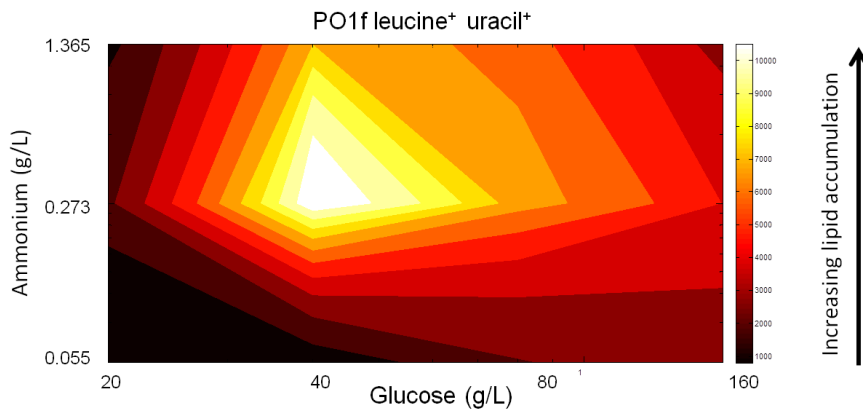


Figure 4.2c
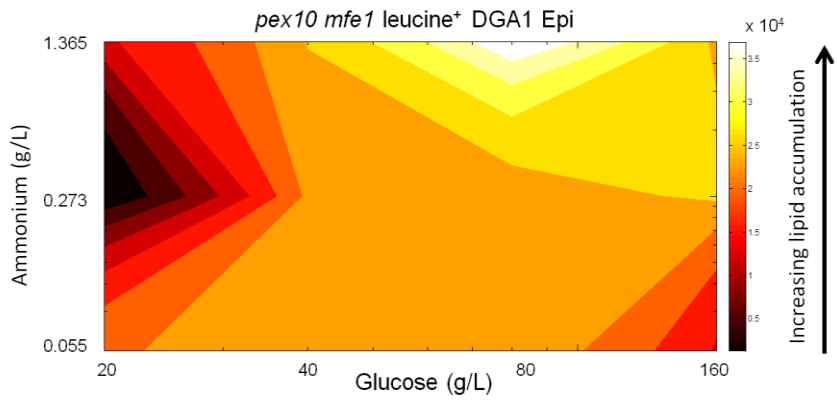
Figure 4.2 cont.

Heat maps of Nile Red stained lipid fluorescence for the (**A**) POlf low lipid accumulating strain, (**B**) POlf leucine[+] uracil[+] moderate lipid accumulating strain, and (**C**) *pex10 mfe1* leucine[+] DGA1 high lipid accumulating strain demonstrate a decoupling of lipogenesis and nitrogen starvation as well as the implication of absolute carbon content as a lipogenesis effector. Fluorescence data is shown for each strain after cultivation and staining in twelve media formulations containing between 20 g/L and 160 g/L glucose and 0.055 g/L and 1.365 g/L ammonium. Lipogenesis is dependent on absolute environmental carbon content, and low lipid accumulators (**A**) require less carbon for optimal lipogenic induction than moderate (**B**) or high (**C**) lipid accumulating strains. In highly lipogenic strains (**C**), high lipogenesis is un-coupled from nitrogen starvation. These studies were conducted with technical duplicates.

### 4.3.3 Controlled fermentation enables superior lipogenesis

Taken together, these dominant lipogenesis targets and nutrient levels (specifically, 80 g/L glucose and 1.365 g/L ammonium) enabled an optimization of fermentation conditions for the *pex10 mfe1* leucine$^+$ uracil$^+$ DGA1 overexpression strain to maximize lipid accumulation in a bioreactor setting. We cultivated this fully prototrophic strain in an inexpensive minimal media formulation consisting of only glucose, ammonium sulfate, and yeast nitrogen base. By additionally controlling pH, temperature, and dissolved oxygen levels, we observed significantly improved lipid titer to 16.1 g/L with cells containing up to 88% lipid cellular content (**Figure 4.3a**). This represents a 5.4 fold increase over a POlf leucine$^+$ uracil$^+$ control and 63% of the theoretical stoichiometric yield with a specific productivity approaching 0.2 g/L hr$^{-1}$ (**Figure 4.3**). Lipogenesis continues in the engineered strain throughout the six day fermentation despite complete depletion of glucose and cessation of biomass production within three days (**Figure 4.3a**). Moreover, this engineered strain exhibits reduced citric acid and biomass production to enable heightened flux towards lipid synthesis (**Figure 4.3a,c**). In contrast, excess carbon flux in the control strain accumulates as citric acid (dispersed throughout the supernatant) before reabsorption and incorporation into biomass (**Figure 4.3c**). Thus, the engineered strain's metabolic processes are in stark contrast to a central tenet of lipid accumulation in oleaginous organisms – that lipid accumulation requires prior production of citric acid (128-130). We hypothesize that our

re-engineered metabolism enables temporary carbon storage in secondary metabolites more amenable to direct incorporation into elongating fatty acids.

Doubling nutrient availability to 160 g/L glucose and 2.73 g/L ammonium further increased lipid titer to 25.3 g/L, the highest reported titer to date (**Figure 4.1d**). This represents an increase in specific productivity to 0.21 g/L/h, but a decrease in cellular lipid content to 71% and a decrease to 44% of theoretical stoichiometric yield. This further demonstrates the need to fully optimize carbon and nitrogen content to maximize lipogenic efficiency. These extremely high lipogenesis levels correlated with a metabolic shift to maintain homeostatic, steady state ammonium levels not seen in the low lipid accumulation background (**Figure 4.3b,d**). Specifically, after an initial drop, engineered cells re-buffered the nitrogen level within the media, thus illustrating a newfound, decoupled relationship between lipogenesis and nitrogen starvation. The control and engineered strain both exhibit similar intracellular protein degradation during the final four days of fermentation (**Figure 4.3e**). However, the control strain produces 4.9 g/L biomass containing ~11% nitrogen content (thus utilizing 0.54 g/L nitrogen) (131), while the engineered strain re-buffers supernatant nitrogen levels to ~0.5 g/L. A simple mass balance indicates that the nitrogen replenishment afforded by engineered cells is originating from protein degradation. Interestingly, the purely lipogenic phase (after biomass accumulation) in the engineered cells corresponds to a reduction in oxygen utilization, evidenced by a large, prolonged spike in dissolved oxygen content in bioreactor run, suggesting that both nitrogen and oxygen utilization are down regulated to reduce metabolite utilization for cell growth to enable enhanced lipogenesis.

Figure 4.3 Fermentation profiles of pex10 mfe1 leucine+ uracil+ DGA1 and POlf leucine+ uracil+
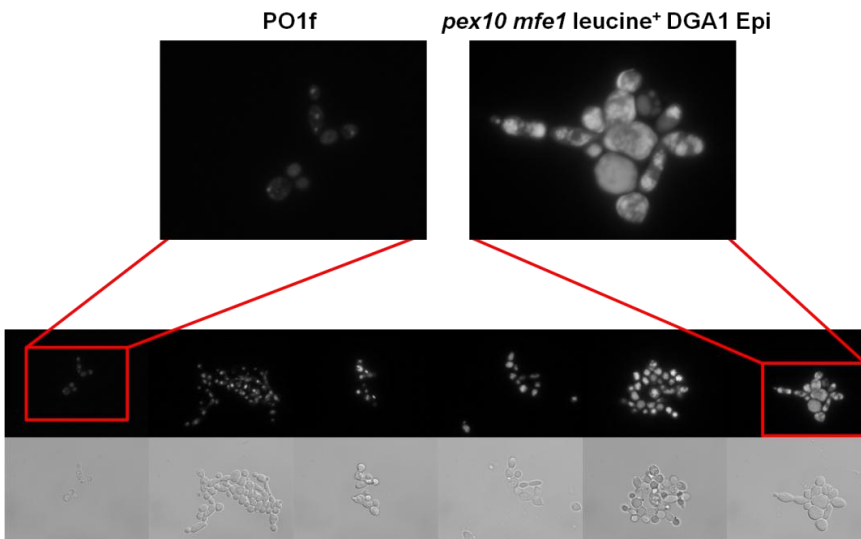
Figure 4.3a
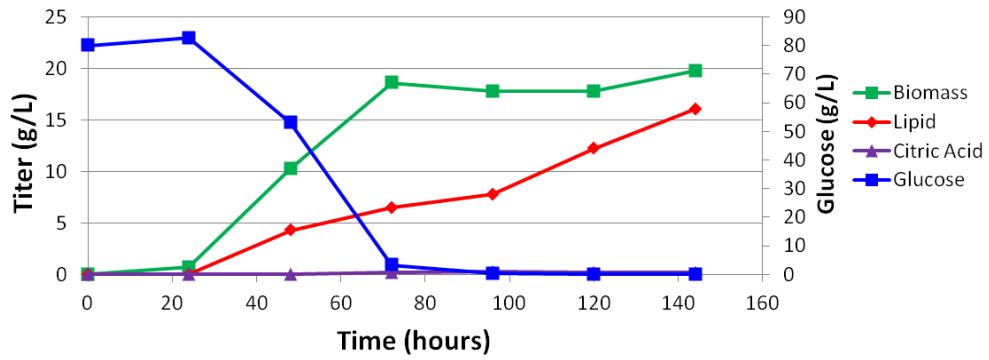


Figure 4.3b
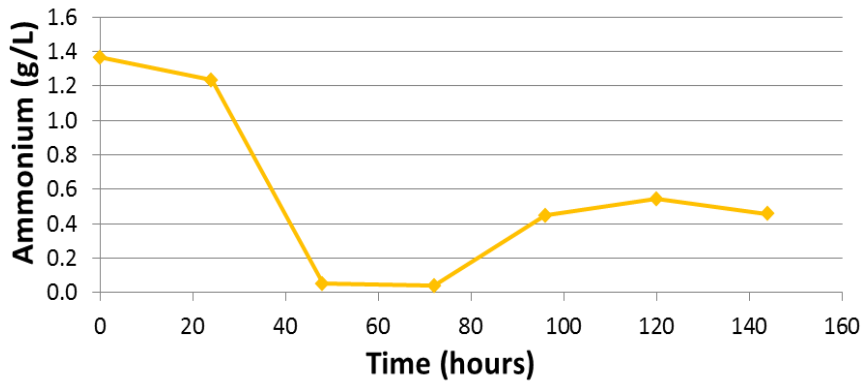
Figure 4.3 cont.

Figure 4.3c



Figure 4.3d

Figure 4.3 cont.

Figure 4.3e

Figure 4.3 cont.

Time courses of the 1.5L scale batch fermentation of the *pex10 mfe1* leucine[+] uracil[+] DGA1 (**A**,**B**) and POlf leucine[+] uracil[+](**C**,**D**) strains in 80 g/L glucose, 6.7 g/L YNB (no amino acids, 1.365 g/L ammonium) are shown, including production of biomass, lipids, and citric acid (left axis **a,c**), consumption of glucose (right axis **a,c**), and ammonium level (**B,D**).  (**A**)  During the *pex10 mfe1* leucine[+] uracil[+] DGA1 fermentation, negligible citric acid was produced, and lipid product accumulated during and after biomass production phases.  This fermentation was run three times in identical conditions, reaching final yields of 15.25 g/L lipids and 20.3 g/L biomass (75% lipid content), 14.96 g/L lipids and 20.6 g/L biomass (73% lipid content), and 16.9 g/L lipids and 19.21 g/L biomass (88% lipid content).  Most time points show average values from the former Figure 4.3 cont.

two fermentations (75% and 73% final lipid content), while endpoints represent averages from all three final values.  Error bars represent standard deviations of these technical replicates.  Glucose and ammonium substrate were fully consumed after 72 hours, but surprisingly, (**B**) ammonium level was replenished to a steady state level of ~0.5 g/L, almost 40% of the original starting level.  (**C**) During the POlf leucine[+] uracil[+] fermentation, citric acid accumulated to more than 14 g/L after 72 hours before quickly reducing to 4 g/L.  Lipid production did not trend with biomass production, reaching a final yield of only 3 g/L lipids, compared to 30 g/L biomass, and glucose was again consumed within 72 hours.  (**D**) Ammonium was fully consumed after 72 hours with no replenishment as observed in the mutant strain. (E) Ammonium is fully utilized by both the *pex10 mfe1* leucine[+] uracil[+] DGA1 and POlf leucine[+] uracil[+] strains after 72 hours of bioreactor batch fermentation.  However, during *pex10 mfe1* leucine[+] uracil[+] DGA1 fermentation, ammonium levels are replenished.  We tested if this could be a result of intracellular protein degradation, by analyzing protein content before, during, and after this dip in ammonium concentration.  However, protein concentration decreases in both *pex10 mfe1* leucine[+] uracil^{+} DGA1 cells and in POlf leucine[+] uracil^{+} cells.  Thus, the metabolic shift to sustain steady state nitrogen levels observed in *pex10 mfe1* leucine[+] uracil[+] DGA1 fermentation is not solely the result of protein degradation.  This experiment was conducted with individual samples.

## 4.3.4 High lipogenesis with alternative carbon sources

We further tested this engineered strain on alternative carbon sources to assay for carbon-source independent lipogenesis. We observed that the *pex10 mfe1* leucine$^+$ uracil$^+$ DGA1 overexpression strain exhibited superior production in nearly all carbon sources, establishing these lipogenesis targets as essential in rewiring this organism into an oleochemical platform strain (**Figure 4.4**).

Figure 4.4 Lipid accumulation on alternative carbon sources
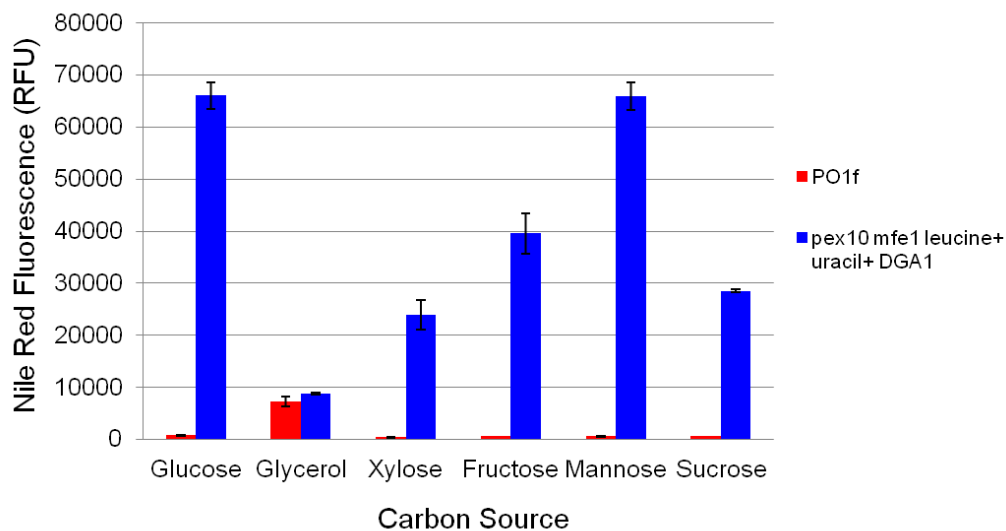


The pex10 mfe1 leucine+ uracil+ DGA1 strain effectively generates high lipid content in a carbon-source independent manner. Error bars represent standard deviations of biological triplicates.

## 4.3.5 Lipid analysis and conversion into soybean-like biodiesel

We analyzed lipid content with GC and saw predominantly C16:0, C16:1, C18:0, C18:1, and C18:2 fatty acids (very similar to soybean), making these lipid reserves ideal feedstock for biodiesel synthesis (**Figure 4.5a**) (132).  Moreover, we observed 127 mg/L accumulation of C17 fatty acids, a very rare metabolite in cells (**Figure 4.5b**).  We hypothesize that extremely active lipogenesis enables less favored odd chained synthesis and such high titers permit detection and characterization.  Finally, a standard methanol transesterification reaction with bioreactor-extracted lipids demonstrated *de novo* biodiesel production (**Figure 4.5c**).  Thus, the microbial production of high lipids in this host can facilitate a renewable biodiesel production process with profiles similar to conventional plant-derived oils.

Figure 4.5 Fatty acid profile characterization and biodiesel conversion

Figure 4.5a
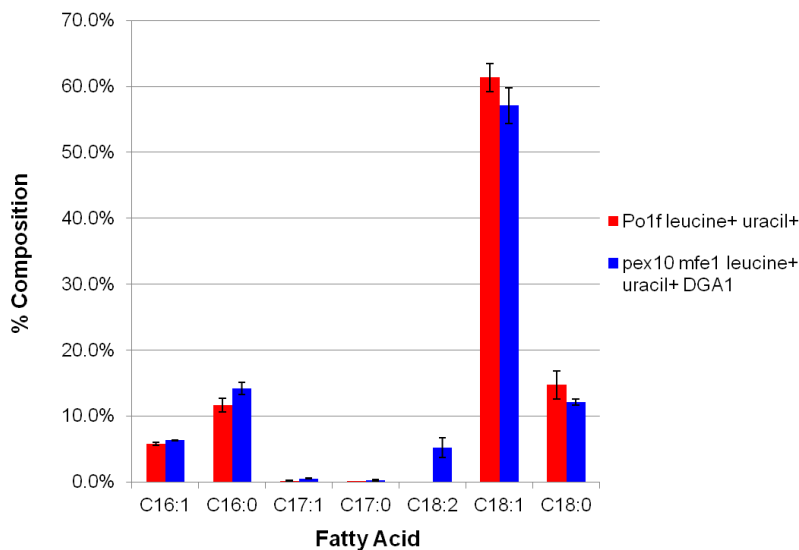
Figure 4.5 cont.

Figure 4.5b
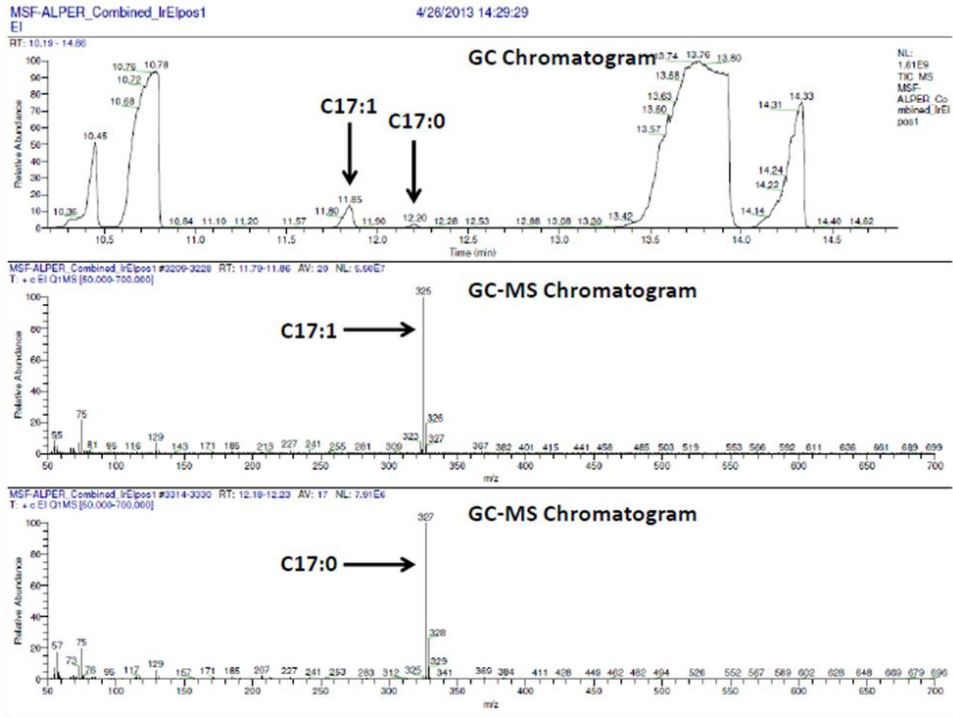


Figure 4.5c

Figure 4.5 cont.

(**A**) Fatty acid profiles of lipid extract from *pex10 mfe1* leucine$^+$ uracil$^+$ DGA1 and POlf leucine$^+$ uracil$^+$ strains after six day bioreactor batch fermentations are shown. We observed predominantly C16 and C18 fatty acid content, as expected, with a noticeable amount of C17 accumulation. We observed C18:2 (linoleic acid) accumulation in the *pex10 mfe1* leucine$^+$ uracil$^+$ DGA1 but not in the POlf leucine$^+$ uracil$^+$ control. Error bars represent standard deviations of technical triplicates. (**B**) GC-MS analysis of *pex10 mfe1* leucine$^+$ DGA1 lipid content. Lipid extract from the *pex10 mfe1* leucine$^+$ DGA1 strain was analyzed with GC (top panel) and MS (bottom two panels). Coinciding with the C17:0 standard retention time, C17:0 was present between 12.16-12.23, and MS analysis showed the expected mass of 327 m/z (bottom panel). C17:1 was present on the GC between 11.79 and 11.86, and analysis with MS (middle panel) revealed the expected mass of 325 m/z, which corresponds to C17:0 losing two hydrogen atoms as it is unsaturated to C17:1. (**C**) Image of transesterified lipid content (FAMEs/biodiesel). Lipid content from *pex10 mfe1* leucine$^+$ uracil$^+$ DGA1 cells fermented in a bioreactor was transesterified with methanol to form FAMEs (biodiesel). Shown is a picture of ~1500 μL sample of biodiesel in a 15 mL Falcon tube against a white backdrop.

### 4.5.6 Probing the link between leucine and lipogenesis

Finally, we sought to explain the lipogenic benefit bestowed by leucine biosynthetic capacity by comparing leucine supplementation to genetic complementation. Leucine supplementation mimicked genotypic complementation in leucine$^-$ strains but did not affect leucine$^+$ backgrounds (**Figure 4.6a,b**). Isoleucine supplementation had no effect, insuring that this leucine-mediated response was not a result of amino acid catabolism (**Figure 4.6a,b**). Leucine supplementation or genetic complementation enabled a pronounced alteration in steady state nitrogen concentration that correlated with lipogenesis in small scale cultivations (**Figure 4.6c,d**). These results implicated leucine as an intracellular trigger to stimulate lipogenesis while regulating nitrogen availability. In this regard, the yeast and mammalian TOR complexes (TORC1) promote cell anabolic processes, such as growth, proliferation, and protein synthesis, in response to amino acid availability and growth factor stimuli (133-134). The leucyl-tRNA synthetase has recently been implicated as an intracellular sensor of amino acid availability for the TORC1, providing a potential link between leucine stimulation and lipogenesis (135-136). To probe this interaction further, we inhibited *Y. lipolytica* TOR kinase activity with rapamycin, revealing a complex TOR-regulated lipogenic phenotype, in which leucine stimulation and TOR inhibition coupled to facilitate lipogenesis in low lipid production backgrounds but reduced lipogenesis in high production strains (**Figure 4.6e**). Thus, we demonstrated here that leucine-mediated lipogenic induction is affected by TOR regulation.

Figure 4.6 Leucine supplementation recovers leucine+ phenotype
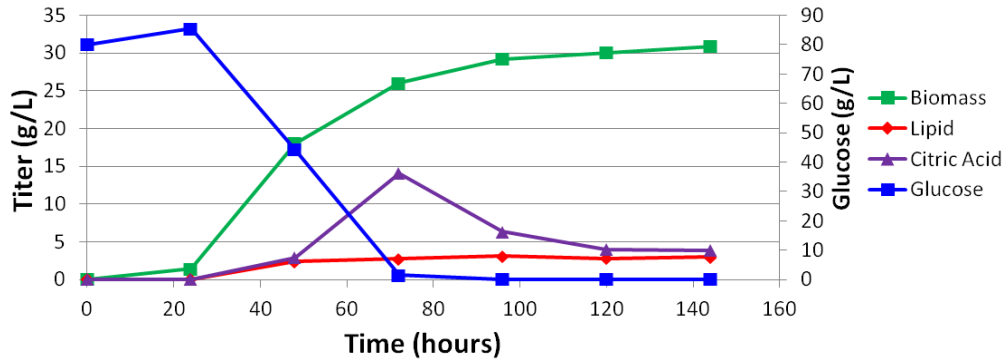
Figure 4.6a
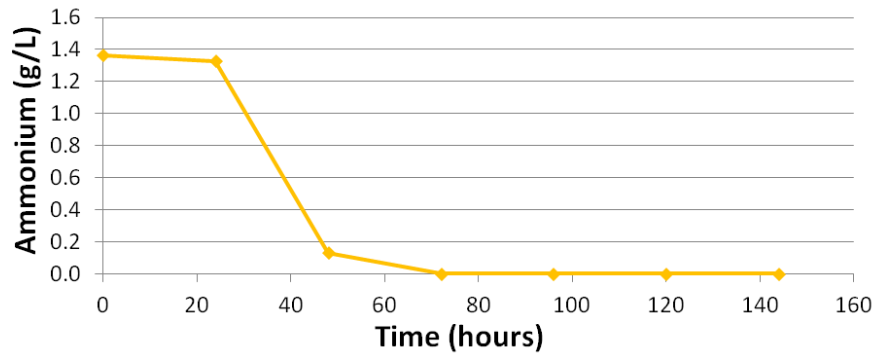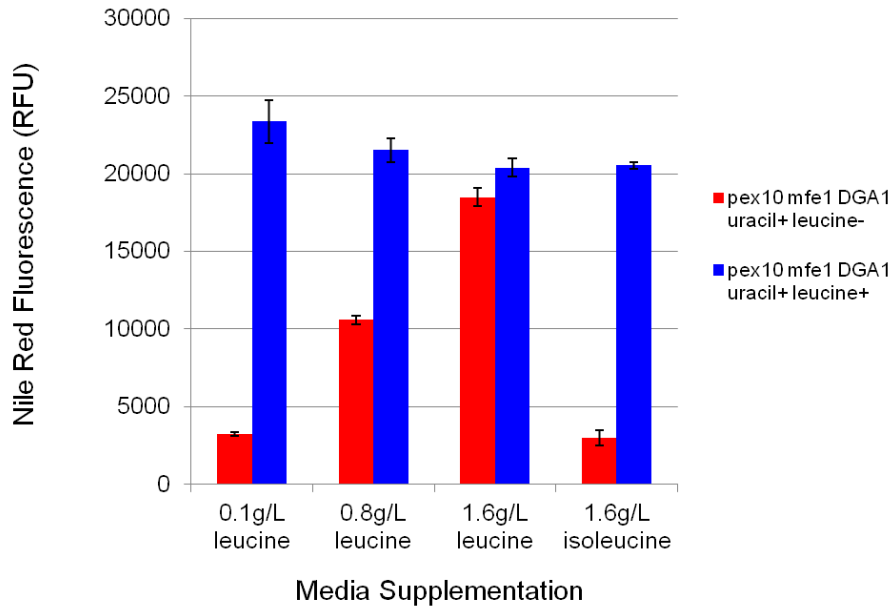


Figure 4.6b
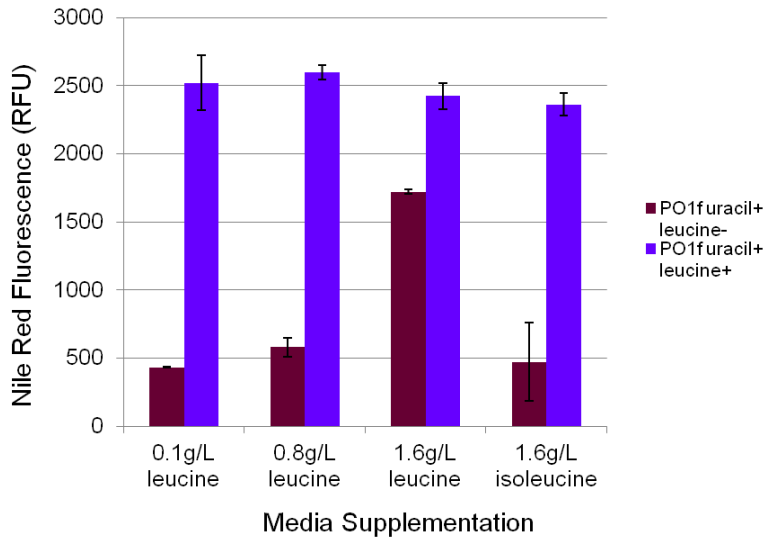
Figure 4.6 cont.
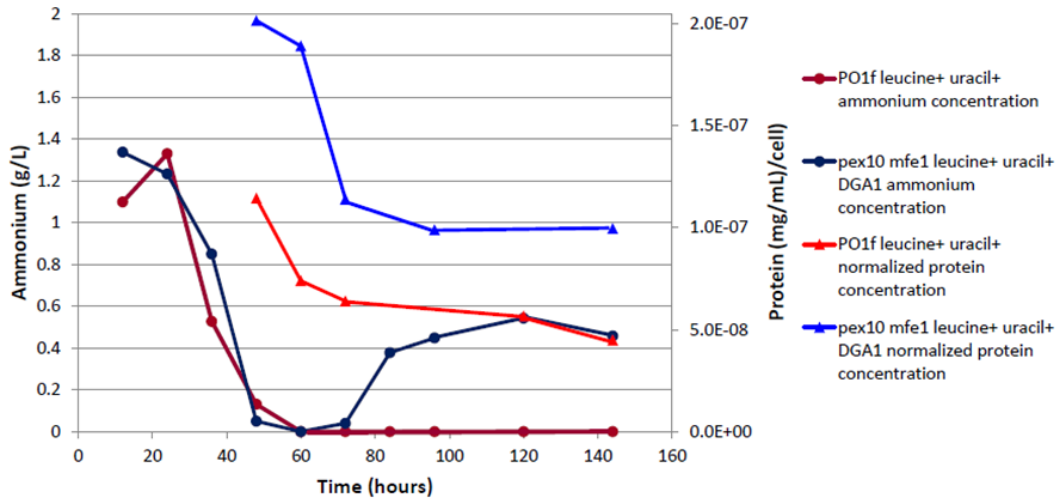
Figure 4.6c
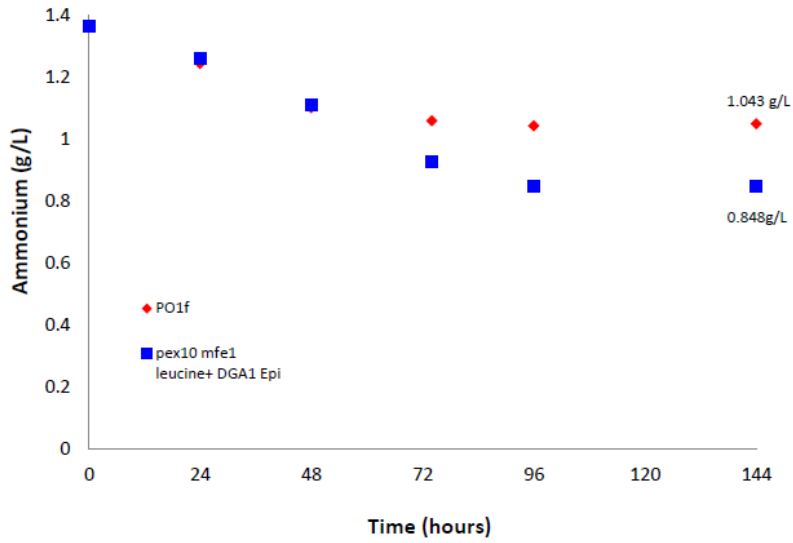


Figure 4.6d
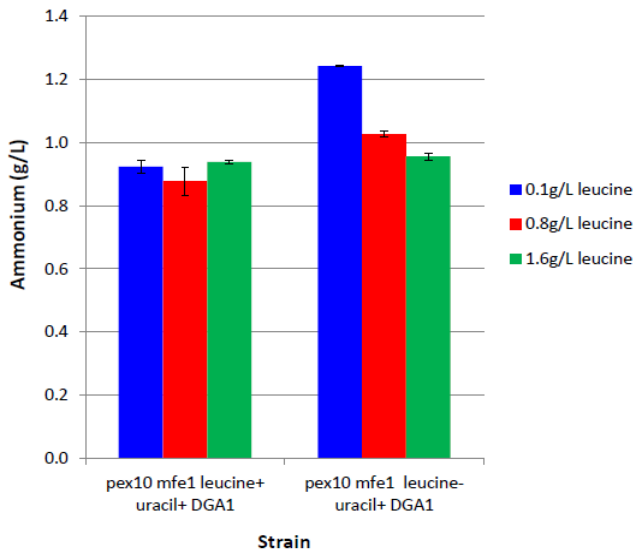
Figure 4.6 cont.

Figure 4.6e
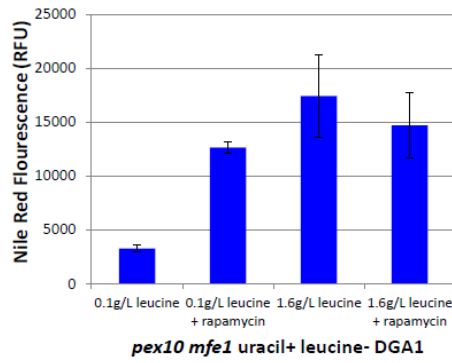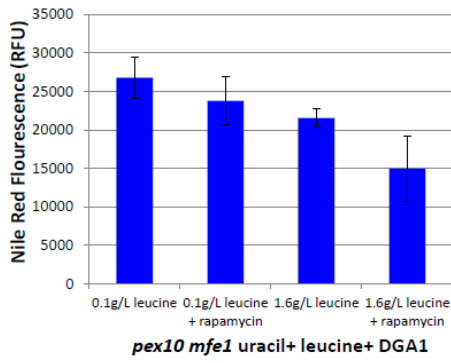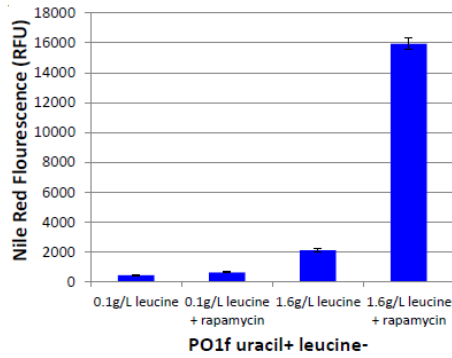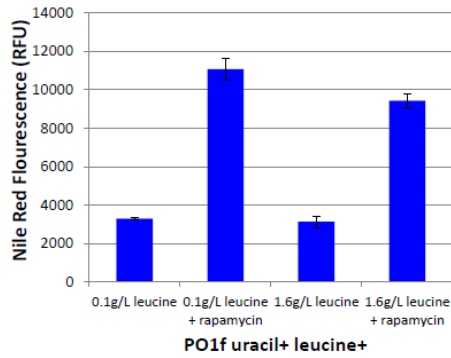
Figure 4.6 cont.

The ability of leucine or isoleucine supplementation to complement the leucine$^+$ phenotype in the **(A)** *pex10 mfe1* leucine$^-$ uracil$^+$ DGA1 and the **(B)** PO1f leucine$^-$ uracil$^+$ backgrounds was tested. 1.6 g/L leucine supplementation complemented the leucine$^+$ phenotype in both the *pex10 mfe1* leucine$^-$ uracil$^+$ DGA1 and the PO1f leucine$^-$ uracil$^+$ backgrounds. Leucine supplementation had no effect on the *pex10 mfe1* leucine$^+$ uracil$^+$ DGA1 background or the PO1f leucine$^+$ uracil$^+$ backgrounds, demonstrating the leucine biosynthetic capacity generates enough leucine to stimulate lipogenesis. Isoleucine had no effect on lipogenesis in either the leucine$^+$ or leucine$^-$ backgrounds. Thus, the benefit of leucine towards lipogenesis is not a result of leucine catabolism for carbon and nitrogen use. Error bars represent standard deviations of biological triplicates. **(C)** The steady state ammonium concentration of PO1f and *pex10 mfe1* leucine$^+$ DGA1 Epi strains were measured during cultivations in 30 mL media containing 80 g/L glucose, 6.7 g/L Yeast Nitrogen Base w/o amino acids (1.365 g/L ammonium), and 0.79 g/L CSM supplement. The engineered *pex10 mfe1* leucine$^+$ DGA1 Epi strain maintains a lower steady state ammonium concentration than the unmodified POlf low lipid production strain. This experiment was conducted with individual samples. **(D)** In addition to effecting higher lipogenesis, leucine biosynthetic capacity results in lower ammonium levels in the *pex10 mfe1* leucine$^+$ uracil$^+$ DGA1 strain than in the *pex10 mfe1* leucine$^-$ uracil$^+$ DGA1 strain. Once again, leucine supplementation of the leucine$^-$ strain complements the phenotype observed in the leucine$^+$ by reducing ammonium levels. Leucine supplementation has no effect on ammonium levels for the leucine$^+$ strain. Thus, leucine biosynthetic capacity, lipogenesis, and nitrogen availability are linked in high lipid accumulating strains of *Y. lipolytica*. Error bars represent standard deviations of biological triplicates. **(E)** 2 μg mL$^{-1}$ rapamycin was used to inhibit *Y. lipolytica* TOR activity. Coupling TOR inhibition with leucine biosynthetic capacity stimulates lipogenesis in the low lipid accumulating PO1f leucine$^+$ background. As this strain has leucine biosynthetic capability, it is unaffected by leucine supplementation. TOR inhibition and leucine supplementation are necessary to induce lipogenesis in the PO1f leucine$^-$ background. Thus, TOR inhibition coupled with leucine-mediated signaling enables high lipogenesis in low accumulation backgrounds. TOR inhibition tends to decrease lipogenesis in the lipogenic *pex10 mfe1* uracil$^+$ DGA1 background, except when leucine biosynthetic capacity and supplementation are absent: TOR inhibition can increase lipogenesis in this instance. Error bars represent standard deviations of biological triplicates.

**4.4 Discussion and conclusion**

Lipogenic organisms offer ideal platforms for biodiesel and oleo-chemical synthesis. To this effect, we rewired *Y. lipolytica's* native metabolism via a combinatorial multiplexing to effect superior *de novo* lipid accumulation. Our analyses revealed that high lipogenesis can be un-coupled from nitrogen starvation, is dependent on leucine-mediated signaling and absolute environmental carbon content, and is adversely affected by citric acid and nitrogen cycling. For the majority of our moderate or highly lipogenic strains, optimal lipid accumulation was enabled in nitrogen-permissive, high carbon conditions. In contrast, low performing strains were optimally induced by low carbon levels, indicating central carbon metabolisms ill-equipped to utilize energy-dense media formulations. Thus, genomic rewiring quickly eliminates the requirement of induction through nitrogen starvation and necessitates a re-optimization of environmental stimulus after each metabolic perturbation. During bioreactor fermentation, a lowly lipogenic strain diverted excess carbon to production of extracellular citric acid before assimilation into biomass (simultaneously utilizing nitrogen derived from protein degradation). In contrast, a highly lipogenic strain avoided citric acid accumulation and prevented incorporation of nitrogen into biomass. In this manner, our final engineered strain mentioned in this chapter maintained nitrogen levels optimal for high lipogenesis and prevented extracellular carbon flux, promoting easier lipid accumulation.

The work from this chapter reports the novel link between leucine signaling and lipogenesis in *Y. lipolytica*. Specifically, we contrasted the effects of leucine and isoleucine supplementation on lipogenesis and demonstrated that only leucine acts to promote lipogenesis. As *Y. lipolytica* possesses degradation pathways for both leucine and isoleucine to acetyl-CoA fatty acid precursors (66, 121-122), leucine must act as an intracellular signal to permit lipid production, rather than as a carbon source. This is further established by the leucine-dependent TOR-inhibition phenotype of the PO1f leucine$^-$ uracil$^+$ and PO1f leucine$^+$ uracil$^+$ strains. Thus, a complex signaling scheme is implicated for high lipid titers in this organism.

In summary, we conducted the largest rewiring of an oleaginous organism, and successfully engineered and enhanced *de novo* lipid accumulation in *Y. lipolytica* by more than 60 fold comparing to the starting strain. In doing so, we identified several unique features of lipogenesis, demonstrated that lipid accumulation approaching 90% of cell mass is possible, determined dominant genotype- phenotype dependencies, decoupled lipogenesis and nitrogen starvation, illustrated carbon-source independence, and demonstrated the feasible conversion of these lipids into FAMEs. We further presented evidence that two central tenets of lipogenesis, the necessity for nitrogen starvation and citric acid cycling, are not universal. The work presented in this chapter reports a high lipid titers to date at 25 g/L and it can be used as starting point for further evolutionary metabolic engineering as described in the next chapter (Chapter 5).

# Chapter 5: Evolutionary metabolic engineering for high lipid production in *Yarrowia lipolytica*

## 5.1 Chapter summary

Through rational metabolic engineering efforts described in Chapter 4, lipogenesis titers in *Yarrowia lipolytica* were significantly enhanced. However, the improvement still suffered from decreased biomass generation rates. Here, we attempted to employ a rapid evolutionary metabolic engineering approach linked with a floating cell enrichment process to improve lipogenesis rates, titers, and yields. Through this iterative process, we were able to ultimately improve yields from our prior strain by over 60% to achieve production titers of 40.5 g/L with upwards of 79% of the theoretical maximum yield of conversation. Isolated cells were saturated with up to 89% lipid content. An average specific productivity of 0.55 g/L/h was achieved with a maximum instantaneous specific productivity of 0.86 g/L/h during the fermentation. Genomic sequencing of the evolved strains revealed a link between a decrease/loss of function mutation of succinate semialdehyde dehydrogenase, uga2, suggesting the importance of gamma-aminobutyric acid assimilation in lipogenesis. This linkage was validated through gene deletion experiments. This chapter presents an improved host strain that can serve as a platform for efficient oleochemical production.

## 5.2 Introduction

Metabolic engineering of a highly oleaginous strain of *Y. lipolytica* capable of producing titers exceeding 25 g/L in bioreactors has been achieved as described in Chapter 4. Nevertheless, even in this organism, improvements in all metrics (productivities, titers, and yields) are essential to make microbial production of chemicals, and especially commodity chemicals and biofuels, economically viable. Thus, here, we take an evolutionary approach to further improve lipogenesis rates.

One particular challenge of rational metabolic engineering is the competition between product titers and yields (137). To this end, improved lipid production is usually accompanied by a decrease in cell growth (138). Specific for engineering lipogenesis in *Y. lipolytica*, rational approaches have mainly produced strains with increased lipid production at the cost of decreased biomass production (23, 139) . Thus, a more balanced evolutionary approach may access a middle ground for these two competing factors.

Evolutionary metabolic engineering of bio-based production of oils and lipids is challenging due to the lack of developed enrichment and selection schemes. Prior work has coupled random mutagenesis with anti-metabolites such as cerulenin screening to evolve oleaginous yeast *Lipomyces starkeyi* (140). However, the improvement was rather limited probably due to the lack of full enrichment and the high specificity of cerulenin screening. An alternative strategy based on physiology has been employed in the case of identifying high lipid containing mutants from a transposon library of *S. cerevisiae* whereby a gradient centrifugation selection step was used (141).  However, these

approaches can be quite sensitive to conditions of the selection, yet demonstrate the potential for an evolutionary approach.

Here, we designed and performed a simple, evolutionary metabolic engineering approach for improving lipogenesis in a pre-engineered starting strain using random mutagenesis and an observed buoyancy property of lipid-filled cells. Specifically, by repeating the process of error generation and floating-based selection, we were able to ultimately improve yields from our prior strain by over 60% to achieve production titers of 40.5 g/L with upwards of 79% of the theoretical maximum yield of conversation and average specific productivities reaching 0.55 g/L/h with a maximum instantaneous productivity of 0.86 g/L/h. More importantly, these improvements simultaneously increase both biomass and titer. Whole genome sequencing reveals a novel lipid production enhancer (*uga2*) and provides important insight into the relationship between glutamate degradation and lipogenesis. Thus, this chapter presents a metabolically evolved, novel platform with substantial lipogenesis potential.

## 5.3 Results

### 5.3.1 High-lipid content cells can be identified via floating cells

By coupling combinatorial multiplexing of lipogenesis targets with phenotypic induction, we successfully rewired *Y. lipolytica*'s native metabolism for high *de novo* lipogenesis through the identification of three dominant genetic targets – *pex10* deletion, DGA1 overexpression and restoration of a complete leucine biosynthetic pathway

(leucine$^+$ phenotype) and created an engineered strain PO1f *pex10 mfe1* leucine$^+$ uracil$^+$ DGA1 with production titer exceeding 25 g/L in bioreactor [139]. During these engineering efforts, we successfully identified a subpopulation of cells with extremely high buoyancy property: these cells can float on top of the medium once the culture settled while normal cells would settle down to the bottom of the tube (**Figure 5.1**). At times, this "floating" subpopulation can even survive conditions of mild centrifugation (e.g. 100 x g). We then examined the lipid bodies inside both cell populations using fluorescence microscopy with Nile Red staining (a dye straining lipid bodies showing yellow-green fluorescence when excited with blue light [125]) and observed that the floating cells were full of lipids whereas cells that settled were not (**Figure 5.1,** this strain is further characterized in Chapter 6). Thus, we concluded that higher lipid containing cells would possess a higher buoyancy property and can be separated based on this "floating" phenotype. Here, we sought to utilize this observation as a method to isolate cells with high lipid content cells by coupling this floating selection with random mutagenesis and evolutionary engineering.

Figure 5.1 High-lipid content cells can be identified via floating cells
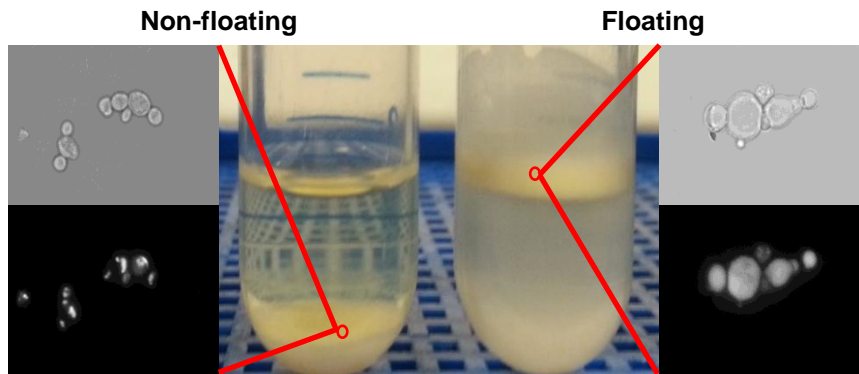


A non-floating strain (left) and culture with a floating subpopulation strain (right) was cultured in high glucose media and then allowed to settled for 4 hours in room temperature in culture tubes to demonstrate the observed floating cell phenotype. Representative fluorescence microscopic pictures show lower lipids content inside the cells staining with Nile Red from the non-floating population (left bottom) than from the floating subpopulation (right top).

## 5.3.2 Random mutagenesis linked with floating cell transfer can identify improved

## lipogenesis traits

Based on the observations described above, we opted to invoke an iterative, evolutionary metabolic engineering approach using our prior engineered strain of *Y. lipolytica* PO1f *pex10 mfe1* leucine[+] uracil[+] DGA1 (Chapter 4) as a starting point. Overall, this process consists of generating a random mutagenesis library using Ethyl methanesulfonate (EMS), enriching for mutants with higher lipid content by sequentially transferring the floating cells, screening individual colonies on Nile Red plates, and finally testing for lipid content and cell growth (**Figure 5.2**). The best lipid producer was tested in a bioreactor to evaluate the overall lipid production performance and was

characterized with whole genome sequencing to identify the causative mutations leading to the enhanced lipogenesis genotype. Moreover, this process can be iterated to further evolve the strain toward an optimal lipogenesis phenotype (**Figure 5.2**). Following this process, early stationary phase cells (our previously engineered strain, PO1f *pex10 mfe1* leucine$^+$ uracil$^+$ DGA1) were first treated with EMS to generate mutations resulting in a library size of approximately $10^8$ cells (142). A sample not treated with EMS was used as a control for this experiment to evaluate the impact of spontaneous mutations during the selection process. Next, the floating subpopulation in this library was subjected to serial transfer in culture tubes for five rounds after which the culture was plated for screening using Nile Red plates to isolated individual colonies with high lipogenesis potential. In total, 31 colonies from the EMS library (named E1 to E31), and 5 colonies from the non-EMS treated control were selected from the plates based on high visual fluorescence. These colonies were then cultured along with the engineered strain at the test tube level to further characterize lipid accumulation level by using the metric of Mean Nile Red fluorescence*OD600 as a reference for lipid production performance and a means of rank-ordering the mutants (**Figure 5.3a**). All of the selected strains exhibited a clear improvement over the engineered strain. Moreover, while spontaneous mutagenesis through the serial transfer process could lead to enhanced lipogenesis, mutation generation was beneficial for the isolation of higher performing strains. Next, we selected the top two strains (E13 and E26, **Figure 5.3a**) as they both exhibited a nearly 3.5 fold-increase over the engineered strain. These two mutants showed both an increase of around 60% improvement based on absolute Nile Red staining (**Figure 5.3b**)

85

as well as an over 60% increase in the final OD600 (cell growth).  Whole genome

sequencing (described in 5.3.5) revealed that these two mutant strains were highly similar

genetically, thus we selected E26 for further characterization.  The fluorescence

micrograph of the E26 mutant clearly illustrated the enhanced lipogenesis with this strain

when compared to the parental, engineering strain (**Figure 5.3c**).  Specifically, the empty

edge without lipid in the engineered stain disappeared in the E26 strain and was engulfed

with lipid instead.

Figure 5.2 Overall schematic for the iterative, evolutionary metabolic engineering approach used to enhance lipogenesis in *Yarrowia lipolytica*
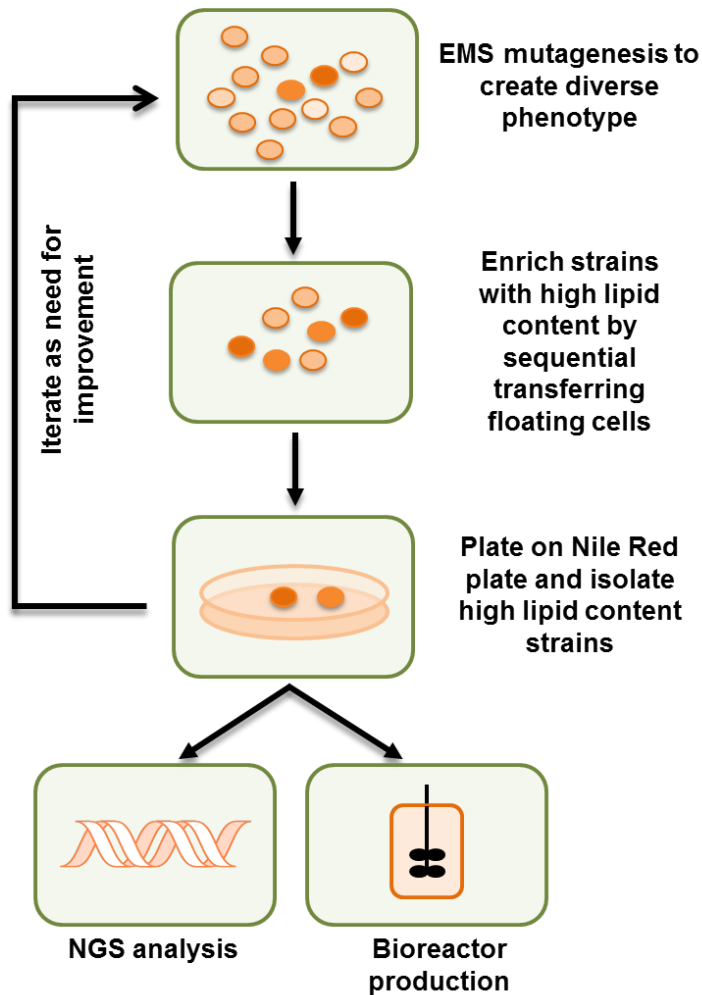


High lipid producing strains were created through first inducing random mutations by EMS, using serial transfer of floating cells, screening colonies on Nile Red plates, and characterizing resulting mutants through both whole genome sequencing and bioreactor production.

### 5.3.3 High lipid production through bioreactor fermentation with E26

To more accurately quantify the improvement achieved through this evolutionary

metabolic engineering approach, we cultivated the E26 strain in an inexpensive minimal

media formulation consisting of only glucose (160 g/L), ammonium sulphate (10 g/L) and yeast nitrogen base while controlling pH, temperature and dissolved oxygen levels at set points we previously found optimal (**Figure 5.3d**). In our previous efforts described in Chapter 4, the engineered strain produced 25.2 g/L lipid with an average productivity of 0.21g/L/h under these condition. After the evolutionary engineering, the E26 strain derived from this engineered host exhibited a significantly improved lipid titer reaching 40.5 g/L with cells containing 89% lipid cellular content (**Table 5.1**). This value represents the highest reported titer of lipid to the date. Moreover, this represents a 61% increase in titer over the engineered strain. This strain achieved 79% of the theoretical stoichiometric yield and had an average specific productivity approaching 0.51 g/L/h (a 2.5-fold increase over the engineered strain). The increased lipid titer was the combined effect of both increase cellular lipid content as well as a higher overall biomass. For the parental, engineered strain, the main period of lipogenesis occurred in the later parts of fermentation (through 144 hours) after glucose depletion and biomass formation (139). In contrast, for the evolved E26 strain, lipogenesis occurred during the biomass accumulation stage and was completed within 96 hours. Thus, the evolved strain's metabolic processes are in clear contrast to the parental, engineered strain and presented improvements in rate, titer, and yield.

Figure 5.3 Random mutagenesis linked with floating cell transfer can identify improved lipogenesis strains.

Figure 5.3a



Figure 5.3b
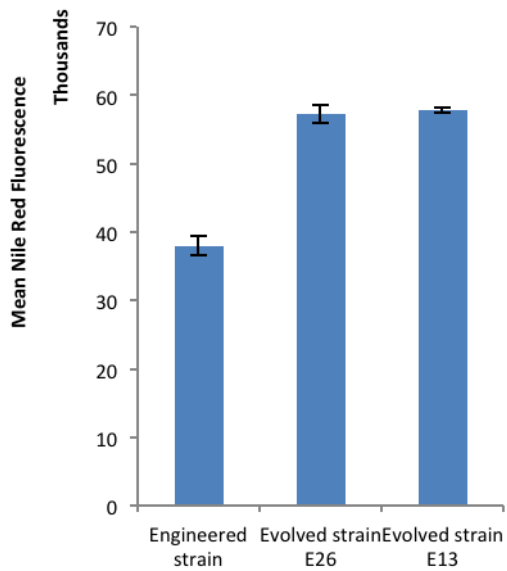
Figure 5.3 cont.

Figure 5.3c



Engineered strain

E26 strain
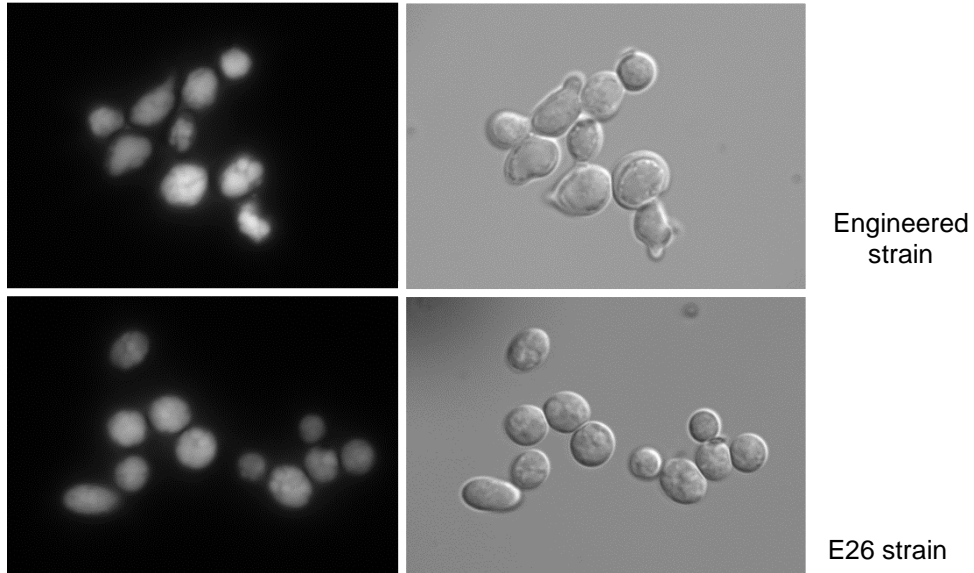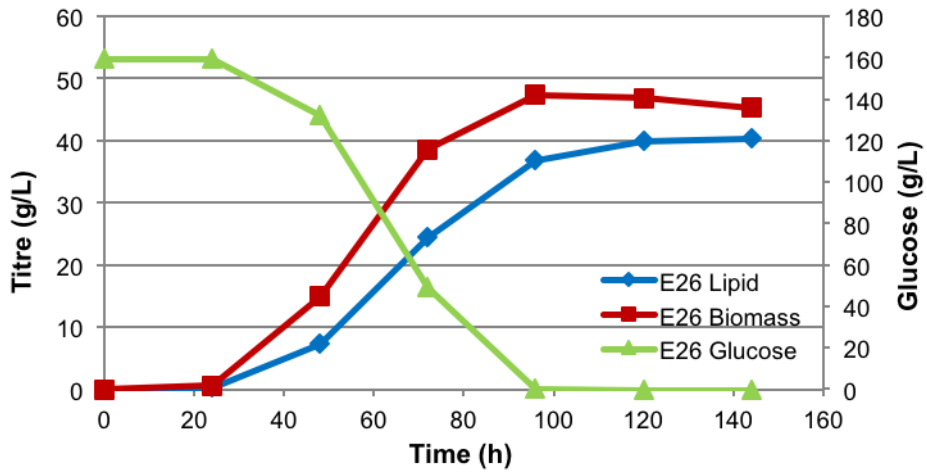
Figure 5.3d

Figre 5.3 cont.

(**A**) Comparison of lipid production using engineered strain (green), non-EMS evolved strain (light blue), and EMS evolved strain (dark blue) using Mean Nile Red fluorescence*OD600 as ranking metric.  Selected strains E13 and E26 are highlighted by a red circle.  (**B**) Enhanced lipogenesis among the isolated evolved strains E13 and E26 were characterized using flow cytometry and compared with the parental, engineered strain.  (**C**) Comparison of lipids stained with Nile Red between the engineered strain and evolved E26 strain using fluorescence microscopy. (**D**) Batch bioreactor fermentation profile of the E26 strain for lipid production.

Table 5.1 Bioreactor metrics with E26 and E26E1 strains

|  | Titer | Biomass | Average specific productivity | Overall yield | Lipid content |
|---|---|---|---|---|---|
| Engineered strain | 25.3 g/L | 35.0 g/L | 0.21 g/L/h | 0.158 g/g | 71% |
| E26 strain | 40.5 g/L | 45.3 g/L | 0.51 g/L/h | 0.253 g/g | 89% |
| E26E1 strain | 40.4 g/L | 47.3 g/L | 0.55 g/L/h | 0.253 g/g | 85% |

Performance metrics for lipid production in batch bioreactor fermentation with the engineered strain (Chapter 4), E26 strain and E26E1 strain.

## 5.3.4 Assemble and analysis of draft genome of PO1f

To enable the SNP analysis described in 5.3.5, we first sequenced and analyzed the genome from control strain PO1f. Although a high quality genome sequence of *Y. lipolytica* strain CLIB122 (E150) has been available (65), this strain is not the most popular for metabolic engineering applications. Specifically, *Y. lipolytica* strain W29 (CLIB 89) and its derivatives such as PO1f  have been more widely used, especially in metabolic engineering studies for value-added chemical production (23, 76, 117, 139, 143-144), therapeutic protein production (145-146) and fundamental microbiology studies (55, 147-148).  As one of the parental strains of the French inbred lines, the wild-type haploid strain, W29, was originally isolated from sewage material (118). A preliminary sequencing effort was conducted with only 4.9 Mb  available (149). In the

work here, we assembled a draft genome of PO1f and analyzed the SNPs through its genome using CLIB122 genome as reference.

The genome of *Y. lipolytica* PO1f was sequenced using the illumina HiSeq DNA sequencing platform (PE2X100). The raw sequence data comprises a total of 8,740,022 reads that together provide very high sampling coverage of the genome (43.7-fold coverage). The reads were assembled using Velvet with *k*-mer size of 55 (150). This led to a genome assembly containing 669 contigs (each at length >= 500 bp). The total length of the genome assembly is 20,282,994 bp with N50 equals 58kbp. The reads were also assembled using A5 pipeline (151) and closed gaps with IMAGE (152) to 348 contigs (each at length >=500 bp) and further scaffolded based on genome sequence of strain CLIB122 using ABACAS (153). Total 19,922,824 bp were placed to the final 6 scaffolds. The final *de novo* assembled genome was analyzed to assign open reading frames (ORF) with Augustus (154) trained with *Y. lipolytica* CLIB122 data. A total of 6,420 putative ORFs were identified and 4,096 were annotated with Blast2Go (155). The genome sequences of PO1f and strain CLIB122 are very similar in nature. By mapping the Illumina reads to the CLIB122 genome using BWA (156) and analyzing using Samtools (156) and BEDTools (157), a total of 24,675 single nucleotide variations were called in PO1f genome sequences (QUAL>=30; DP>=10). Moreover, LTR-retrotransposon elements are confirmed being absent in stain PO1f, matching prior information about this strain (149). There is one large deletion in chromosome A with four ORF missing. Two of them are weakly similar to the SMC5/6 complex (YALI0A01562p and YALI0A01602p), which are related to double strand break repairing and homologous

recombination (158). These absences may give rise to differences in homologous recombination efficiencies in this strain.

**5.3.5 Whole genome sequencing revealed enhanced lipogenesis genotype**

To establish a genotype-phenotype linkage in our evolved strains, we performed whole genome sequencing for isolated strains E13 and E26 using an Illumina platform. An average of 65X coverage over the genome was obtained and a single nucleotide polymorphism (SNP) analysis was performed by mapping the sequences to the CLIB122 genome (65) and comparing with SNPs identified from our recent draft genome sequence of the PO1f strain described in 5.3.4. The SNPs identified in both E13 and E26 are highly similar suggesting both successful enrichment of the enhanced lipogenesis subpopulation as well as a co-occurrence of common mutations within this population. After filtering the sequences (QUAL>30), a total of 182 SNPs were identified in E13 and 179 SNPs in E26 with 93 of them in common between the two strains. Using the IGV genome browser (159), a total of 16 SNPs in E13 and 19 SNPs in E26 were determined to be in coding regions. Further analysis taking into account read quality revealed that E13 and E26 shared 9 authentic coding region mutations (**Table 5.2**). Out of these 9 coding regions, three of these ORFs had linkages with lipogenesis, namely YALI0A02354g (YOX1), YALI0E20449g (OSH6) and YALI0F26191g (UGA2). YOX1 encodes for a homeobox transcriptional repressor and has been suggested to bind with leucine tRNA genes in *Y. lipolytica*, which could affect the leucine synthesis regulation (141). OSH6, a member of the oxysterol-binding protein family, is associated with the activity of the TOR (target of rapamycin) complex 1 (160). Both leucine and TOR were demonstrated to

be linked with lipogenesis in our prior engineering efforts (139). Finally, UGA2 encodes for succinate semialdehyde dehydrogenase (SSADH) and participates in the GABA (gamma-aminobutyric acid) assimilation pathway, converting succinate semialdehyde to succinate following 4-aminobutyrate aminotransferase (161). Further analysis and investigation into the non-coding mutations may also be necessary to fully investigate the genotype-phenotype linkage.

Table 5.2 Authentic SNP shared in coding region in genome of E13 and E26 with their annotation

| Chrom | Position | Base changes | | | Annotation |
|---|---|---|---|---|---|
| Yali0A | 297474 | G | A | YALI0A02354g | similar to *S. cerevisiae* OSH6; member of an oxysterol-binding protein family |
| Yali0C | 138994 | T | C | YALI0C01001g | no similarity |
| Yali0C | 139014 | A | G | YALI0C01001g | no similarity |
| Yali0C | 953493 | G | A | YALI0C07150g | similar to *S. cerevisiae* IRC20; E3 ubiquitin ligase and putative helicase |
| Yali0C | 2966661 | C | T | YALI0C22231g | weakly similar to *Schizosaccharomyces pombe* RNA polymerase III Transcription factor (TF)IIIC subunit |
| Yali0C | 3047264 | G | A | YALI0C22726g | no similarity |
| Yali0D | 1576990 | G | A | YALI0D12628g | similar to *Fusarium solani* cutinase transcription factor 1 alpha |
| Yali0E | 2424790 | T | G | YALI0E20449g | weakly similar to *S. cerevisiae* YOX1 |
| Yali0F | 3369592 | C | T | YALI0F26191g | similar to *S. cerevisiae* UGA2 |

SNP analysis in isolated strains. Authentic SNPs shared in coding region in genome of E13 and E26 with their annotation. (All are missense mutations except mutation in YALI0C22231g is a silence mutation)

## 5.3.6 uga2 pro209ser may play a critical role for improving lipid production

As an initial test, we sought to investigate whether individual overexpression of these mutants in the engineered strain background would elicit a dominant lipogenesis

phenotype. To this end, no significant improvements were achieved through these efforts. We were particularly intrigued by the *uga2* mutant as it was functionally related to nitrogen metabolism and relatively well studied (161-162). The identified mutation site in *uga2*, Proline 209 is a highly conserved residue based on sequence alignment using Geneious software (**Figure 5.4a**). Through the use of the i-tasser protein structure prediction server (163) and structural analysis to a homologue (*Synechococcus sp.* succinic semialdehyde dehydrogenase, PDB 3VZ3), Pro209 sits at a starting point of a helix and is in close proximity to a hydrogen bond forming serine that provides critical binding to the cofactor $NADP^+$ (164) (**Figure 5.4b**). Thus, we hypothesized that the mutation from proline to serine could distort the helix, decrease enzyme function, and thus alter the GABA assimilation pathways. To test whether the *uga2* P209S was a reduced function allele, we cultivated the E26 strain and the engineered strain with either GABA or $NH_4^+$ as the sole nitrogen source and tested the ratio of cell densities as a measurement of the GABA assimilation function. E26 showed reduced growth and thus a significant decrease in GABA assimilation (**Figure 5.4c**). To further link *uga2* mutations to increased lipogenesis, we knocked out the UGA2 gene from the engineered strain. This modification improved lipogenesis as measured by an over 30% increase in a Nile Red staining assay (**Figure 5.4d**). Collectively, this data suggests the *uga2* mutation identified from genome sequencing is indeed a beneficial mutation for enhanced lipogenesis.

Figure 5.4 Functional and structural analysis of uga2 as an elicitor of lipogenesis
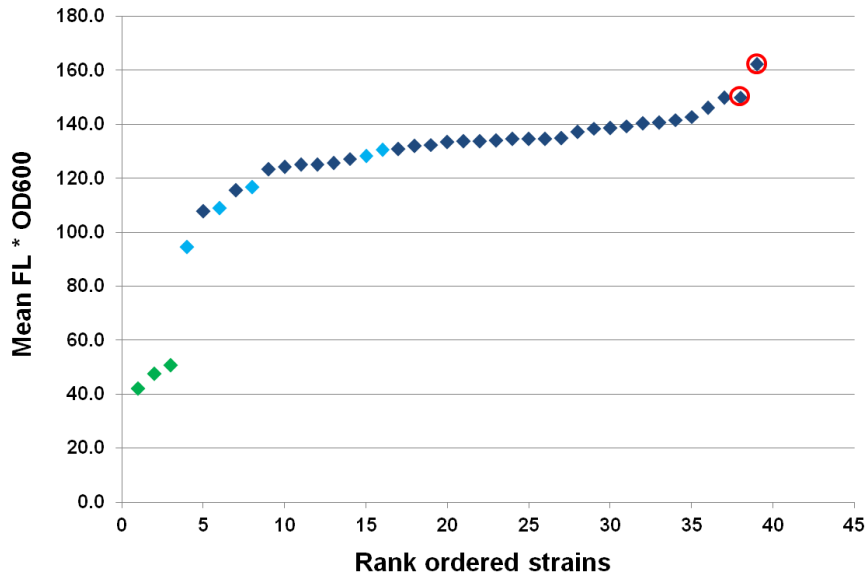
Figure 5.4a
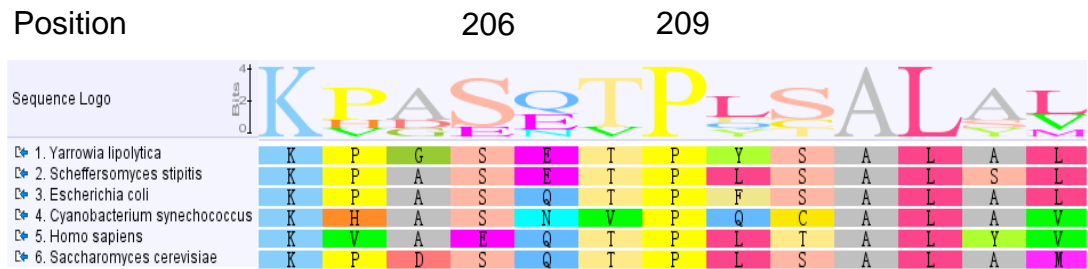


Figure 5.4b
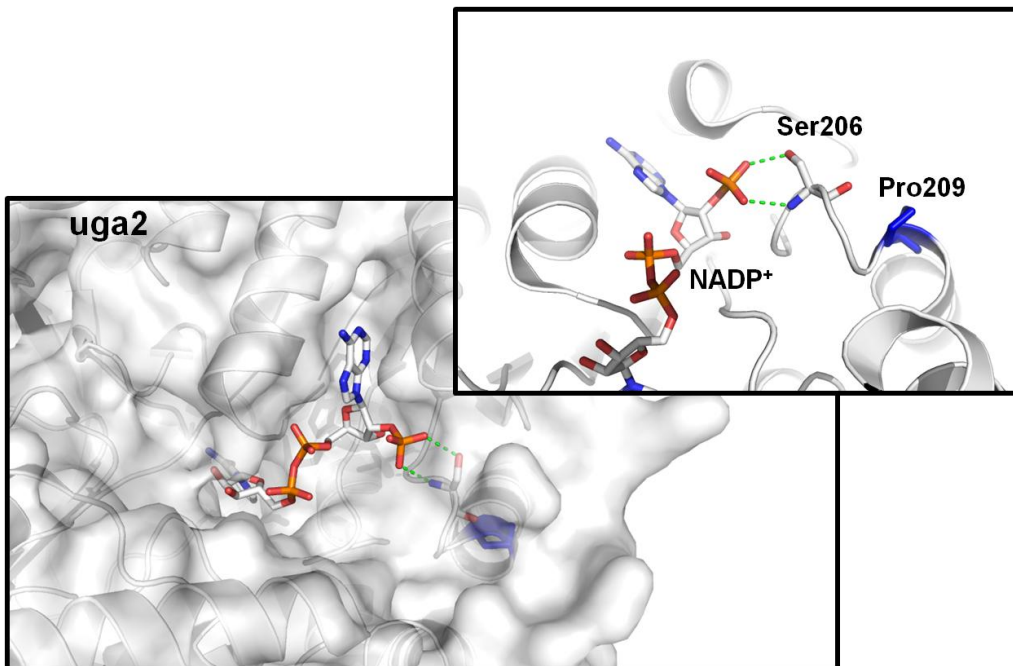
Figure 5.4 cont.

Figure 5.4c
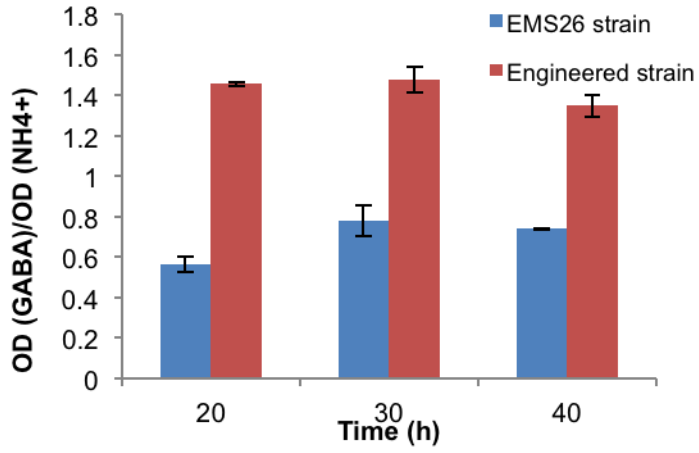


Figure 5.4d
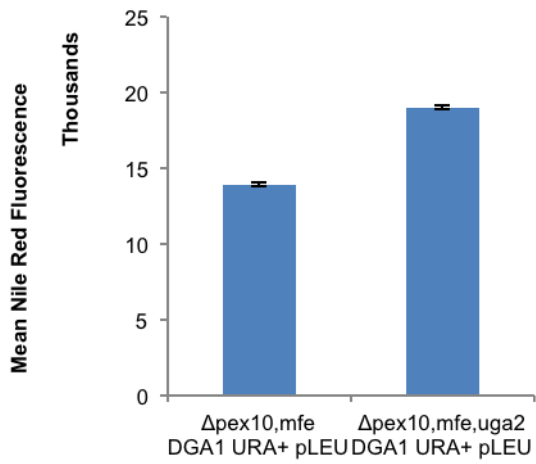
Figure 5.4 cont.

**(A)** Alignment of *Y. lipolytica* uga2 amino acid sequence with different species to demonstrate the conservation of the proline 209 residue. **(B)** Structural illustration of the conserved proline209 residue. The proline 209 is positioned at the starting point of a helix which harbors serine that has a key interaction with co-factor NADP's phosphate residue. Illustration is made using PyMOL. **(C)** Growth of the E26 strain and the engineered strain using GABA or $NH4^+$ as sole nitrogen source. The ratio of OD (GABA) / OD ($NH4^+$) represents the ability of using GABA as sole nitrogen source. **(D)** Evaluation of uga2 deletion on lipogenesis using a Nile Red staining assay.

### 5.3.7 Iterative evolutionary engineering to further improve lipogenesis rates

The first round of evolutionary metabolic engineering produced strains such as E26 that exhibited improved rates, titers, and yields of lipids. Thus, we sought to iterate this process using E26 as the parental strain to further enhance lipogenesis rates. In this round, we opted to carry out the floating selection using flasks instead of culture tubes in hopes of obtaining strains that were better suited for bioreactor conditions. After five rounds of enrichment, screening and selection, we first characterized 34 isolated mutants from this round and chose the top candidate, E26E1, for further testing (**Figure 5.5a**). E26E1 had a 31% increase of our lipid ranking metric (OD600*Nile Red mean fluorescence) compared to the E26 strain and a 97% increase compared to the engineered strain. Visualization of the E26E1 strain using fluorescence microscopy showed fully saturated cells (**Figure 5.5b**). To further evaluate the lipid production performance of E26E1, we cultivated this strain in a bioreactor with the same conditions as for E26 and the engineered strain (**Figure 5.5c**). Overall, E26E1 showed an improved lipogenesis capacity with a titer of 40.4 g/L and an average specific productivity of 0.55 g/L/h (a slight increase over E26). The final lipid content reached 85% with a yield of 0.253 g/g glucose (**Table 5.1**). More interestingly, between 48 and 72 hours of fermentation, the instantaneous specific productivity reached 0.86 g/L/h, a 20% increase over the E26 strain. Thus, this further evolved strain could benefit from fed-batch fermentation operation.

Figure 5.5 Iterative evolutionary engineering can further improve lipogenesis rates

Figure 5.5a



Figure 5.5b



E26E1
strain
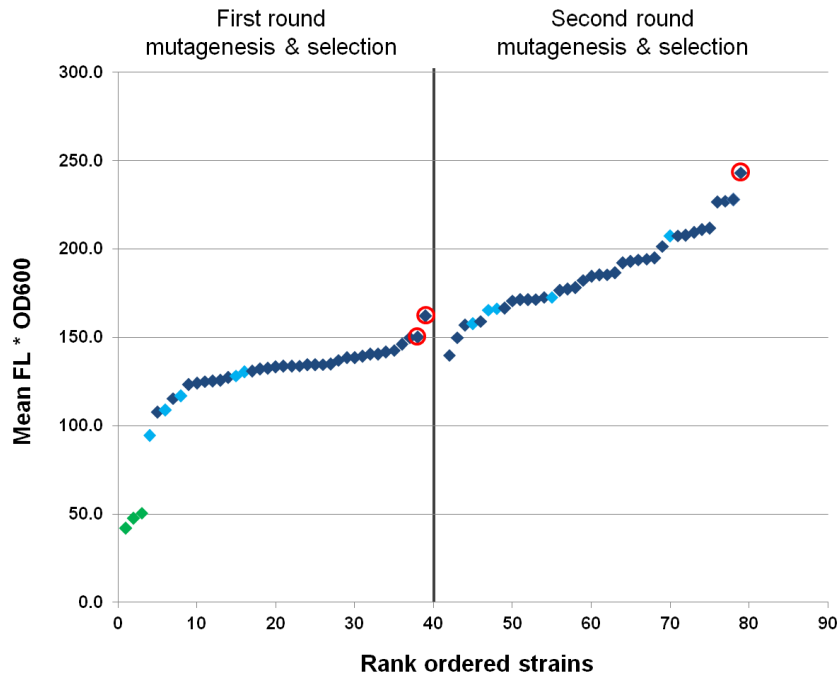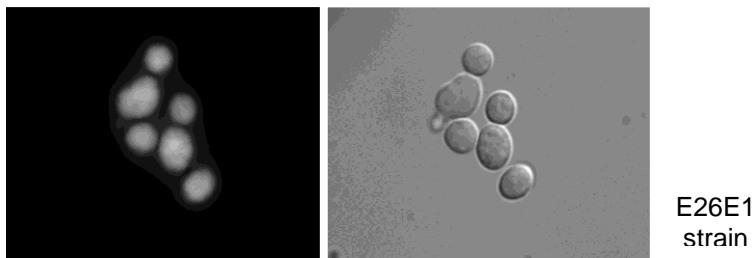
Figure 5.6 cont.

Figure 5.5c
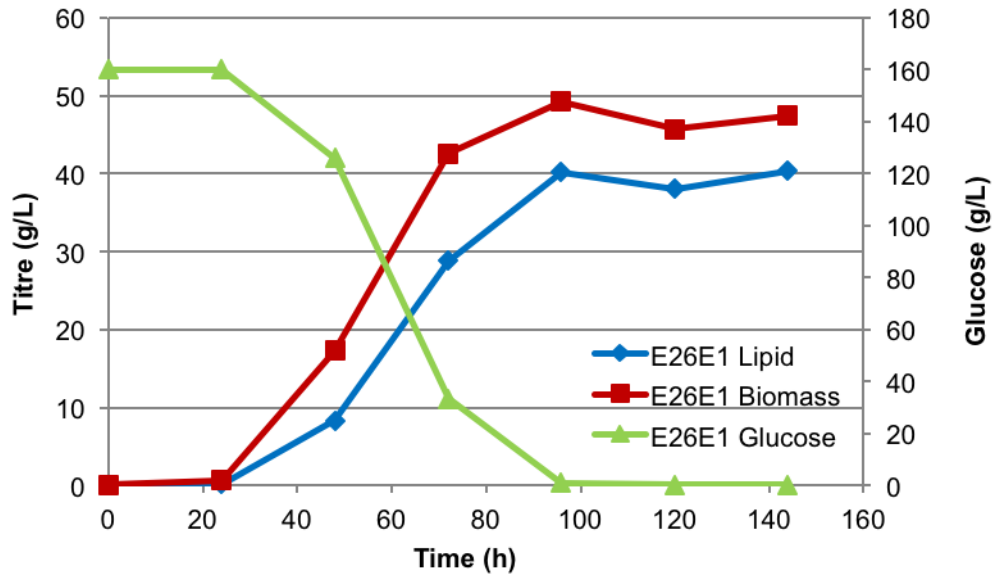
Figure 5.6 cont.

**(A)** Overall performance of iterative evolutionary metabolic engineering using Mean Nile Red fluorescence * OD 600 as metric to rank the strains. Green: the engineering strain; light blue: non EMS mutagenized control strains; dark blue: isolated EMS mutants. The selected mutant, E26E1 is circled in red.  **(B)** Fluorescence microscopy pictures of the E26E1 strain stained with Nile Red to visualize lipids**.  (C)** Batch bioreactor fermentation profile of the E26E1 strain for lipid production.

## 5.3.8 RNA-Seq analysis revealed the importance of glutamate degradation and DHAP biosynthesis

To further exam the transcriptome level changes in the high lipogenesis strain, we performed RNA-Seq analysis with E26 stain and the control strain (PO1f leu$^+$ ura$^+$). Due to the identified beneficial mutation in uga2 from E26 and E13, we first took a look into the glutamate degradation pathway genes and compared their expression (based on log2 fold change) to their expression in PO1f leu+ ura+. There are two metabolic pathways for glutamate degradation in *Y. lipolytica*. The first pathway (along with expression fold changes) uses glutamate decarboxylase (GAD1, YALI0F08415g, -0.82 and YALI0F16753g, -0.37), GABA transaminase (UGA1, YALI0F18238g, no significant change) and succinate semialdehyde dehydrogenase (UGA2, YALI0F26191g, -0.27). The second pathway (along with expression fold changes) uses glutamate dehydrogenase (GDH2, YALI0F17820g, +0.20). These transcriptional changes suggest a downregulated glutamate decarboxylase pathway and a slightly upregulated glutamate dehydrogenase pathway. In the glutamate decarboxylase pathway, degradation costs one 2-oxoglutarate and generates one succinate, however, the glutamate dehydrogenase pathway generates one 2-oxoglutarate. From this analysis, it is again possible that the glutamate dehydrogenase pathway can lead to an unbalanced TCA cycle and subsequently lead to increased citrate secretion from mitochondria. Interestingly, glutamate dehydrogenase also releases one ammonia molecule during the reaction and we indeed found

accumulation of ammonia in the medium as characterized in the high lipid production strain described in Chapter 4.

To gain a more holistic, global view of gene expression changes in the evolved strain, we also sought to examine the top overexpressing genes in the E26 strain. Several of the most highly expressed genes are related to important aspects of lipogenesis such YCF1 (YALI0E08969g) for antioxidation, SPS19 (YALI0F01650g) for denoyl-CoA reductase, ACP1 (YALI0D24629g) for acyl-carrier protein. Interestingly, dihydroxyacetone kinase (YALI0E20691g) was also upregulated.  This enzyme generates dihydroxyacetone phosphate (DHAP), a backbone precursor for triacylglycerol synthesis, which could be a very important molecule in lipogenesis. Interestingly, further analysis of DHAP biosynthesis related gene expression demonstrates that both transketolase and transaldolase were downregulated in E26 (-0.77 and -0.38). This data suggested a reduced exchange between PPP and glycolysis, which could lead to an accumulation of glyceraldehyde 3-phosphate (G3P) that can then be converted to DHAP or continue through glycolysis. The reversible reaction between DHAP and G3P could be an important regulatory node for lipogenesis, since the carbon flux can go to DHAP (for lipid biosynthesis), PPP (for generating NADPH and pentose) or continue into glycolysis to TCA cycle (for most biosynthetic pathway including fatty acid biosynthesis).

## 5.4 Discussion and conclusion

Evolutionary metabolic engineering strategies have been successfully applied to improve production of molecules such as lactic acid, L-ornithine and isobutanol (31, 165-166).  Here we developed a floating based selection scheme that was able to significantly increase: (1) lipid titers from 25 g/L to over 40 g/L, (2) average specific productivity from 0.21 g/L/h to 0.55 g/L/h and (3) overall yield from 0.158 g/g to 0.253 g/g.  Moreover, we were able to achieve maximum instantaneous productivities of 0.86 g/L/h during the fermentation.  Previous rational engineering efforts resulted in unbalanced strains with increased lipid production at the cost of decreased biomass production and fitness.  In contrast, the floating cell enrichment scheme used here resulted in concurrent enhanced lipogenesis and biomass formation. Thus, we have efficiently resolved the competition between product titers and yields by evolutionary engineering following our rational engineering approach.

The balance of lipogenesis and biomass generation developed here could serve as a key for industrialized and economically viable production of oleochemcials using *Y. lipolytica.*  The titer of over 40 g/L is the highest titer reported to the date for this organism.  Furthermore, this evolved strain exhibits lipid accumulation during the cell growth phase without the need for extensive nitrogen starvation.  The result is improvements in all three metrics for a process: rate, titer, and yield.

In addition to the improvements in lipid production, whole genome sequencing of the evolved strain produced critical information about the underlying metabolism. Among the many SNPs identified in this analysis, a major contributing factor to the observed phenotype was a reduced/loss of function mutation in the *uga2* allele. Uga2p

107

functions in the GABA assimilation pathway, which serves as one of two pathways for glutamate degradation and thus related to nitrogen assimilation, a key factor for triggering lipogenesis in *Y. lipolytica* (56). Moreover, previous studies suggest that nitrogen sources, especially glutamate, can be a critical factor for lipid accumulation inside the cells (167). In *Saccharomyces cerevisiae*, *uga2* null mutants result in an accumulation of α-ketoglutarate (168) as well as a decrease in succinic acid (more than 5 fold decrease) (169). Moreover, reductive glutamine metabolism has been suggested as a function of the α-ketoglutarate to citrate ratio in cells (170). Collectively, this information suggests the decrease of GABA assimilation could lead to large changes in carbon flux and result in an imbalance of TCA cycle intermediates which then stalls the TCA cycle allowing for more flux through to fatty acid biosynthesis. In this regard, this rewiring may be similar to the function of AMP deaminase as proposed before (56). It is also likely that decreased GABA assimilation can alter the nitrogen metabolic flux during the protein degradation stage and also lead to increased lipogenesis. Beyond both carbon and nitrogen flux, it is known that the glutamate metabolic node is critical in many processes and can act to buffer redox changes in the cell (171). Furthermore, the relation between GABA metabolism and the TOR pathway, an important signaling pathway for lipid accumulation (139), has been suggested (172-173). Thus, it is likely that the overall rewiring achieved through this evolutionary approach is quite complex. Beyond the GABA target, two additional notable mutations, YOX1 and OSH6, were also closely related to known lipogenesis elicitors (i.e. leucine biosynthesis, TOR pathway) (139). While the overexpression of these mutant alleles did not immediately improve phenotype,

they merit further investigation and can likely be novel engineering targets in the future. Further analysis of the evolved strain E26 with RNA-Seq supported the beneficial effect of uga2 mutation and revealed the potential importance of DHAP in high lipogenesis.

Overall, as described in this chapter, we developed an evolutionary metabolic engineering approach that successfully enhanced lipogenesis of a previously engineered *Y. lipolytica* strain to achieve lipid titers of 40.5 g/L with an average specific productivity reaching 0.55 g/L/h, both representing the highest to the date in this organism. Moreover, cells were saturated with upwards of 89% lipid content in bioreactors. Through whole genome sequencing and RNA-Seq, we were able to provide a link between GABA assimilation and lipogenesis. This evolutionary metabolic engineering approach linked with a simple floating enrichment to enrich high lipogenesis potential presents a platform for engineering a number of other oleaginous systems including potentially microalgae to increase lipid production without compromising cell growth. The resulting strains developed in this chapter should serve as a stepping stone towards creating a robust, efficient engineering platform for converting carbon sources into value-added oelochemical and biofuels.

# Chapter 6: A mutant mga2 protein confers improved lipogenesis in *Yarrowia lipolytica*

## 6.1 Chapter summary

Lipogenic organisms represent great starting points for engineering high lipid production. While previous engineering efforts were able to significantly improve lipogenesis in *Yarrowia lipolytica* (Chapters 4 and 5), understanding of its lipogenesis process was rather limited. In this chapter, we started from a superior lipid accumulation strain, L36, and employed whole genome sequencing and inverse metabolic engineering to identify a mutant mga2 protein conferring improved lipogenesis. Phenotypic characterization revealed this mutant's newly-acquired role in regulating the profile of unsaturated fatty acids. Furthermore, transcriptomic analysis suggested that this mutant enhancer operates by redirecting the net carbon flux difference from an upregulated glycolysis pathway and a downregulated TCA cycle into an upregulated fatty acid synthesis pathway.

**6.2 Introduction**

In Chapters 4 and 5, we described our efforts of exploring the metabolic landscape of lipogenesis through rational and evolutionary engineering, thus driving production to titers exceeding 40 g/L in bioreactors. This exploration can also be done in other ways, such as combining systems and combinatorial engineering of metabolic enzymes (174), engineering the sensor-regulator system (175) or metabolic switches (11) as well as engineering global transcriptional regulators (176-177). The landscape scanned by these approaches contains overlapping phenotypes despite the fact that these engineering efforts targeted different enzymes and pathways, illustrating the complex regulation and crosstalk inherent to this system.

Lipogenesis is regulated in a complex manner (178). This complexity can lead to a disconnection between the expected and actual results of rational engineering. Regulators play a key role in the lipogenesis regulatory network. Thus, identification and engineering of global regulators related to lipogenesis could potentially de-bottleneck lipid production, enriching our understanding over the process and enhancing our engineering ability. A recent study of SNF1 (179), a regulator for lipid accumulation, showed that deletion of SNF1 conferred a 2.6 fold improvement to lipid production . Moreover, results from studies of UBX2 (180) and MIG1 (181) also indicated important function as regulators of lipogenesis.

In this chapter, we report the identification and characterization of a mutant mga2 protein functioning as a lipogenesis enhancer from the L36 mutant strain. In doing so, we further engineered the strain into a high lipid producer and explored the altered transcriptomic landscape caused by the mutation. Specifically, we identified a mutant mga2 exhibiting a similar regulatory effect on unsaturated fatty acid biosynthesis as the mga2 knockout but which is better able to enhance lipogenesis in *Y. lipolytica*. Transcriptomic analysis suggested that a carbon flux imbalance was created by the upregulation of glycolysis and the downregulation of TCA cycle, leading to upregulated biosynthesis of acetyl-CoA/acyl-CoA from pyruvate and hence fatty acid production.

**6.3 Results**

**6.3.1 Isolation and whole-genome sequencing of a high lipid producer revealed a mutant mga2**

During the course of metabolic engineering approach to improve lipid production through construction genomic library (overexpression library on plasmid) and following screening, we isolated mutant strain (L36) exhibiting a dark purple color when grown on solid media containing Nile Red, indicative of high lipid content. Strikingly, during growth in liquid media, this strain settled at the liquid surface while cells from the parent strain remained at the bottom, indicating a reduced mass density in the mutant, consistent with increased lipid production. Indeed, Nile Red staining of the mutant strain followed by fluorescence microscopy indicated almost nothing but lipid inside the cells (**Figure**

112

**5.1**, Chapter 5). Furthermore, TLC plate analysis of cell extracts indicated that the majority of accumulated lipids were in the form of triacylglycerol (**Figure 6.1a**). However, this significant improvement is not due to the plasmid the strain contained due to no beneficial effect was detected when the plasmid was transformed into a control strain.

In order to identify the mechanism underlying this superior lipid accumulation phenotype, we isolated genomic DNA and performed whole-genome sequencing with strain L36 using the Illumina HiSeq platform yielding 2x100bp reads. A 47x coverage was obtained and single nucleotide polymorphism (SNP) analysis was performed by mapping the sequences to the CLIB122 genome (65) and comparing these to the SNPs identified from the draft genome sequence of the PO1f strain (Chapter 5). After filtering the sequences (Q>30), a total of 259 SNPs were identified in L36. Manual curation using the IGV genome browser (159) revealed that there is only one coding region mutation in L36: YALI0B12342g (g1927a), corresponding to MGA2 (g1927a). Mga2 has been well-studied as regulator for multiple cellular processes. It is known to be proteolytically processed on the ER membrane before translocation into the nucleus to function as a transcriptional regulator for delta-9 desaturase gene expression with its homolog spt23 (182-185). Overexpression of mga2 can also influence the chromatin accessibility (186). Mga2 has also been associated with hypoxia as well as with glucose sensing (187-188). Its linkage with lipogenesis has also been studied in *S. cerevisiae*, showing that overexpression of mga2 was accompanied by the appearance of large lipid particles due

to accumulation of unsaturated triacylglycerol (189). To understand the potential impact

of the isolated mutation on mga2 function, we first analyzed the mga2 protein sequence

from *Y. lipolytica* using the Simple Modular Analysis Research Tool (SMART) (190).

This analysis revealed the presence of putative functional domains which were identical

and arranged similarly to other mga2 proteins: an IPT domain (DNA-binding domain), an

ankyrin-like domain (protein binding domain) and a transmembrane (TM) domain. The

isolated mutation occurs in the middle of the DNA-binding domain and the protein

binding domain at position amino acid 643, changing a glycine into arginine

(mga2G643R).

## 6.3.2 MGA2 (g1927a) leads to superior lipogenesis compared with MGA2 deletion

We sought to test the importance of the mga2G643R mutation using inverse

metabolic engineering. We first knocked out the mutant mga2 gene from L36.  The lipid

accumulation from the resulting strain L36 Δmga2(g1927a) leu$^+$ was dramatically

decreased compared with L36 leu$^+$, confirming the importance of this SNP to the superior

lipogenesis phenotype in L36 (**Figure 6.1b**). Subsequently, we deleted wild-type mga2

from the parent strain PO1f (PO1fΔmga2 leu$^+$) and then integrated the mutant mga2

(including 1000bp upstream of the start codon to preserve native expression/regulation)

to test whether this SNP is the dominant mutation causing a superior lipogenesis

phenotype.  The resulting strain PO1fΔmga2 MGA2(g1927a) leu$^+$ exhibits an almost, if

not all, restored phenotype compared to L36 leu$^+$ (**Figure 6.1b,c**).  In particular, knockout

of mga2 from PO1f resulted in an over 2 fold increase in Nile Red signal, and

introduction of mutant mga2 restored the superior lipogenesis phenotype as characterized

by Nile Red straining (**Figure 6.1b**) as well as the floating phenotype (**Figure 6.1c**).

Hence, mga2 is an important lipogenesis regulator in *Y. lipolytica*. While knockout can

improve lipogenesis, the mutant mga2 identified here functions as a superior lipogenesis

enhancer. Collectively, these results suggest that this mutant mga2 protein results in a

gain-of-function in the context of lipogenesis.

Figure 6.1 MGA2 (g1927a) leads to superior lipogenesis and is better than an MGA2

deletion

Figure 6.1a
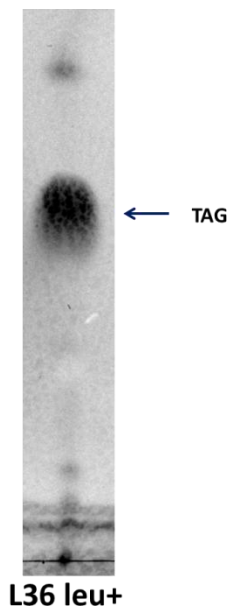
Figure 6.1 cont.

Figure 6.1b
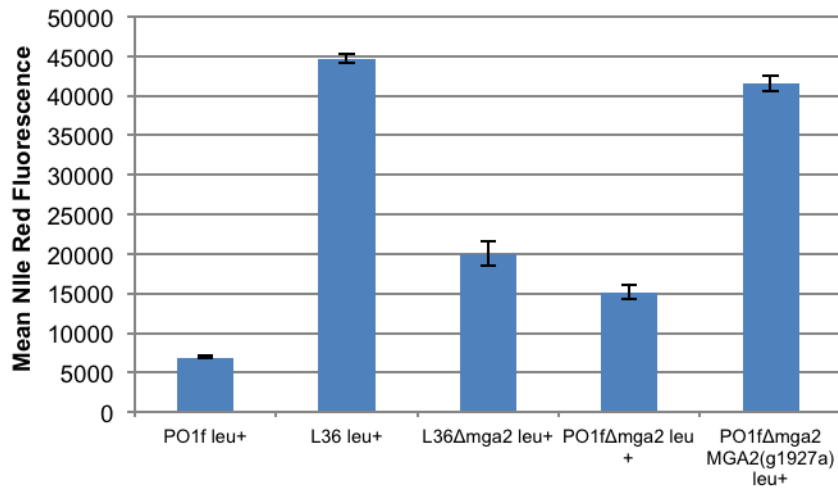


Figure 6.1c
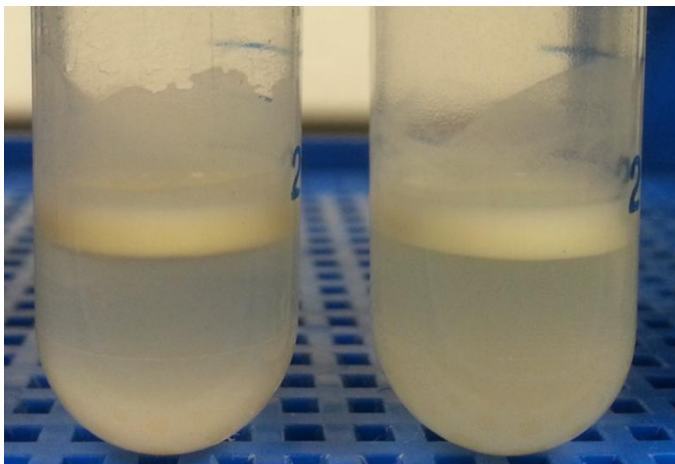


L36 leu⁺        PO1fΔmga2 MGA2(g1927a) leu⁺

Figure 6.1 cont.

**(A)** TLC plate analysis showing that majority of lipid accumulated in L36 is in the form of triacylglycerol. **(B)** Nile Red staining characterized with flow cytometry for strains through inverse metabolic engineering process. (C) Floating phenotype exhibited with L36 leu$^+$ and PO1fΔmga2 MGA2(g1927a) leu$^+$ after cultivation.

### 6.3.3 Metabolic engineering of strain L36 for high lipid production

While L36 showed promising lipid accumulation traits, its lipid production potentials were not yet fully explored. To further enhance its lipid production capacity, we sought to introduce two previously identified lipogenesis enhancers: PEX10 (pexisome biogenesis factor 10) knockout and DGA1(diacylglycerol acyltransferase 1) overexpression, as identified in Chapter 4. We first integrated DGA1 into L36 with leucine and uracil biosynthesis capacity, improving Nile Red fluorescence by 13% (**Figure 6.2a**). Intriguingly, knockout PEX10 significantly decreased lipid accumulation inside the cells (**Figure 6.2a).** To further examine the lipid production performance of the engineered mutant strain, cultivation in a bioreactor was undertaken (**Figure 6.2b**). The lipid titer reached 25 g/L with a specific productivity of 0.142 g/L/h, suggesting its potential for use as an industrial production host. Both measures are comparable to those from the rational metabolic engineering efforts described in Chapter 4.

Figure 6.2 Metabolic engineering lipid production in strain L36

Figure 6.2a
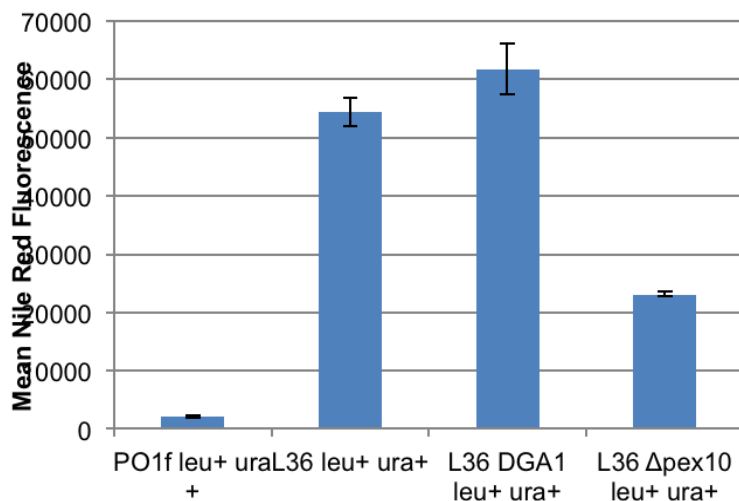


Figure 6.2b
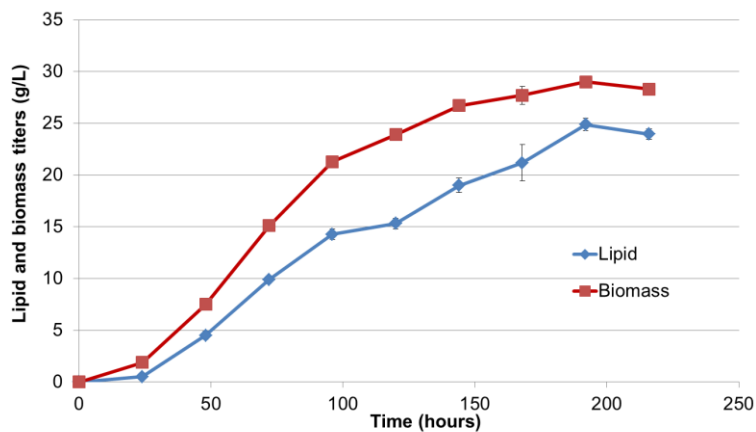


(**A**) Lipogenesis among control strain, L36 leu$^+$ ura$^+$, engineered strains L36 DGA1 leu$^+$ ura$^+$ and L36 Δpex10 leu$^+$ ura$^+$ were characterized using flow cytometry with Nile Red strained cells. (**B**) Fed batch bioreactor fermentation profile of the L36 DGA1 leu$^+$ ura$^+$ strain for lipid production.

**6.3.4 Rag- phenotype and elevated unsaturated fatty acid levels associated with mga2**

To further understand this mutant mga2 protein, we cultivated PO1f leu$^+$, L36 leu$^+$, PO1fΔmga2 leu$^+$ and PO1fΔmga2 MGA2 (g1927a) leu$^+$ on solid media containing YPD, GAA (a rich glucose medium supplemented with the mitochondrial inhibitor antimycin A) and GAA+UFA (GAA with unsaturated fatty acids). All strains grew well on YPD plates, while only PO1f leu$^+$ could grow on GAA plates. The addition of unsaturated fatty acids (GAA+UFA) was required to rescue the growth of L36 leu$^+$, PO1fΔmga2 leu$^+$ and PO1fΔmga2 MGA2 (g1927a) leu$^+$ (**Figure 6.3a**). These phenotypes are comparable to what has been reported for *S. cerevisiae* and *Kluyveromyces lactis* during mga2 knockout (187-188). This impaired growth on GAA plates is known as the Rag$^-$ phenotype (191) and is usually ascribed to defective glycolysis and/or fermentation. Interestingly, this phenotype can be rescued by UFA, suggesting a functional correlation mediated by mga2 between UFA biosynthesis and defective growth, which is similar to observations in *K. lactis*. Following this, we studied the fatty acid profile changes in these strains. In *Y. lipolytica*, both the knockout and the mutant mga2 protein led to an increase in C16:1 and C18:1 fatty acid production at the cost of C16:0 and C18:0 (**Figure 6.3b**). These results stand in contrast to results from *S. cerevisiae* and *K. lactis,* suggesting a different function of mga2 in regulating desaturase gene expression in *Y. lipolytica*. The elevated C16:1 and C18:1 production from the knockout strain indicated an upregulation of delta-9 desaturase gene (OLE1), suggesting that mga2 functions as a repressor for

OLE1 expression in *Y. lipolytica*. The results demonstrated here, which show similar Rag⁻ phenotype and UFA profile from the mga2 deletion and mutant mga2 protein expression, suggest that the mutant functions similarly to a deletion in terms of regulating glycolysis/fermentation and UFA biosynthesis. However, the improved lipogenic capacity of the mutant mga2 protein confirmed that there are preserved functions in this mutant which are important for lipid accumulation.

Figure 6.3 Mga2 is related to Rag- phenotype and unsaturated fatty acid level

Figure 6.3a
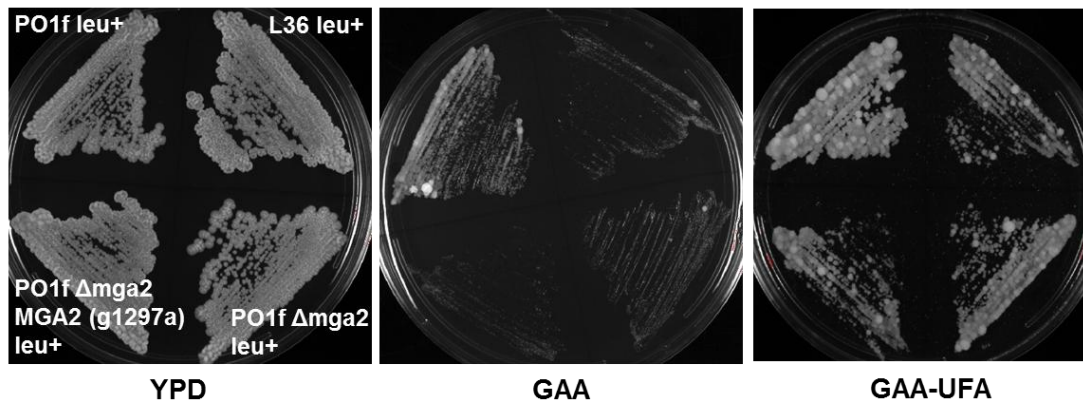


Figure 6.3b
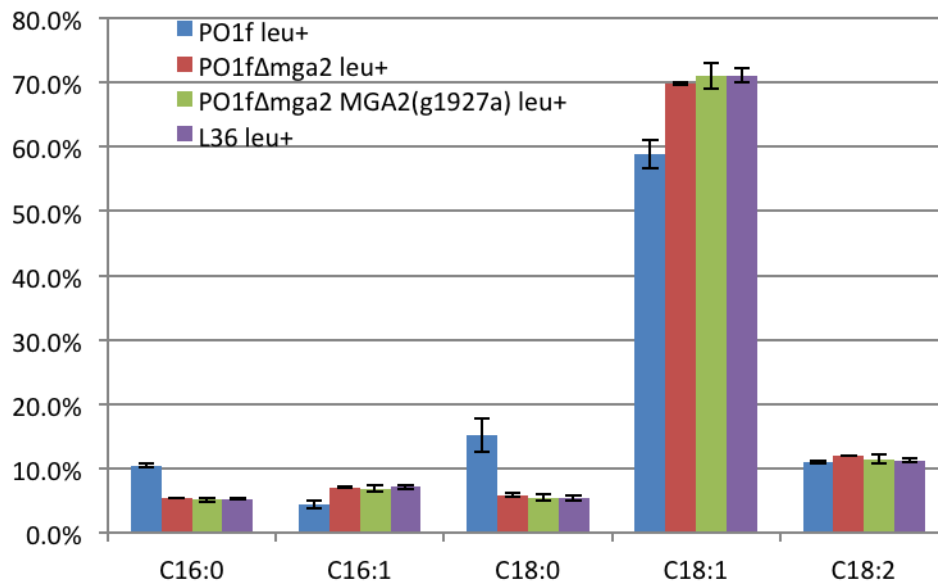


**(A)** Plate growth assay with different inverse metabolic engineering strains on YPD, GAA and GAA-UFA plates. **(B)** Fatty acid profile from GC analysis with different inverse metabolic engineering strains.

### 6.3.5 Link the mga2G643R with phenotype using RNA-Seq

To further probe the mechanisms underlying the phenotypic changes resulting from mga2G643R, we performed RNA-Seq analysis with PO1f leu$^+$ and PO1fΔmga2 MGA2 (g1927a) leu$^+$. Overall, we identified 429 upregulated and 467 downregulated genes (> 1-fold change) with edgeR (192). Due to changes in the fatty acid profile, we first examined the expression of desaturase genes. Indeed, the expression of delta-9 desaturase (YALI0C05951g) and delta-12 desaturase (YALI0B10153g) were upregulated in the inverse engineered strain, explaining the increased level of C16:1/C18:1 and C18:2 fatty acids.

Due to the importance of acetyl-CoA/malonyl-CoA and glycerol-3-phosphate (G3P) in lipid biosynthesis, we also examined the expression of genes related to their biosynthesis (**Figure 4**). We found that while most of the genes involved in glycolysis were significantly upregulated in the mutant strain, genes related to TCA cycles were not, especially the genes close to citrate biosynthesis. This observation raises the possibility that the improved lipogenesis in the inverse engineered strain results from the generation of extra carbon flux due to an imbalance between increased glycolysis and reduced TCA cycle. This net carbon flux could then be funneled into acetyl-CoA biosynthesis through the upregulated pyruvate dehydrogenase and citrate synthase. However, it is also interesting to note that pyruvate decarboxylase, another possible route to generate acetyl-CoA from pyruvate, is downregulated. While pyruvate dehydrogenase yields one NADH

123

to generate an acetyl-CoA, pyruvate decarboxylase costs one, indicating a substantial benefit for the cell to use pyruvate dehydrogenase instead of pyruvate decarboxylase. The acetyl-CoA in mitochondria can be converted into citrate, exported efficiently through the upregulated citrate transporters, and converted into acetyl-CoA with the upregulated ATP citrate lyases. The overproduced acetyl-CoA can then be converted into malonyl-CoA by the 6-fold upregulated acetyl-CoA carboxylase. Besides acetyl-CoA/malony-CoA, the increased dihydroxyacetone phosphate (DHAP) from glycolysis can also be transformed into G3P through a 6-fold upregulated G3P dehydrogenase. Overall, mutant mga2 improves lipogenesis through regulating carbon metabolism genes. In addition, we also examined the expression of the glutamate degradation pathway due to its importance in the control of the carbon/nitrogen flux distribution and the aforementioned discussion of its importance as described in Chapter 5. We found that all the genes related to glutamate degradation exhibit either a downregulation or no significant change, suggesting that protein degradation may not be the major source of carbon for lipid biosynthesis in the context of this mutation.

To gain an overall view of transcriptomic changes caused by mutant mga2, we performed gene set enrichment analysis with significantly upregulated genes and downregulated genes (>1-fold change) (**Table 1**). Overall, the analysis supported the improved lipogenesis phenotype. In particular, fatty acid biosynthesis pathways were enriched in upregulated genes and fatty acid metabolisms as well as glycerolipid metabolism were enriched in downregulated genes. Interestingly, among the upregulated

124

genes, analysis with INTROPRO suggested the enrichment of mitochondrial substrate carrier genes. Among these, citrate and oxoglutarate carrier protein (YALI0B10736g) exhibited a 6.2-fold overexpression, which could be very important as this protein functions to export citrate from mitochondria and import oxoglutarate, with a net export of NADPH (193). As a consequence, this gene could supply citrate for acetyl-CoA biosynthesis as well as NADPH as cofactor for fatty acid biosynthesis. Oxaloacetate carrier (OAC1, YALI0E04048g) also represents an important link to citrate export: it takes in oxaloacetate, which is produced by ATP citrate lyases when converting citrate to acetyl-CoA, thus recycling carbon back to the TCA cycle. Furthermore, one ATP–ADP translocase protein (AAC, YALI0A10659g), which is responsible for importing ADP into and exporting ATP out of the mitochondria, is also overexpressed. This protein could supply ATP to the ATP citrate lyases for production of acetyl-CoA, as well as supply energy to other cellular processes. Among the significantly downregulated genes, we found that the fatty acid metabolism pathway (KEGG) was enriched in significantly downregulated genes, including POX2 (YALI0F10857g), POX3 (YALI0D24750g), POX5 (YALI0C23895g), enoyl-CoA dehydrase (YALI0B10406g) confirming a decrease in fatty acid degradation. We also found that glycerolipid metabolism was enriched, in particular DGA1 (YALI0D07986g), a very important lipogenesis enhancer as identified in Chapter 4, suggesting that the improvement to lipid accumulation is mainly due to initial carbon flux rewiring, further verifying the previous beneficial results obtained from the metabolic engineering of L36.

As a transcriptional regulator, this mutant mga2 protein could also regulate the expression of other regulators to achieve this complex rewiring of cellular metabolism. To understand this process a more deeply, we analyzed the upregulated and downregulated genes separately using SCOPE to investigate the enrichment of motifs in the promoter region (-800). When comparing the top 10 candidates from both sets to the known transcription factor binding sites in *S. cerevisiae* (194), we found that enriched motifs showed similarity to the binding sites of mig1,2,3 proteins (aytttcwgt and thttatta) and sko1 protein (tacgtab) in the promoters of upregulated genes, and leu3 protein (gttaacd) and azf1 protein (aaaga) in the downregulated genes. These transcription factors are closely linked with cellular metabolism, in particular the regulation of carbon and nitrogen uptake. Collectively, mutant mga2 improved lipogenesis by rewiring cellular metabolism related to carbon flux, fatty acid related biosynthesis and degradation as well as other cellular metabolic regulators.

Figure 6.4 Differential expression level of genes related to central carbon flux for lipid biosynthesis
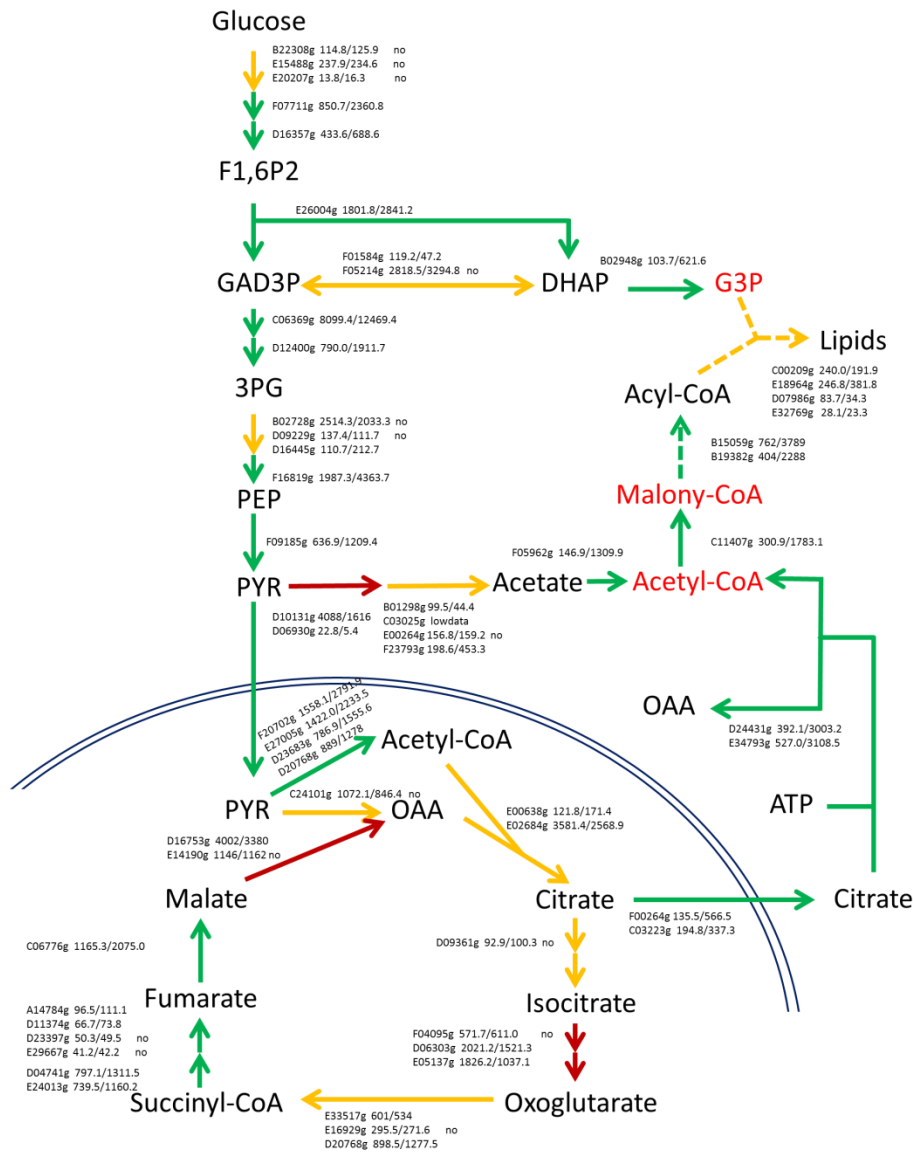


Differential expression level of genes related to central carbon flux for lipid biosynthesis. PFKM change showing as PFKM from PO1f leu2$^+$/PFKM from PO1f Δmga2 MGA2 (g1297a) leu$^+$. All the changes are significant unless labeled with no (Green: upregulation; Red: downregulation; yellow: change cannot be determined). PFKM is from cufflink calculation and statistical analysis is using data from edgeR analysis.

Table 6.1 Gene set enrichment analysis with significant differential expressed genes from RNA-Seq experiments

| Upregulated genes | Downregulated genes |
|---|---|
| **GOTERM** ||
| GO:0018130~heterocyclebiosyntheticprocess | GO:0030001~metaliontransport |
| GO:0016053~organicacidbiosyntheticprocess | GO:0046942~carboxylicacidtransport |
| GO:0046394~carboxylicacidbiosyntheticprocess | GO:0015837~aminetransport |
| GO:0008610~lipidbiosyntheticprocess | GO:0015849~organicacidtransport |
| GO:0044271~nitrogencompoundbiosyntheticprocess | GO:0006865~aminoacidtransport |
| GO:0055114~oxidationreduction | GO:0055114~oxidationreduction |
| GO:0042278~purinenucleosidemetabolicprocess | GO:0006812~cationtransport |
| GO:0046128~purineribonucleosidemetabolicprocess | GO:0006811~iontransport |
| GO:0051188~cofactorbiosyntheticprocess | GO:0000041~transitionmetaliontransport |
| GO:0016021~integraltomembrane | GO:0006825~copperiontransport |
| GO:0031224~intrinsictomembrane | GO:0006071~glycerolmetabolicprocess |
| GO:0033293~monocarboxylicacidbinding | GO:0019400~alditolmetabolicprocess |
| GO:0004806~triacylglycerollipaseactivity | GO:0019751~polyolmetabolicprocess |
| GO:0016836~hydro-lyaseactivity | GO:0051252~regulationofRNAmetabolicprocess |
| GO:0009374~biotinbinding | GO:0006355~regulationoftranscription,DNA-dependent |
| | GO:0045449~regulationoftranscription |
| | GO:0016021~integraltomembrane |
| | GO:0031224~intrinsictomembrane |
| | GO:0005576~extracellularregion |
| | GO:0046873~metaliontransmembranetransporteractivity |
| | GO:0046915~transitionmetaliontransmembranetransporteractivity |
| | GO:0015171~aminoacidtransmembranetransporteractivity |

Table 6.1 cont.

| | GO:0005275~aminetransmembranetransporteractivity |
|---|---|
| | |
| | GO:0015082~di-,tri-valentinorganiccationtransmembranetransporteractivity |
| | GO:0005375~copperiontransmembranetransporteractivity |
| | GO:0004175~endopeptidaseactivity |
| | GO:0048037~cofactorbinding |
| | GO:0004371~glyceronekinaseactivity |
| | GO:0004190~aspartic-typeendopeptidaseactivity |
| | GO:0070001~aspartic-typepeptidaseactivity |
| | GO:0003700~transcriptionfactoractivity |
| | GO:0050662~coenzymebinding |
| | GO:0046914~transitionmetalionbinding |
| | GO:0043167~ionbinding |
| | GO:0043169~cationbinding |
| | GO:0046872~metalionbinding |
| | GO:0070011~peptidaseactivity,actingonL-aminoacidpeptides |
| | GO:0030528~transcriptionregulatoractivity |
| **KEGG PATHWAY** | |
| yli00061:Fattyacidbiosynthesis | yli00071:Fattyacidmetabolism |
| | yli00561:Glycerolipidmetabolism |
| | yli00650:Butanoatemetabolism |
| | yli00410:beta-Alaninemetabolism |
| | yli00010:Glycolysis/Gluconeogenesis |
| | yli00640:Propanoatemetabolism |
| | yli00330:Arginineandprolinemetabolism |
| | yli00350:Tyrosinemetabolism |
| | yli00280:Valine,leucineandisoleucinedegradation |
| | yli00980:MetabolismofxenobioticsbycytochromeP450 |
| **INTROPRO** | |
| IPR001993:Mitochondrialsubstratecarrier | IPR011701:MajorfacilitatorsuperfamilyMFS-1 |

Table 6.1 cont.

| | |
|---|---|
| IPR018108:Mitochondrialsubstrate/solutecarrier | IPR005828:Generalsubstratetransporter |
| IPR011701:MajorfacilitatorsuperfamilyMFS-1 | IPR002293:Aminoacid/polyaminetransporterI |
| IPR000873:AMP-dependentsynthetaseandligase | IPR004648:Tetrapeptidetransporter,OPT1/isp4 |
| IPR002113:Adeninenucleotidetranslocator1 | IPR004841:Aminoacidpermease-associatedregion |
| IPR003819:TaurinecatabolismdioxygenaseTauD/TfdA | IPR016040:NAD(P)-bindingdomain |
| IPR005482:Biotincarboxylase,C-terminal | IPR004813:OligopeptidetransporterOPTsuperfamily |
| IPR011764:Biotincarboxylationregion | IPR004840:Aminoacidpermease,conservedsite |
| IPR013816:ATP-graspfold,subdomain2 | IPR018289:MULEtransposase,conserveddomain |
| IPR002123:Phospholipid/glycerolacyltransferase | IPR009007:Peptidaseaspartic,catalytic |
| IPR006139:D-isomerspecific2-hydroxyaciddehydrogenase,catalyticregion | IPR001461:PeptidaseA1 |
| IPR006140:D-isomerspecific2-hydroxyaciddehydrogenase,NAD-binding | IPR003663:Sugar/inositoltransporter |
| | IPR002198:Short-chaindehydrogenase/reductaseSDR |
| | IPR000209:PeptidaseS8andS53,subtilisin,kexin,sedolisin |
| | IPR001969:Peptidaseaspartic,activesite |
| | IPR001509:NAD-dependentepimerase/dehydratase |
| | IPR002347:Glucose/ribitoldehydrogenase |
| | IPR002328:Alcoholdehydrogenase,zinc-containing,conservedsite |
| | IPR015500:PeptidaseS8,subtilisin-related |
| | IPR004007:Dakphosphatase |
| | IPR004006:Dakkinase |
| | IPR007274:Ctrcoppertransporter |
| | IPR001092:Basichelix-loop-helixdimerisationregionbHLH |
| | IPR013154:AlcoholdehydrogenaseGroES-like |
| | IPR002085:Alcoholdehydrogenasesuperfamily,zinc-containing |
| | IPR013149:Alcoholdehydrogenase,zinc-binding |

Table 6.1 cont.

| | |
|---|---|
| | IPR004843:Metallophosphoesterase |
| | IPR013112:FAD-binding8 |
| | IPR005829:Sugartransporter,conserved site |

## 6.4 Discussion and conclusion

Lipogenesis is a complex and energy-consuming process. Rewiring this process usually requires complex cellular metabolic engineering, which is time and labor intensive. The mutant mga2 protein conferring improved lipogenesis identified here strongly validated the power of transcriptional regulators in altering a complex cellular phenotype. Strikingly, when compared to the rational metabolic engineering for high lipogenesis in this yeast as presented in Chapter 4, which required a large scale exploration of lipogenesis-related targets, this single SNP in the genome placed its *de novo* lipid accumulation on par with the engineered strain (139). The nature of this result is characteristic of the gTME (global transcriptional machinery engineering) approach (177); single mutations in enzymatic proteins are usually not enough to dramatically improve complex cellular phenotypes and sequential beneficial mutations are hard to achieve without strong selection pressure. However, simple mutations to global transcriptional regulators can alter the metabolism of the whole cell to a very large extent, thus efficiently improving a complex phenotype.

Although the results of plate assays for the Rag⁻ phenotype resembled those from *K. lactis* and *S. cerevisiae*, the alterations to the fatty acids profile was different. In *K. lacis*, there is an increase of C18:1 at the cost of C18:2 and C18:3 (188) while in *S. cerevisiae*, there is reduction of C16:1 and an increase in C18:1 (195). This data suggests a difference in mga2's function in *Y. lipolytica*. In addition, the changes in UFA with mutant mga2 could also explain the detrimental effect of the PEX10 knockout in L36.

Moreover, the mga2 knockout strain contained a similar fatty acid profile to the strain with mutant mga2, indicating a similar loss of function over the control of OLE1 from this mutation. However, the clearly improved lipogenesis as illustrated by the floating phenotype and Nile Red staining suggests that the mutant protein functions differently than the knockout. Indeed, previous studies also suggested that mga2 could regulate the stability of OLE1 mRNA through exosome-mediated mechanisms (182) as well as influencing chromatin accessibility (186), presenting the possibility of an incomplete loss of function from the mutation.

Despite the lack of a conversed domain predicted to contain the mutation, alignment of mga2 sequences from different species showed that the mutant position and adjacent sequences are actually highly conserved with other yeast species such as *S. cerevisiae* and *Scheffersomyces stipitis* (196) (**Figure 6.5**). Interestingly, this conserved region in *S. cerevisiae* (VGLKMNG<u>K</u>LEDAR) has been predicted to be subject to ubiquitination on the second lysine (197). A recent study also suggested that the region between the IPT domain and the ANK domain are putative sites of initial degradation and processing of mga2 in *S. cerevisiae* (198). This process is similar to its human homolog NFκB (199). However, in *Y. lipolytica* mga2 as well as in the homologous sequences from two other oleaginous yeast sequences *Rhodosporidium toruloides* (200) and *Rhodotorula glutinis* (201), there is an arginine in the position of lysine, which is likely to stop ubiquitination and the resulting degradation. Moreover, in sequence of the homologous regulator spt23, there remains a lysine at this position (**Figure 6.5**). In

addition, two lysine residues within membrane-anchored mga2 have also been studied as targets of Rsp5p ubiquitination for cleavage (202). These results suggest the possibility of multi-step processing of mga2, and hence a complex underlying regulation mechanism. A previous study with its human relative, NFκB, indicated the possibility of non-ubiqutination dependent processing in the conserved region aforementioned (203), raising the possibility that due to the level of sequence conservation, processing can occur with native mga2 in *Y. lipolytica* but not the mutant one. As a consequence, mga2G643R does not get activated to carry out its full function as a transcriptional factor yet still functions in other ways such as improving RNA stability, which could explain both the similarities and differences between mga2G643R and mga2 deletion.

When comparing the differential gene expression data obtained here with that obtained from another regulator (SNF1 knockout) for lipogenesis in *Y. lipolytica* (179), out of 49 targets identified for SNF 1 knockout, 32 of these showed differential expression in mutant mga2 strain, with 3 out of 8 downregulated genes and 24 out of 41 upregulated genes overlapping. This suggests there are similar underlying lipogenesis rewiring mechanisms shared between the two modifications. However, the large number of targets identified through this study may indicate a more complex and complete rewiring over cellular metabolism using the mutant mga2 protein, which also led to a better lipogenesis phenotype comparing to the SNF1 knockout. Indeed, through the promoter motif enrichment analysis, the potential of involvement of several transcriptional factors was revealed. Mig1,2,3 proteins have been studied for their role in

mediating glucose repression and  sko1 protein has been shown to interact with mig proteins as well as to regulate cellular metabolism under oxidative stress (204-205). Leu3 is a key transcriptional regulator for branched-chain amino acid metabolism in *S. cerevisiae* (206) and azf1 (207) has also been linked with nitrogen assimilation. This information indicates a global regulatory change resulting from the mutant mga2 to rewire whole cellular metabolism through the glucose repression and nitrogen assimilation.

There is an increased level of unsaturated fatty acids in the mutant strain and the mga2 deletion strain.  This increment should result from upregulated desaturase gene expression. Desaturases such as OLE1 in yeast and the mammal homolog Stearoyl-CoA desaturase-1 (SCD1) have been shown to be functionally important to fatty acid biosynthesis. Deletion of OLE1 (ole1$\Delta/\Delta$) in *Candida parapsilosis* severely impaired lipid droplet formation inside the cells (208). Furthermore, increases to SCD1 activity in CHO cells is sufficient to increase triglyceride accumulation when supplemented with exogenous palmitic acid, and this increased triglyceride synthesis associated with SCD1 overexpression can also protect against lipoapoptosis (209). In addition, SCD in *C. elegans* also showed an ability to regulate fatty acid biosynthesis (184). Unsaturated fatty acid biosynthesis is usually tightly regulated due to its importance to membrane fluidity. This elevated unsaturated fatty acids level along with improved lipogenesis indicates that regulation over UFA biosynthesis could be one of the bottlenecks for improving lipogenesis.

Lipogenic organisms provide an ideal platform for biodiesel and oleochemical production. However, to fully develop a platform for industrial level production, understanding the regulatory aspects of lipogenesis can be very beneficial. In this chapter, we successfully identified and confirmed a mutant mga2 protein as a novel lipogenesis regulator through whole genome sequencing. This mutant mga2 protein leads to a superior lipid accumulation phenotype and an elevated unsaturated fatty acids level. Through probing the transcriptomic changes associated with the mutant mga2, we were able to show that mutant mga2 acts to funnel carbon flux to fatty acid biosynthesis. Further metabolic engineering of this mutant strain led to a high lipid producer with a titer of 25 g/L. The altered fatty acid profile of this strain makes it a unique starting point for downstream engineering for tailored oleochemical production. Collectively, the information supplied in this chapter along with the identified mutations and the strains could accelerate understanding of the complex regulation of lipogenesis as well as the creation of a robust, efficient engineering platform for converting carbon sources into value-added oleochemicals and biofuels.

Figure 6.5 Illustration of mga2 protein with IPT and ANK domains and sequence alignment over mga2 and its homologues
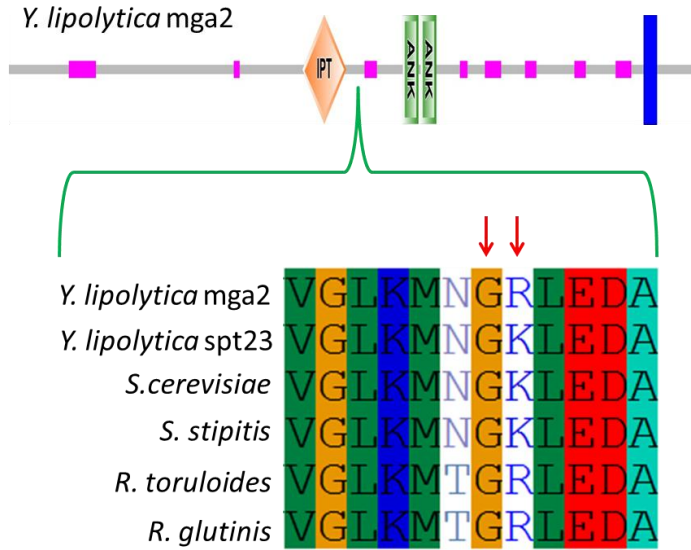


Blue indicates transmembrane domain, purple indicates low complexity and grey indicates unknown region (illustration made by SMART). Sequence alignment is performed using clustralW.

# Chapter 7: Major findings and proposal for future work

## 7.1 Major findings

The experiments described herein had three major goals. The first goal was to develop tools for controlling gene expression in *Yarrowia lipolytica*. We first performed hybrid promoter engineering by creating a library of promoters with a 400-fold dynamic range based on mRNA expression levels. We then created a set of plasmids with a dynamic range of 2.7-fold using different promoters upstream of the centromeric region. The results presented in Chapters 2 demonstrated that the hybrid promoter approach is an efficient strategy for promoter engineering by fusing a core promoter region with upstream activation sequences, and the results presented in Chapter 3 illustrated that using a promoter repressed centromere could alter the plasmid copy number and expression level to enable an additional layer for controlling gene expression. Both methods developed here are based on fundamental molecular biology principles, thus, could be easily adapted into other organisms with an ill-defined gene expression toolbox. Furthermore, the combination of these two methods would further expand the range of expression level.

The second goal was to metabolically engineer *Y. lipolytica* for high lipid production. In order to achieve this goal, we employed rational and evolutionary metabolic engineering strategies. Rational metabolic engineering efforts included combinatorially engineering several targets related to lipogenesis, which successfully improved the lipid production in this yeast. The lipid content reached upwards of 90% in the engineered strain while the initial strain only amassed up to 10% under the same

condition. The engineered strain was able to produce over 25 g/L lipid in a bioreactor without requiring nitrogen starvation. By further employing a self-developed evolutionary engineering method, the lipid production titer exceeded 40 g/L with both increased yield and productivity at the same time. Moreover, unlike other rational metabolic engineering cases, this improved lipid production was not accompanied by decreased biomass. The results here clearly showed a significant improvement over lipid production performance in *Y. lipolytica* through a combination of rational and evolutionary metabolic engineering. The evolutionary metabolic engineering method for improving lipid production could be easily applied to other microorganisms to enhance lipid production.

The third goal was to gain novel understanding over the lipogenesis process in *Y. lipolytica*. Through the engineering experiments and whole genome sequencing efforts, we successfully identified several lipogenesis enhancers such as DGA1 overexpression, PEX10 knockout, UGA2 mutation/knockout. Leucine biosynthetic capacity was also identified as essential for high lipogenesis. These findings supplied clues to the basic mechanism of lipid accumulation in this yeast; more specifically, they revealed the limiting rate of triacylglycerol biosynthesis, the importance of glutamate degradation, and the essence of target of rapamycin pathway (TOR) in lipogenesis process. Transcriptomic analysis with the evolved strain confirmed the importance of glutamate degradation and further illustrated the potential of DHAP serving as a key molecule to high lipogenesis. In addition to the knowledge gained from the strain engineering process, we also identified a

mutant mga2 protein functioning as a novel lipid enhancer. Further characterization of mga2 protein uncovered its function for regulating unsaturated fatty acid biosynthesis in *Y. lipolytica*. Ultimately, this mutant mga2 protein redirected carbon flux towards fatty acid biosynthesis using pyruvate as a key intermediate.

Overall, through the experiments described in this work, we employed synthetic biology concepts rooted in fundamental molecular biology to gain control over gene expression and utilized rational metabolic engineering in combination with evolutionary engineering to improve lipid production in *Y. lipolytica*. In addition, we successfully identified and characterized a novel lipogenesis enhancer, a mutant mga2 protein. Moreover, we performed genomic and transcriptomic analyses to further explore the underlying mechanism that contributed to improved lipogenesis. The resulting strains and information would serve as stepping stones for industrial development and production studies. A recent study of the oleaginous yeast *Lipomyces starkeyi* fed with soluble starch proposed a biodiesel factory gate price of $2.30 per gallon, which is economically viable (210). This study suggests that the *Y. lipolytica* strain with high lipid production titer, yield, and productivity developed in this work could serve as an industrial production platform. Since the cost of lipid production was strongly influenced by the cost of medium nutrients required for cultivation of cells (50%) and the cost of solvent required to extract lipids from biomass (25%), decreases in raw materials cost and engineering fatty acid secretion in this organism could improve economic viability (210). Furthermore, the methodologies, tools, and information gained in this work could be transferred into

other microorganisms in order to engineer them for producing a variety of value-added chemicals.

**7.2 Proposal for future work**

The research described here represents a metabolic engineering flow for engineering high lipid production in a microorganism. Since most of the methods and targets used here are based on general biological mechanisms and concepts, it would be interesting to apply these similar strategies in order to engineer other organisms for high lipid production. Although *Y. lipolytica* is a very attractive host, there are other natural hosts that are amenable to industrial-scale processes and have better alternative carbon source utilization (more importantly, different types of biomass), such as other oleaginous yeasts like *L. starkeyi* and *Rhodosporidium toruloides* (211) as well as non-oleaginous yeast such as *Ustilago maydis* (212). Specifically, the evolutionary engineering scheme developed in this work could be very effective when applied to other organisms.

The information gained from rational metabolic engineering, especially the importance of leucine biosynthetic capacity to high lipogenesis is very interesting. Although the studies showed here suggest relation to the TOR pathway, detailed study could further reveal its function in lipogenesis. Since rapamycin addition actually improved lipogenesis as described in Chapter 4, further engineering of the FK506-binding protein of 12 kDa (FKBP) that binds rapamycin should impact lipogenesis inside the cells (213). In addition, RNA-Seq experiments would be especially helpful to

illustrate the changes in lipid accumulation with or without the leucine biosynthesis capacity. Furthermore, additional analysis of the RNA-Seq results from the evolved strain E26 as well as mutant strain L36 could further supply novel understanding over the lipogenesis mechanism in this yeast. The importance of DHAP and glutamate degradation pathway can be further studied with metabolic engineering strategies such as feeding DHAP and overexpression of the GDH2 (glutamate dehydrogenase 2) to examine the lipogenesis changes. Nitrogen starvation is also a very key component for lipogenesis. While the studies described here test the effect of nitrogen starvation through optimizing the carbon/nitrogen ratio in the medium, more detailed genetic modifications could supply better understanding underlying this requirement, such as identifying the resulting signaling pathway regulation caused by nitrogen starvation through engineering one of the key regulatory knot, the URE2/GLN3 transcriptional regulator pairs (214-215). Although we studied and characterized the mutant mga2's function over lipogenesis, the results from sequence alignments and previous studies suggested a complex regulation and important function over the identified conserved region. Follow-up studies mixed with biochemical characterization to identify different processing events and resulting phenotype changes could further explain the function of this regulator. More importantly, this study could lead to identification of one of the key factors in creating oleaginous yeast.

While high lipid production has been engineered in *Y. lipolytica*, their actual use for industrial scale production would depend on other factors such as its ability to utilize alternative carbon sources (xylose, arabinose, cellulose etc.) in addition to the optimal

production medium. Thus, engineering *Y. lipolytica* for xylose consumption is another important task. This can be tackled with overexpressing native genes predicted to code for xylose metabolic enzymes and complementing with heterologous genes from other xylose metabolizing microorganisms such as *Scheffersomyces stipitis* (216) and *Piromyces sp.* (217).  Furthermore, micronutrients such as minerals and small molecules have been studied as beneficial factors to improve growth and hydrocarbon or lipid production in algae (218-219). Similar work has been done with oleaginous yeast such as *Lipomyces starkeyi* to improve lipid production (220).  For *Y. lipolytica*, a medium optimization study was performed to improve its heterologous protein production and lipase production (146, 221). Mineral supplementation was also studied in order to increase erythritol biosynthesis from glycerol in *Y. lipolytica* (222). However, the effect of micronutrients on lipid accumulation has not been studied in detail. More importantly, not only the available study is rather limited but also almost all of those have been carried with the wild type strain rather than a metabolic engineered strain for increased lipid production. The responses to micronutrients from the genetic engineered strains need to be addressed in comparison with the wild type strain in order to fully understand their impact on lipogenesis in these strains and to enable their complete and optimal utilization during lipid production.

Collectively, my research led to successfully improving lipid production in *Y. lipolytica*. In doing so, we developed novel promoter engineering and plasmid engineering strategies, and an efficient evolutionary engineering method for increasing lipid production. Concurrently, we revealed sufficient knowledge over the lipogenic

143

pathway in this yeast, such as the importance of leucine biosynthetic capacity and the

novel functions of a mutant mga2 in lipogenesis.

# Chapter 8: Materials and methods

## 8.1 Common materials and methods

## 8.1.1 Strains and media

$E.$ $coli$ strain DH10β was used for all cloning and plasmid propagation.  DH10β

was grown at $37^{o}$C with constant shaking in Luria-Bertani (LB) Broth (Teknova)

supplemented with 50μg/ml ampicillin for plasmid propagation.  $Yarrowia$ $lipolytica$

strain PO1f (ATCC # MYA-2613), a leucine and uracil auxotroph devoid of any secreted

proteasic activity (82) was used for all studies.  $Y.$ $lipolytica$ PO1f containing plasmid was

routinely cultivated at $30^{o}$C with constant agitation in YSC-LEU media consisting of

20g/L glucose purchased from Fisher Scientific, 0.69g/L CSM-Leucine supplement

purchased from MP Biomedicals, and 0.67g/L Yeast Nitrogen Base purchased from

Becton, Dickinson, and Company.  Solid media for $E.coli$ and $Yarrowia$ $lipolytica$ was

prepared by adding 15g/L agar (Teknova) to liquid media.

## 8.1.2 Cloning procedures

All restriction enzymes were purchased from New England Biolabs and all

digestions were performed according to standard protocols.  PCR reactions were set up

with recommended conditions using Phusion high fidelity DNA polymerase (Finnzymes).

Ligation reactions were performed overnight at $16^{o}$C using T4 DNA Ligase (Fermentas).

Gel extractions were performed using the GeneClean gel extraction kit purchased from

MP Biomedicals.  Purification of small DNA fragments (<200 bp) generated during

plasmid construction were performed using the MERmaid Spin Kit (Qbiogene).  $E.$ $coli$

minipreps were performed using the Zyppy Plasmid Miniprep Kit (Zymo Research Corporation). *Y. lipolytica* minipreps were performed using Zymoprep Yeast Plasmid Miniprep II kit (Zymo Research Corporation). Transformation of *E. coli* strains was performed using the standard electroporator protocols (223). Transformation of *Y. lipolytica* was performed using the Zymogen Frozen EZ Yeast Transformation Kit II (Zymo Research Corporation). Genomic DNA was extracted from *Y. lipolytica* using the Wizard Genomic DNA Purification kit (Promega).

## 8.1.3 Fatty acid characterization by Nile Red staining

Nile Red (MP Biomedicals) is commonly utilized to stain oleaginous cellular material and can be coupled with fluorescence flow cytometry to gauge relative lipid content (125). *Y. lipolytica* strains were routinely inoculated from glycerol stock in biological triplicate in appropriate media for 72 hours at 30 $^o$C with shaking. Cell concentrations were normalized to a specific $OD_{600}$ for reinoculation in fresh media and further incubation. For assays in which the effect of media formulation was not being investigated, this media contained 0.79 g/L CSM (or 0.69 g/L CSM-Leucine if necessary), 1.7 g/L Yeast Nitrogen Base w/o amino acid and w/o $(NH_4)_2SO_4$, 80 g/L carbon source, and 5 g/L ammonium sulfate, as this formulation was shown to strongly induce lipid accumulation in the highest lipid producing strains . For large experiments, 2 mL cultures were utilized to test large number of cultures and were inoculated to an $OD_{600}$ =2.5, and larger volume cultures were inoculated to an $OD_{600}$ = 0.1. Cultures were incubated for two to eight days at 30 $^o$C with constant agitation. 2 mL cultures were incubated in a rotary drum (CT-7, New Brunswick Scientific) at speed seven. Flasks

were shaken at 225 rpm in a standing incubator, and bioreactors were agitated by rotor at no less than 250 rpm and no more than 800 rpm.  To harvest, one $OD_{600}$ unit of culture was spun down at 1000 x g for three minutes and resuspended in 500 μL Phosphate Buffered Saline solution (PBS) (Sigma Aldrich).  6 μL of 1 mM Nile Red (dissolved in DMSO) was added, and then cells were incubated in the dark at room temperature for 15 minutes.  Cells were spun down at 1000 x g for three minutes, resuspended in 800 μL ice cold water, spun down again, and resuspended again in 800 μL ice cold water.  300 μL of stained cells was added to 1ml ice cold water and tested with a FACS Fortessa (BD Biosciences), a voltage of 350, a 10,000 cell count, a forward scatter of 125, a side scatter of 125, and the 535LP and 585/42BP filters for fluorescence detection using the GFP fluorochrome.  Samples were kept on ice and in the dark during the test and fluorescence data was analyzed using FlowJo software (Tree Star Inc., Ashland, OR) to compute mean fluorescence values. Day-to-day variability was mitigated by analyzing all comparable strains on the same day.  An average fluorescence and standard deviation were calculated from the mean values of biological replicates.  Stained cells were routinely examined with fluorescence microscopy under a 100X oil immersion objective using the FITC channel on an Axiovert 200M microscope (Zeiss).

### 8.1.5 Bioreactor fermentations

Bioreactor fermentations were run in minimal media (described above) as batch processes.  All fermentations were inoculated to an initial OD600 = 0.1 in 1.5L of media. Dissolved oxygen was maintained at 50% of maximum by varying rotor speed between 250 rpm and 800 rpm with a constant air input flow rate of 2.5 v/v/m. PH was maintained

at 3.5 or above with 2.5M NaOH, and temperature was maintained at 28 $^{\circ}$C. 10-15 mL samples were taken every twenty-four hours.

### 8.1.4 Lipid, biomass and glucose quantification from samples

Lipids from approximate 2mg dry weight culture were extracted following the procedure described by Folch et al. (224) and modified for yeast (225). Lipid weights were determined through gravity method. For biomass, 500ul culture were washed and dried overnight in 65 $^{\circ}$C until the weight become constant. Glucose concentrations were measured with supernant from bioreactor samples using Glucose (HK) Assay Kit (Sigma GAHK) following the manufacturer instruction.

### 8.2 Materials and methods for Chapter 2

### 8.2.1 Calculation of codon adaptation index

Codon Adaption Indices were calculated for the hrGFP, mStrawberry, EGFP, and yECitrine genes using the CAIcal server (226) and the codon usage table for *Y. lipolytica* available on the Codon Usage Database(227).

### 8.2.2 Plasmid construction

Detailed information for primers can be found in **Table 8.1**.

Construction of endogenous promoter fluorescence cassettes : All plasmids employed for gene expression in *Y. lipolytica* were centromeric, replicative vectors based off plasmid pSl16-Cen1-1(227), which was initially modified to include a new multicloning site and redubbed pMCSCen1 (85). The cyc1 terminator (cyc1t) was amplified from p416-TEF-yECitrine (16, 228) and inserted into pMCSCen1 with an

EcoNI/BlpI digestion to form pMCScyc1t. Endogenous promoters EXP1, GPAT, GPD, TEF, YAT1, FBA and XPR2 were amplified from *Yarrowia lipolytica* PO1f genomic DNA and ligated into pMCScyc1t using XmaI/AscI for FBA and BstBI/AscI for the rest to form pMCS-Promoter serial constructs. Reporter genes including yECitine (16), mStrawberry (pmstrawberry, Clonetech), EGFP (229), hrGFP (pIRES-hrGFP, Agilent) and lacZ (230) were amplified and inserted into appropriate pMCS-Promoter constructs to form different pMCS-Promoter-Reporter constructs.

Constructions of $UAS1B_1$-Leum through $UAS1B_{32}$-Leum expression cassettes: Leum (minimal leucine promoter) was amplified from *Y. lipolytica* genomic DNA and ligated into pUC19 plasmid using SphI/HindIII. Following that, serial and reciprocal insertions of UAS1B (upstream activating sequence 1B) elements were performed with different restriction sites to form $pUC-UAS1B_n$-Leum plasmids. $UAS1B_n$-Leum promoter elements were cut out using BstBI/AscI and inserted upstream of hrGFP and lacZ reporter genes in pMCS-Promoter-Reporter constructs (pMCS-hrGFP and pMCS-lacZ).

Construction of TEF-based promoters and expression cassettes: TEF serial truncation promoters, including TEF(1004), TEF(804), TEF(604), TEF(504), TEF, TEF(203), TEF(136), were amplified from *Yarrowia lipolytica* PO1f genomic DNA and inserted in the pUC19 vector (pUC-TEF(n)) and further digested with BstBI/AscI and ligated into pMCS-hrGFP to form pTEF(n)-hrGFP. $UAS1B_8$ and $UAS1B_{16}$ fragments were cut out from the appropriate vectors and ligated into pUC19 vectors to form pUC-$UAS1B_{8/16}$. TEF truncation promoters were amplified and inserted into these vectors

149

using HindIII/AscI resulting in pUC-UAS1B$_{8/16}$-TEF(n) vectors.  UAS1B$_{8/16}$-TEF(n) promoters were cut out and ligated into the pMCS-hrGFP vector to form pUAS1B$_{8/16}$-TEF(n)-hrGFP.

## 8.2.3 Promoter characterization with flow cytometry

*Y. lipolytica* PO1f strains, transformed with different plasmids, were inoculated directly from glycerol stock (in biological duplicate or triplicate) in YSC-LEU media for 48 hours at 30$^o$C with shaking, and then normalized to an OD$_{600}$ of 0.03 in 2ml fresh YSC-LEU and incubated for another 48 hours at 30$^o$C in a rotary drum (CT-7, New Brunswick Scientific) at speed seven.  To harvest, the cultures were spun down at 500g for five minutes, washed in cold water, and resuspended in 5ml ice cold water before testing with a FACSCalibur (BD Biosciences) using 488nm excitation; FL1 detector; and 10,000 cell count for hrGFP detection.  Standard, optimized protocols were used for other reporter proteins tested in this chapter.  The samples were kept on ice during the test and the data was analyzed using FlowJo software (Tree Star Inc., Ashland, OR) to compute mean fluorescence values.

## 8.2.4 Promoter characterization through β–galactosidase assay

*Y. lipolytica* PO1f strains, transformed with different plasmids, were inoculated directly from glycerol stock (in biological triplicate) in YSC-LEU media for 48 hours at 30$^o$C in a rotary drum (CT-7, New Brunswick Scientific) at speed seven, and then normalized to an OD$_{600}$ of 0.03 in 2ml fresh YSC-LEU and incubated for another 48 hours in the same conditions.  The cultures were washed twice in 1ml Z buffer , resuspended in 1 ml of Z buffer, and their OD$_{600}$ readings were recorded (93-94).  β-

galactosidase assays were performed as described by Miller (93) using 10μl of

chloroform-permeabilized cells, with a reaction length of 17 minutes.

### 8.2.5 Promoter characterization through qRT-PCR

*Y. lipolytica* PO1f strains, transformed with different plasmids, were inoculated

directly from glycerol stock (in biological triplicate) in YSC-LEU media for 48 hours at

$30^{o}C$ with shaking, and normalized to an $OD_{600} = 0.03$ in 2ml fresh YSC-LEU media and

incubated for another 48 hours at $30^{o}C$ in a rotary drum (CT-7, New Brunswick Scientific)

at speed seven. The cells were pelleted and total RNA was extracted using the

RiboPureTM-Yeast Kit (Ambion). 1000ng of RNA from each sample was used for a

reverse transcription reaction with the High-Capacity cDNA Reverse Transcription Kit

(Applied Biosystems). A 1.2μl sample from each reaction was used to set up a qPCR

reaction (in triplicate) with FastStart SYBR Green Master (Roche) using primers 5'-

TCAGCGACTTCTTCATCCAGAGCTTC-3' and 5'-

ACACGAACATCTCCTCGATCAGGTTG-3' as described in the manual with a non-

template control. The reactions were run with Applied Biosystems 7900HT Fast Real-

Time PCR System (Applied Biosystems) using fast 96 well plates (Applied Biosystems).

The data was analyzed with ABI 7900HTsequence detection systems (version 2.4;

Applied Biosystems).

### 8.2.6 Plasmid stability test

*Y. lipolytica* PO1f strains containing plasmids pUAS1B$_{12}$-Leum-hrGFP or

pUAS1B$_{16}$-Leum-hrGFP were grown for 48 hours from glycerol stock and thereafter

subcultured in fresh YSC-LEU media at an $OD_{600}=0.01$ every 48 hours. After a total

continuous culture time of 192 hours, corresponding to 36 cell doublings, yeast cells were

miniprepped to extract the plasmid.  Individual plasmids were isolated by transformation

into *E. coli*, and sequencing and restriction enzymes digests of isolated plasmids were

used to confirm the stability of the UAS1B$_{12}$-Leum and UAS1B$_{16}$-Leum promoters over

this timeframe.

Table 8.1 Primers used for Chapter 2

| Primer | Sequence (5'-3') |
| --- | --- |
| JB085 | CGGGATCCCCCCCGGGAATTCGAATTGGCGCGCCCCTTAATT AAGGCACGTGCCTAAAAAAGGCGGACCGGGCTTAGCTTGTTT AAACAACTGCAGTTTT |
| JB088 | GGTTCGAAGACGCAGTAGGATGTCCTGCA |
| JB089 | TTGGCGCGCCGTTGATGTGTGTTTAATTCAAGAATGA |
| JB090 | GG TTCGAAATAAGTTTGCAAAAAGATCGTATTATAGT |
| JB091 | TTGGCGCGCCTTGTGAATTAGGGTGGTGAGA |
| JB092 | TCCCCCCGGGTAAACAGTGTACGCAGTACTATAGA |
| JB093 | TTGGCGCGCCGGAGAGCTGGGTTAGTTTGT |
| JB094 | GG TTCGAACAACTTTTCTTGTCGACCTGAGAT |
| JB095 | TTGGCGCGCCTTAGCGTGTCGTGTTTTTGTTGT |
| JB096 | GGTTCGAAGGAGTTTGGCGCCCGTTTTT |
| JB097 | TTGGCGCGCCTGCTGTAGATATGTCTTGTGTGTAAGGG |
| JB099 | AAAACTGCAGTTGTTTAAACAAGCTAAGCCCGGTCCGCCTT TTTTAGGCACGTGCCTTAATTAAGGGGCGCGCCAATTCGAA TTCCCGGGCCGGATCCCG |
| JB102 | GGCCTAAAAAAGGATCGATACCGTCGACCTCGAG |
| JB103 | GGGCTTAGCCGAGCGTCCCAAAACCTTCTC |
| JB153 | TTGGCGCGCCATGGTGAGCAAGGGCGAGGA |
| JB155 | CCTTAATTAACTACTTGTACAGCTCGTCCATGCC |
| JB156 | TTGGCGCGCCATGTCTAAAGGTGAAGAATTATTCA |
| JB158 | CCTTAATTAATTATTTGTACAATTCATCCATACCA |
| JB160 | TTGGCGCGCCATGGTGAGCAAGCAGATCCTGAAG |
| JB161 | CCTTAATTAATTACACCCACTCGTGCAGGC |
| JB162 | ACATGTGCATGCACTGATCACGGGCAAAAGTGCGTATATAT |
| JB163 | CAACCCAAGCTTTTAGTTTCGGGTTCCATTGTGG |

Table 8.1 cont.

JB164      GACACGCGTCGACCTGAGGTGTCTCACAAGTGC
JB165      GACACATGCATGCCCGGATCGAGGTGGGCGGG
JB166      GACACATGCATGCGAGCTCCCGGATCGAGGTGGGCGGG
JB167      CGCGGATCCCTGAGGTGTCTCACAAGTGCC
JB168      GACACGCGTCGACCCGGATCGAGGTGGGCGGG
JB169      CACACACGAGCTCCTAGTCTAGACTGAGGTGTCTCACAAGTGCC
JB170      CGCGGATCCCCGGATCGAGGTGGGCGGG
JB171      CACACACGAGCTCCTGAGGTGTCTCACAAGTGCC
JB172      CTAGTCTAGACCGGATCGAGGTGGGCGGG
JB173      CCGGAATTCCTGAGGTGTCTCACAAGTGCC
JB174      CACACACGAGCTCCTGAGGTGTCTCACAAGTGC
JB177      CTGAGGTGTCTCACAAGTGCCGTGCAGTCCCGCCCCCACTT
               GCTTCTCTTTGTGTGTAGTGTACGTACATTATCGAGA
               CCGTTGTTCCCGCCCACCTCGATCCGG
JB178      CCGGATCGAGGTGGGCGGGAACAACGGTCTCGATAA
               TGTACGTACACTACACACAAAGAGAAGCAAGTGGGG
               GCGGGACTGCACGGCACTTGTGAGACACCTCAG
JB249      CATATGCGGTGTGAAATACCGC
JB250      GGAATTCGGGTACCAACTGCAGTTCGAAACTGGCCGTCGTT
               TTACAAC
JB251      AAGCTTCAGGCGCGCCATCATGGTCATAGCTGTTTCCTG
JB252      CCCACATGTTCTTTCCTGCGTTATCC
JB253      GGAATTCAACTGCAGACTGGCCGTCGTTTTACAAC
JB254      ACATACATGCATGCGGTACCCGGGCAAAAGTGCGTATAT
               ATACAA
JB289      GGAATTCCATATGTGTAAAACGACGGCCAGTTTCGAAGGT
               ACCAAGGAAGCATGCCTGCAGAAGCTTGGGAAGA
JB290      TCTTCCCAAGCTTCTGCAGGCATGCTTCCTTGGTACCT
               TCGAAACTGGCCGTCGTTTTACACATATGGAATTCC
JB311      TTGGCGCGCCATGACCATGATTACGGATTCACTG
JB312      ACTGTTGGCGCGCCACCATGATTACGGATTCACTGGC
JB313      CCTTAATTAATTATTTTTGACACCAGACCAACTGG
LQ9        CCAATTGGTTCGAAATGTCCCAACTTGCCAAATT
LQ10       CCAATTGGTTCGAAATTGCACCCCAGCCAGACCG
LQ12       CCAATTGGTTCGAATTGCGTTTCGCTCCCACAC
LQ13       CCAATTGGTTCGAATCTGTAAAAGTCTCTACAAG
LQ14       CCAATTGGTTCGAATTGTGGTTGGGACTTTAG
LQ15       CCAATTGGTTCGAATTTCTTTGTCTGGCCATC
LQ16       CCAATTGGTTCGAACCCACACTTGCCGTTAAG
LQ17       TTAAAGCTTAGAGACCGGGTTGGCG
LQ18       TATAAGCTTGGCGCGCCTCATTTTGAATGATTCTTATAC

Table 8.1 cont.

| | |
|---|---|
| LQ19 | CCAATTGGTTCGAACGGGCAAAAGTGCGTAT |
| LQ20 | TTGGCGCGCCTGAAGCTTTTAGTTTCG |
| LQ25 | CCAATTGGAAGCTTATGTCCCAACTTGCCAAATT |
| LQ26 | CCAATTGGAAGCTTATTGCACCCCAGCCAGACCG |
| LQ28 | CCAATTGGAAGCTTTTGCGTTTCGCTCCCACAC |
| LQ29 | CCAATTGGAAGCTTTCTGTAAAAAGTCTCTACAAG |
| LQ30 | CCAATTGGAAGCTTTTGTGGTTGGGACTTTAG |
| LQ31 | CCAATTGGAAGCTTTTTCTTTGTCTGGCCATC |
| LQ32 | CCAATTGGAAGCTTCCCACACTTGCCGTTAAG |

## 8.3 Materials and methods for Chapter 3

### 8.3.1 Plasmid construction

Primer sequences can be found in the primer list in **Table 8.2**. All plasmids employed for gene expression in *Y. lipolytica* were centromeric, replicative vectors based on plasmid pSl16-Cen1-1(227) (85), which was initially modified to pMCSCEN1 (103). Promoters with partial open reading frame TEF(404), TEF(272), TEF(136) (primer pair LQ105/LQ110, LQ106/LQ110, LQ107/LQ110), GPD (LQ125/LQ126), EXP (LQ127/LQ128), POT1 (LQ123/LQ124), CDC2 (LQ172/LQ173), MET2 (LQ170/LQ171), YOX1 (LQ178/LQ179) were amplified from *Y. lipolytica* PO1f genomic DNA and ligated into pMCSCEN1 by using KpnI/NdeI and then digested out Promoter-CEN region with NdeI/BstBI and ligated into pMCSUAS1B16-LeumhrGFP (103). CDC2 and POT1-CEN regions were digested out with BglII/XmaI and ligated into pMCSUAS1B16-LeumlacZ and pMCSEXPlacZ (103).

### 8.3.2 Plasmid characterization with flow cytometry

*Y. lipolytica* PO1f strains, transformed with different plasmids, were inoculated directly from glycerol stock (in biological triplicate) in YSC-LEU media for 48 hours at $30^{\circ}$C with shaking, and then normalized to an $OD_{600}$ of 0.03 in 2ml fresh YSC-LEU and

incubated for another 48 hours at 30$^\circ$C in a rotary drum (CT-7, New Brunswick Scientific) at speed seven. To harvest, the cultures were spun down at 500g for five minutes, washed in cold water, and resuspended in 5ml ice cold water before testing with a FACS LSRFortessa (BD Biosciences) using 488nm excitation; FL1 detector; and 10,000 cell count for hrGFP detection. The samples were kept on ice during the test and the data was analyzed using FlowJo software (Tree Star Inc., Ashland, OR) to compute mean fluorescence values. The sorting was performed with FACSAria Cell Sorter (BD Biosciences) using the same setting to collect 10^6 cells from two subpopulation.

### 8.3.3 Plasmid characterization through β–galactosidase assay

*Y. lipolytica* PO1f strains, transformed with different plasmids, were inoculated directly from glycerol stock (in biological triplicate) in YSC-LEU media for 48 hours at 30$^\circ$C in a rotary drum (CT-7, New Brunswick Scientific) at speed seven, and then normalized to an OD$_{600}$ of 0.03 in 2ml fresh YSC-LEU and incubated for another 48 hours in the same conditions. The cells were characterized using Gal-Screen™ β-Galactosidase Reporter Gene Assay System for Yeast or Mammalian Cells (life technologies) following manufacturer's manual.

### 8.3.4 Plasmid copy number characterization through qRT-PCR

*Y. lipolytica* PO1f strains, transformed with different plasmids, were inoculated directly from glycerol stock (in biological triplicate) in YSC-LEU media for 48 hours at 30$^\circ$C with shaking, and normalized to an OD$_{600}$ = 0.03 in 2ml fresh YSC-LEU media and incubated for another 48 hours at 30$^\circ$C in a rotary drum (CT-7, New Brunswick Scientific) at speed seven. Plasmid copy numbers were quantified using quantitative PCR (qPCR) from the total DNA extracts. Total DNA extraction was performed as described previously (107). Lyticase from Arthrobacter luteus was purchased from Sigma Aldrich (St. Louis, MO). Quantitative PCR was performed on a ViiA7 qPCR system (Life Technologies, Carlsbad, CA) using SYBR Green Master Mix from Roche (Penzberg, Germany) with primer set 5'-TCAGCGACTTCTTCATCCAGAGCTTC-3' and 5'-

ACACGAACATCTCCTCGATCAGGTTG-3', following the manufacturer's instructions with an annealing temperature of 58 ℃ and 1 μL of total DNA extract per 20-μL reaction volume.

Table 8.2 Primers used for Chapter 3

| Primer | Descriptions | Sequences |
|--------|-------------|-----------|
| LQ105 | Translation elongation factor EF-1α promoter (P-TEF) forward primer | ACTGCATATG AGAGACCGGGTTGGCG |
| LQ106 | Truncated translation elongation factor EF-1α promoter (P-TEF(272)) forward primer | ACTGCATATG CCCACACTTGCCGTTAAG |
| LQ107 | Truncated translation elongation factor EF-1α promoter (P-TEF(136)) forward primer | ACTGCATATG TTGTGGTTGGGACTTTAG |
| LQ110 | Translation elongation factor EF-1α promoter (P-TEF) reverse primer | ACTGGGTACC AACGTGAGTCTTTTCC |
| LQ123 | 3-ketoacyl-CoA thiolase, peroxisomal promoter (P-POT1) forward primer | GTACATATG GGAGGCGACGTGGCAG |
| LQ124 | 3-ketoacyl-CoA thiolase, peroxisomal promoter (P-POT1) reverse primer | TACGGTACC TTGGCGGGGTTCTGCTC |
| LQ125 | Glyceraldehyde-3-phosphate dehydrogenase promoter (P-GPD) forward primer | GTACATATG ATGATAGTTGGGGGTGTG |
| LQ126 | Glyceraldehyde-3-phosphate dehydrogenase promoter (P-GPD) reverse primer | TACGGTACC GCCTCGACCTTGCCCTTG |
| LQ127 | Export protein (P-EXP1) forward primer | GTACATATG GGAGTTTGGCGCCCGTT |
| LQ128 | Export protein (P-EXP1) reverse primer | TACGGTACC GCAAACATGAAAATGAG |
| LQ170 | homoserine O-acetyltransferase possible transmembrane segment (P-MET2) forward primer | GTACATATG AAACTCGCGAGAAAAAAAG |
| LQ171 | homoserine O-acetyltransferase possible transmembrane segment (P-MET2) reverse primer | TACGGTACC AGTCCCGAGAAGGGGTTTTC |
| LQ172 | CDC2 DNA-directed DNA polymerase delta catalytic 125 KD subunit (P-CDC2) forward primer | GTACATATG AAAACAGGAAAAGCGCA |
| LQ173 | CDC2 DNA-directed DNA polymerase delta catalytic 125 KD subunit (P-CDC2) reverse primer | TACGGTACC ACGTCGTCGCCCGTTCGC |
| LQ178 | YOX1 homoeodomain protein (p-YOX1) forward primer | GTACATATG GTACAATGATCCGGGCG |
| LQ179 | YOX1 homoeodomain protein (p-YOX1) reverse primer | TACGGTACC GACGAGGTCTCGTGCTTG |

## 8.4 Materials and methods for Chapter 4

### 8.4.1 Base strains and media

**Table 8.3** contains a complete list of PO1f derivatives produced in this chapter. *Y. lipolytica* was cultivated at 30 $^{\circ}$C unless otherwise stated with constant agitation. 2 mL cultures of *Y. lipolytica* used in large-scale screens were grown in a rotary drum (CT-7, New Brunswick Scientific) at speed seven, and larger culture volumes were shaken in flasks at 225 rpm or fermented in a bioreactor.

YSC media consisted of 20 g/L glucose (Fisher Scientific), 0.79 g/L CSM supplement (MP Biomedicals), and 6.7 g/L Yeast Nitrogen Base w/o amino acids (Becton, Dickinson, and Company). YSC-URA, YSC-LEU, and YSC-LEU-URA media contained 0.77 g/L CSM-Uracil, 0.69 g/L CSM-Leucine, or 0.67 g/L CSM-Leucine-Uracil in place of CSM, respectively. YPD media contained 10 g/L yeast extract (Fisher Scientific), 20 g/L peptone (Fisher Scientific) and 20 g/L glucose, and was often supplemented with 300 μg mL$^{-1}$ Hygromycin B (Invitrogen) for knockout selection. Lipid accumulation response towards media formulation was investigated by cultivation in varying concentrations of glucose and nitrogen. These media formulations contained 0.79 g/L CSM, 1.7 g/L Yeast Nitrogen Base w/o amino acid and w/o $(NH_4)_2SO_4$ (Becton, Dickinson, and Company), between 20 g/L and 160 g/L glucose, and between 0.2 g/L and 5 g/L ammonium sulfate - $(NH_4)_2SO_4$ (Fisher Scientific) – which corresponds to between 0.055 g/L and 1.365 g/L ammonium. Minimal media formulations utilized for bioreactor fermentations typically contained 80 g/L glucose and 6.7 g/L Yeast Nitrogen Base w/o

amino acids (1.7 g/L YNB and 5 g/L $(NH_4)_2SO_4$).  When utilizing alternative carbon

sources, glucose was replaced by 80 g/L arabinose (Fisher Scientific), 80 g/L fructose

(Alfa Aesar), 80 g/L galactose (Fisher Scientific), 80 g/L glycerol (Fisher Scientific), 80

g/L mannose (Alfa Aesar), 80 g/L maltose (Acros Organics),  80 g/L ribose (MP

Biomedicals), 80 g/L sucrose (Acros Organics), or 80 g/L Xylose (Acros Organics).

Leucine (MP Biomedicals) and isoleucine (Sigma Aldrich) supplementation was used to

analyze the effect of leucine biosynthetic capacity.  Leucine was added at a concentration

of 0.8 g/L or 1.6 g/L, while isoleucine was added at concentration of 1.6 g/L.  Inhibition

of the TOR protein was caused by supplementation with 200 ng/mL rapamycin (LC

Laboratories).

Table 8.3 Strain information for Chapter 4

| Host Strain Name | Genotype | Reference or Source |
|---|---|---|
| *Escherichia coli* **strains** | | |
| DH10B | F⁻ mcrA Δ(*mrr-hsd*RMS-*mcr*BC) Φ80d*lac*ZΔM15 Δ*lac*X74 *end*A1 *rec*A1 *deo*R Δ(*ara,leu*)7697 *ara*D139 *gal*U *gal*K *nup*G *rps*L λ | OpenBiosystems |
| *Yarrowia lipolytica base* **strains** | | |
| PO1f | MatA, leucine-, uracil-, xpr2-322, axp1-2 | (82) |
| *pex10* | MatA, leucine-, uracil-, xpr2-322, axp1-2, Δmfe1 | (117) |
| *mfe1* | MatA, leucine-, uracil-, xpr2-322, axp1-2, Δpex10 | (117) |
| *pex10 mfe1* | MatA, leucine-, uracil-, xpr2-322, axp1-2, Δpex10, Δmfe1 | This work |
| *Yarrowia lipolytica* **overexpression strains** | | |
| **PO1f background** | | |

Table 8.3 cont.

| | | |
|---|---|---|
| PO1f uracil[+] | MatA, leucine-, uracil+, xpr2-322, axp1-2 | This work |
| PO1f leucine[+] | MatA, leucine+, uracil-, xpr2-322, axp1-2 | This work |
| PO1f leucine[+] uracil[+] | MatA, leucine+, uracil+, xpr2-322, axp1-2 | This work |
| PO1f leucine[+] Epi | MatA, leucine+, uracil-, xpr2-322, axp1-2 | This work |
| PO1f uracil[+] AMPD | MatA, leucine-, uracil+, xpr2-322, axp1-2, AMPD | This work |
| PO1f leucine[+] AMPD | MatA, leucine+, uracil-, xpr2-322, axp1-2, AMPD | This work |
| PO1f uracil[+] MAE | MatA, leucine-, uracil+, xpr2-322, axp1-2, MAE | This work |
| PO1f leucine[+] MAE | MatA, leucine+, uracil-, xpr2-322, axp1-2, MAE | This work |
| PO1f leucine[+] uracil[+] AMPD MAE | MatA, leucine+, uracil+, xpr2-322, axp1-2, AMPD, MAE | This work |
| PO1f leucine[+] DGA1 Epi | MatA, leucine+, uracil-, xpr2-322, axp1-2, DGA1 | This work |
| PO1f leucine[+] DGA2 Epi | MatA, leucine+, uracil-, xpr2-322, axp1-2, DGA2 | This work |
| PO1f leucine[+] DGA1 | MatA, leucine+, uracil-, xpr2-322, axp1-2, DGA1 | This work |
| *mfe1* **background** | | |
| *mfe1* uracil[+] | MatA, leucine-, uracil+, xpr2-322, axp1-2, *mfe1* | This work |
| *mfe1* leucine[+] | MatA, leucine+, uracil-, xpr2-322, axp1-2, *mfe1* | This work |
| *mfe1* leucine[+] uracil[+] | MatA, leucine+, uracil+, xpr2-322, axp1-2, *mfe1* | This work |
| *mfe1* uracil[+] AMPD | MatA, leucine-, uracil+, xpr2-322, axp1-2, *mfe1*, AMPD | This work |
| *mfe1* leucine[+] AMPD | MatA, leucine+, uracil-, xpr2-322, axp1-2, *mfe1*, AMPD | This work |
| *mfe1* uracil[+] MAE | MatA, leucine-, uracil+, xpr2-322, axp1-2, *mfe1*, MAE | This work |

Table 8.3 cont.

| | | |
|---|---|---|
| *mfe1* leucine⁺ MAE | MatA, leucine+, uracil-, xpr2-322, axp1-2, *mfe1*, MAE | This work |
| *mfe1* leucine⁺ uracil⁺ AMPD MAE | MatA, leucine+, uracil+, xpr2-322, axp1-2, *mfe1*, AMPD, MAE | This work |
| *mfe1* leucine⁺ uracil⁺ ACL1 ACL2 | MatA, leucine+, uracil+, xpr2-322, axp1-2, *mfe1*, ACL1, ACL2 | This work |
| *mfe1* leucine⁺ DGA1 Epi | MatA, leucine+, uracil-, xpr2-322, axp1-2, *mfe1*, DGA1 | This work |
| *mfe1* leucine⁺ DGA2 Epi | MatA, leucine+, uracil-, xpr2-322, axp1-2, *mfe1*, DGA2 | This work |
| *mfe1* leucine⁺ DGA1 | MatA, leucine+, uracil-, xpr2-322, axp1-2, *mfe1*, DGA1 | This work |
| *mfe1* leucine⁺ DGA2 | MatA, leucine+, uracil-, xpr2-322, axp1-2, *mfe1*, DGA2 | This work |
| **pex10 background** | | |
| *pex10* uracil⁺ | MatA, leucine-, uracil+, xpr2-322, axp1-2, *pex10* | This work |
| *pex10* leucine⁺ | MatA, leucine+, uracil-, xpr2-322, axp1-2, *pex10* | This work |
| *pex10* leucine⁺ uracil⁺ | MatA, leucine+, uracil+, xpr2-322, axp1-2, *pex10* | This work |
| *pex10* uracil⁺ AMPD | MatA, leucine-, uracil+, xpr2-322, axp1-2, *pex10*, AMPD | This work |
| *pex10* leucine⁺ AMPD | MatA, leucine+, uracil-, xpr2-322, axp1-2, *pex10*, AMPD | This work |
| *pex10* uracil⁺ MAE | MatA, leucine-, uracil+, xpr2-322, axp1-2, *pex10*, MAE | This work |
| *pex10* leucine⁺ MAE | MatA, leucine+, uracil-, xpr2-322, axp1-2, *pex10*, MAE | This work |
| *pex10* leucine⁺ uracil⁺ AMPD MAE | MatA, leucine+, uracil+, xpr2-322, axp1-2, *pex10*, AMPD, MAE | This work |
| *pex10* leucine⁺ DGA1 Epi | MatA, leucine+, uracil-, xpr2-322, axp1-2, *pex10*, DGA1 | This work |
| *pex10* leucine⁺ DGA2 Epi | MatA, leucine+, uracil-, xpr2-322, axp1-2, *pex10*, DGA2 | This work |
| *pex10* leucine⁺ DGA1 | MatA, leucine+, uracil-, xpr2-322, axp1-2, *pex10*, DGA1 | This work |

Table 8.3 cont.

| *pex10 mfe1* **background** | | |
|---|---|---|
| *pex10 mfe1* uracil⁺ | MatA, leucine-, uracil+, xpr2-322, axp1-2, *pex10*, *mfe1* | This work |
| *pex10 mfe1* leucine⁺ | MatA, leucine+, uracil-, xpr2-322, axp1-2, *pex10*, *mfe1* | This work |
| *pex10 mfe1* leucine⁺ uracil⁺ | MatA, leucine+, uracil+, xpr2-322, axp1-2, *pex10*, *mfe1* | This work |
| *pex10 mfe1* uracil⁺ AMPD | MatA, leucine-, uracil+, xpr2-322, axp1-2, *pex10*, *mfe1*, AMPD | This work |
| *pex10 mfe1* leucine⁺ AMPD | MatA, leucine+, uracil-, xpr2-322, axp1-2, *pex10*, *mfe1*, AMPD | This work |
| *pex10 mfe1* uracil⁺ MAE | MatA, leucine-, uracil+, xpr2-322, axp1-2, *pex10*, *mfe1*, MAE | This work |
| *pex10 mfe1* leucine⁺ MAE | MatA, leucine+, uracil-, xpr2-322, axp1-2, *pex10*, *mfe1*, MAE | This work |
| *pex10 mfe1* leucine⁺ uracil⁺ AMPD MAE | MatA, leucine+, uracil+, xpr2-322, axp1-2, *pex10*, *mfe1*, AMPD, MAE | This work |
| *pex10 mfe1* leucine⁺ uracil⁺ ACL1 ACL2 | MatA, leucine+, uracil+, xpr2-322, axp1-2, *pex10*, *mfe1*, ACL1, ACL2 | This work |
| *pex10 mfe1* leucine⁺ DGA1 Epi | MatA, leucine+, uracil-, xpr2-322, axp1-2, *pex10*, *mfe1*, DGA1 | This work |
| *pex10 mfe1* leucine⁺ DGA2 Epi | MatA, leucine+, uracil-, xpr2-322, axp1-2, *pex10*, *mfe1*, DGA2 | This work |
| *pex10 mfe1* leucine⁺ uracil⁺ DGA1 Epi | MatA, leucine+, uracil+, xpr2-322, axp1-2, *pex10*, *mfe1*, DGA1 | This work |
| *pex10 mfe1* leucine⁺ DGA1 | MatA, leucine+, uracil-, xpr2-322, axp1-2, *pex10*, *mfe1*, DGA1 | This work |
| *pex10 mfe1* uracil⁺ DGA1 | MatA, leucine+, uracil-, xpr2-322, axp1-2, pex10, mfe1, DGA1 | This work |
| *pex10 mfe1* leucine⁺ uracil⁺ DGA1 | MatA, leucine+, uracil+, xpr2-322, axp1-2, *pex10*, *mfe1*, DGA1 | This work |
| *pex10 mfe1* leucine⁺ uracil⁺ AMPD DGA1 | MatA, leucine+, uracil+, xpr2-322, axp1-2, *pex10*, *mfe1*, AMPD, DGA1 | This work |
| *pex10 mfe1* leucine⁺ uracil⁺ MAE DGA1 | MatA, leucine+, uracil+, xpr2-322, axp1-2, *pex10*, *mfe1*, MAE, DGA1 | This work |

## 8.4.2 Cloning and transformation procedures

All restriction enzymes were purchased from New England Biolabs and all digestions were performed according to standard protocols. PCR reactions were set up with recommended conditions using Phusion high fidelity DNA polymerase (Finnzymes), or LongAmp *Taq* DNA polymerase (New England Biolabs). Ligation reactions were performed overnight at room temperature using T4 DNA Ligase (Fermentas). Gel extractions were performed using the Fermentas GeneJET extraction kit purchased from Fisher ThermoScientific. *E. coli* minipreps were performed using the Zyppy Plasmid Miniprep Kit (Zymo Research Corporation). *E. coli* maxipreps were performed using the Qiagen HiSpeed Plasmid Maxi Kit. Transformation of *E. coli* strains was performed using standard electroporator protocols (223). Large amounts of linearized DNA (>20 μg), necessary for *Y. lipolytica* PO1f transformation were cleaned and precipitated using a standard phenol:chloroform extraction followed by an ethanol precipitation.

Transformation of *Y. lipolytica* with episomal expression plasmids was performed using the Zymogen Frozen EZ Yeast Transformation Kit II (Zymo Research Corporation), with plating on YSC-LEU plates. Transformation of *Y. lipolytica* PO1f with linearized cassettes was performed as described previously (117), with selection on appropriate plates. Briefly, *Y. lipolytica* strains were inoculated from glycerol stock directly into 10 mL YPD media, grown overnight, and harvested at an $OD_{600}$ between 9 and 15 by centrifugation at 1000 x g for 3 minutes. Cells were washed twice in sterile water. $10^8$ cells were dispensed into separate microcentrifuge tubes for each transformation, spun

down, and resuspended in 1.0 mL 100 mM LiOAc.  Cells were incubated with shaking at 30 $^{\circ}$C for 60 minutes, spun down, resuspended in 90 µL 100 mM LiOAc, and placed on ice.  1-5 µg of linearized DNA was added to each transformation mixture in a total volume of 10 µL, followed by 25 µL of 50 mg mL$^{-1}$ boiled salmon sperm DNA (Sigma-Aldrich).  Cells were incubated at 30 $^{\circ}$C for 15 minutes with shaking, before adding 720 µL PEG buffer (50% PEG8000, 100 mM LiOAc, pH = 6.0) and 45 µL 2M Dithiothreitol.  Cells were incubated at 30 $^{\circ}$C with shaking for 60 minutes, heat shocked for 10 minutes in a 39 $^{\circ}$C water bath, spun down and resuspended in 1 mL sterile water.  200 µL of cells were plated on appropriate selection plates.  All auxotrophic or antibiotic selection markers were flanked with LoxP sites to allow for retrieval of integrated markers with the pMCS-UAS1B$_{16}$-TEF-Cre replicative vector (117).

### 8.4.3 Plasmid construction

Primer sequences can be found in the **Table 8. 4**.  All *Y. lipolytica* episomal plasmids were centromeric, replicative vectors derived from  plasmid pSl16-Cen1-1(227) (85) after it had been modified to include a multi-cloning site, a hrGFP green fluorescent reporter gene (pIRES-hrGFP, Agilent) driven by the strong UAS1B$_{16}$-TEF promoter (103), and a cyc1 terminator (228) to create plasmid pMCS-UAS1B$_{16}$-TEF-hrGFP. Integrative plasmids were derived from plasmids pUC-S1-UAS1B$_{16}$-Leum or  pUC-S1-UAS1B$_{16}$-TEF (117) that contained 5' and 3' rDNA integrative sequences surrounding the following elements - (from 5' to 3') a uracil section marker surrounded by LoxP sites for marker retrieval, the strong UAS1B$_{16}$-Leum or UAS1B$_{16}$-TEF promoter, AscI and

164

PacI restriction enzyme sites for gene insertion, and a XPR2 minimal terminator. These integrative plasmids were also designed to contain two identical NotI restriction enzyme sites directly outside of the rDNA regions so that plasmid linearization would simultaneously remove *E. coli* pUC19-based DNA. All plasmids containing expression cassettes were sequenced confirmed before transformation into *Y. lipolytica*.

Table 8.4 Primers used for Chapter 4

| JB320 | actactacgagctcagcggccgcagatcttggtggtagtagcaaa |
|---|---|
| JB387 | Ttggcgcgccatgccgcagcaagcaatgg |
| JB388 | Ccttaattaattaaccatgcagccgctcaaac |
| JB402 | Ttggcgcgccatgtctgccaacgagaacat |
| JB403 | Ttggcgcgcctctgccaacgagaacatctc |
| JB404 | Ccttaattaactatgatcgagtcttggccttg |
| JB405 | Ttggcgcgccatgtcagcgaaatccattcacg |
| JB406 | Ttggcgcgcctcagcgaaatccattcacgag |
| JB407 | Ccttaattaattaaactccgagaggagtggaa |
| JB862 | ccaccgcggataacttcgtataatgtatgctatacgaagttatgagtctttattggtgatgggaaga |
| JB863 | cggttcgaaataacttcgtatagcatacattatacgaagttatcagtcgccagcttaaagatatcta |
| JB911 | cattcaaaggcgcgccatgactatcgactcacaatactaca |
| JB912 | Gcggatccttaattaattactcaatcattcggaactctgg |
| JB913 | Cattcaaaggcgcgccatggaagtccgacgacgaaa |
| JB914 | Gcggatccttaattaactactggttctgcttgtagttgt |
| AH020 | Gactggcgcgccatgttacgactacgaaccatgc |
| AH021 | Gtccttaattaactagtcgtaatcccgcacatg |
| SJB143 | Caaagacgggattttgccac |
| SJB165 | Ggcatgcactgatcacgg |
| SJB165 | Ggcatgcactgatcacgg |
| SJB173 | Catggatctggaggatctcat |
| SJB205 | Ccggtaccgagctccaataa |
| SJB206 | Accgatggctgtgtagaagta |
| SJB234 | gattttgccacctacaagcc |
| SJB234 | gattttgccacctacaagcc |
| SJB234 | gattttgccacctacaagcc |
| SJB249 | Gttttgttcgacttggtatg |
| SJB250 | Gttttggaaacagaaccttc |
| SAH001 | Cttaatgcagcctgaaatgaggt |
| SAH002 | Gcacaaatgacgtggcaaac |
| SAH003 | Tgtatttccgaatgggtgagag |
| SAH004 | Cgagtgtgatcaagagtgtctg |
| SAH019 | Acattgactacattgtcgtgactg |
| SAH023 | Cagtcgccagcttaaagatatcta |
| SAH034 | Ctaacagttaatcttctggtaagcct |

**8.4.4 Construction of episomal expression cassettes**

The following genes were PCR amplified from *Y. lipolytica* PO1f gDNA and inserted into vector pMCS-UAS1B$_{16}$-TEF-hrGFP in place of hrGFP with an AscI/PacI digest: AMPD, ACL subunit 1 (ACL1), ACL subunit 2 (ACL2), MAE1, DGA1, and DGA2 with primers JB387/388, JB402/404, JB405/407, AH020/021, JB911/912, and JB913/914, respectively. This formed plasmids pMCS-UAS1B$_{16}$-TEF-AMPD, pMCS-UAS1B$_{16}$-TEF-ACL1, pMCS-UAS1B$_{16}$-TEF-ACL2, pMCS-UAS1B$_{16}$-TEF-MAE1, pMCS-UAS1B$_{16}$-TEF-DGA1, and pMCS-UAS1B$_{16}$-TEF-DGA2.

A leucine marker containing plasmid containing the Cre-Recombinase gene, pMCS-UAS1B$_{16}$-TEF-Cre enables constitutive, high-level Cre expression(117).

**8.4.5 Construction of integrative expression cassettes**

The following genes were gel extracted from the previously constructed episomal expression vectors and inserted into vector pUC-S1-UAS1B$_{16}$-TEF with an AscI/PacI digest: AMPD, ACL subunit 1 (ACL1), ACL subunit 2 (ACL2), MAE1, DGA1, and DGA2. This formed plasmids pUC-S1-UAS1B$_{16}$-TEF-AMPD, pUC-S1-UAS1B$_{16}$-TEF-ACL1, pUC-S1-UAS1B$_{16}$-TEF-ACL2, pUC-S1-UAS1B$_{16}$-TEF-MAE1, and pUC-S1-UAS1B$_{16}$-TEF-DGA1, and pUC-S1-UAS1B$_{16}$-TEF-DGA2. The loxP-surrounded uracil marker of these integrative plasmids was replaced with a loxP-surrounded leucine marker created by amplification of pMCSCen1 template with primers JB862/863 followed by insertion using a BstBI/SacII digest. These plasmids enabled integrative selection with leucine auxotrophy and co-expression of two enzymes without marker retrieval. These leucine marker integrative plasmids were dubbed plasmids pUC-S2-UAS1B$_{16}$-TEF-

AMPD, pUC-S2-UAS1B$_{16}$-TEF-ACL1, pUC-S2-UAS1B$_{16}$-TEF-ACL2, pUC-S2-UAS1B$_{16}$-TEF-MAE1, and pUC-S2-UAS1B$_{16}$-TEF-DGA1, and pUC-S2-UAS1B$_{16}$-TEF-DGA2. ACL1 and ACL2 were similarly inserted into pUC-S1-UAS1B$_{16}$-Leum with primers JB403/404 and JB406/407, respectively, to form plasmids pUC-S1-UAS1B$_{16}$-Leum-ACL1 and pUC-S1-UAS1B$_{16}$-Leum-ACL2.

**8.4.6 Strain construction**

All strains were confirmed through gDNA extraction and PCR. We previously constructed two markerless single-gene deletion strains in the *Y. lipolytica* PO1f background, PO1f-Δmfe1 and PO1f-Δpex10, deficient in their β-oxidation and peroxisomal biogenesis capacity, respectively (117). Following our previous protocol, the PEX10 gene was deleted from strain PO1f-Δmfe1 to form the markerless double mutant PO1f-Δmfe1-Δpex10. These four strains, referred to as PO1f, *pex10*, *mfe1*, and *pex10 mfe1* were utilized as backgrounds for single and double overexpression of the AMPD, ACL1, ACL2, MAE1, DGA1, and DGA2 proteins, including variation in selective marker utilized, i.e., leucine (chromosomal or episomal expression cassette) vs. uracil (chromosomal expression cassette). Integrative cassettes were linearized, transformed into the four background strains, and selected for on appropriate dropout plates. Integrative vectors without open reading frames to express, pUC-S1-UAS1B$_{16}$-TEF and pUC-S2-UAS1B$_{16}$-TEF, were utilized to create strains with leucine, uracil, or both leucine and uracil prototrophies, but without enzyme overexpression.

**8.4.7 Lipid quantification and fatty acid profile analysis**

Lipids from a 500 μL volume of culture, or approximately 1.0 mg dry cell weight, were extracted following the procedure described by Folch *et al.* (224) and modified for yeast (231). Briefly, *Y. lipolytica* cells were spun down and washed with water twice, and then resuspended in a chloroform/methanol solution (2:1) and vortexed on high with glass beads for 20 minutes. The organic solution was extracted and washed with 0.2 volumes of 0.3% NaCl solution before being dried at 60 $^o$C overnight and weighed to quantify lipid production. Lipids in the culture medium were tested for, but no extracellular lipids were detected. Dry cell weight was determined after washing cells twice with $H_2O$ and drying overnight at 60 $^o$C. The dried lipids were transesterified with N-tert-Butyldimethylsilyl-N-methyltrifluoroacetamide (Sigma-Aldrich) following the procedure of (Paik et al., 2009), and 2 μL samples were injected into a GC-FID (Agilent Technologies 6890 Network GC System) equipped with an Agilent HP-5 column (5% phenyl-95% methylsiloxane - product number 19091J-413) to analyze fatty acid fractions. Briefly, the following settings were used: Detector Temp = 300 $^o$C, He Flow = 1.0 mL min$^{-1}$, Oven Temp = 80 $^o$C for 2 min, increased at 30 $^o$C min$^{-1}$ to 200 $^o$C, increased at 2 $^o$C min$^{-1}$ to 229 $^o$C, increased at 1 $^o$C min$^{-1}$ to 232 $^o$C, increased at 50 $^o$C min$^{-1}$ to 325 $^o$C. Fatty acid standards for C16:0 palmitic acid, C16:1(n-7) palmitoleic acid, C17:0 heptadecanoic acid, C18:0 stearic acid, C18:1(n-9) oleic acid, and C18:2(n-6) linoleic acid were purchased from Sigma-Aldrich, transesterified, and analyzed by GC to identify fatty acid peaks. Similarly, C16:1(n-9) palmitoleic acid was purchased from Cayman Chemical and used a standard. GC-MS confirmation of fatty acid type was performed with a Thermo Scientific TSQ Quantum Triple Quad using chemical ionization and a 1.5

mL min$^{-1}$ flow rate.  Lipid quantification obtained using both methods converge within an error of less than 20%; thus, we determine both methods are suitable for quantifying lipid levels in the cells.

### 8.4.8 Citric acid quantification

A 2 mL culture sample was pelleted down for 5 minutes at 3000 x g, and the supernatant was filtered using a 0.2 mm syringe filter (Corning Incorporated).  Filtered supernatant was analyzed with a HPLC Ultimate 3000 (Dionex) and a Zorbax SB-Aq column (Agilent Technologies).  A 2.0 µL injection volume was used in a mobile phase composed of a 99.5:0.5 ratio of 25 mM potassium phosphate buffer (pH=2.0) to acetonitrile with a flow rate of 1.25 mL min$^{-1}$.  The column temperature was maintained at 30 $^{o}$C and UV–Vis absorption was measured at 210 nm.  A citric acid standard (Sigma-Aldrich) was used to detect and quantify citric acid production.

### 8.4.9 Ammonium quantification

1 mL of culture was heated to 80 $^{o}$C for 15 minutes, and then centrifuged at 17,900 x g for 3 minutes.  Supernatant was stored at 4 $^{o}$C for less than 1 week, and ammonium concentration was determined using the R-Biopharm Ammonium Assay kit following the manufacturer's instructions.  Ammonium Assay kit accuracy was assessed by measuring ammonium concentration in solutions with varying concentrations of Yeast Nitrogen Base w/o amino acids.  Minor necessary adjustments were made using the resulting standard curve.

### 8.4.10 Bioreactor fermentations

Typically, bioreactor fermentations were run in minimal media (described above) as batch processes. However, one fermentation included a spike of an additional 80 g/L glucose at the 72 hour timepoint, and another had a doubled media formulation that contained 160 g/L glucose and 13.4 g/L YNB w/o amino acids. All fermentations were inoculated to an initial $OD_{600} = 0.1$ in 1.5 L of media. Dissolved oxygen was maintained at 50% of maximum by varying rotor speed between 250 rpm and 800 rpm with a constant air input flow rate of 2.5 v $v^{-1}$ $min^{-1}$ (3.75 L $min^{-1}$). PH was maintained at 3.5 or above with 2.5 M NaOH, and temperature was maintained at 28 $^o$C. 10-15 mL samples were taken every twelve hours, and fermentations lasted 6-7 days. We ran several fermentations with suboptimal conditions before settling on the above parameters. Supernatant was diluted 1:10 and glucose concentration was quantified using a YSI Life Sciences Bioanalyzer 7100MBS.

**8.4.11 Transesterification**

*Y. lipolytica* lipid reserves were transesterified using acid-promoted direct methanolysis of cellular biomass (232). 1L of *pex10 mfe1* leucine$^+$ uracil$^+$ DGA1 fermented in a bioreactor for seven days as described above was washed twice in 400 mL water. Cells were dried on a hotplate at 140 $^o$C for 3 hours. The dried cell mass was transesterified with 2% w $v^{-1}$ $H_2SO_4$ in 200 mL methanol at a fast boil with reflux and constant agitation for 72 hours. The reaction mixture was centrifuged to remove cellular debris. FAMEs were extracted from the supernatant by adding 0.2 volumes water, mixing, centrifuging, and removing the polar phase. Additional FAMEs were extracted

in the polar phase with a second extraction using 0.4 volume of water. FAMEs were washed in 1 volume of water and analyzed with TLC and GC.

### 8.4.12 Protein extraction

Protein content from 0.5 to 1.0 mL of culture was extracted using the Pierce BCA Protein Assay Kit following the manufacturer's instructions. Protein concentration (mg mL$^{-1}$) was normalized per mL of culture and per culture OD$_{600}$ to normalize to the individual cellular level. PO1f leucine$^+$ uracil$^+$ and *pex10 mfe1* leucine$^+$ uracil$^+$ DGA1 strains were analyzed in this manner after fermentation in a bioreactor.


## 8.5 Material and Method for Chapter 5

### 8.5.1 Culture media

For testing growth with GABA as a nitrogen source, 1 g/L GABA were added in place of ammonia sulfate. Lipid accumulation was promoted by cultivation in media with high glucose, containing 80 g/L glucose, 0.79 g/L CSM supplement, 6.7 g/L Yeast Nitrogen Base w/ ammonia sulfate w/o amino acid. Minimal media formulations utilized for bioreactor fermentations contained 160 g/L glucose and 13.4 g/L Yeast Nitrogen Base w/ ammonia sulfate w/o amino acids (3.4 g/L YNB and 10 g/L (NH4)$_2$SO$_4$). Solid media for *E. coli* and *Y. lipolytica* were prepared by adding 15 g/L agar (Teknova) to liquid media formulations. Nile Red plates were made by adding 1mM Nile Red (MP biomedicals) stock solution dissolved in DMSO (Fisher Scientific) to a final concentration of 1 μM.

### 8.5.2 Transformation procedures

Transformation of *Y. lipolytica* PO1f with linearized cassettes was performed as described previously (233), with selection on appropriate plates. All auxotrophic or antibiotic selection markers were flanked with LoxP sites to allow for retrieval of integrated markers with the pMCS-UAS1B16-TEF-Cre replicative vector (103).

**8.5.3 Plasmid construction**

Primer sequences can be found in the **Table 8.5**. All *Y. lipolytica* episomal plasmids were centromeric, replicative vectors derived from plasmid pSl16-Cen1-1(227) (85) as described in (103). Integrative plasmids were derived from plasmids pUC-S1-UAS1B16-TEF as described in (139). All plasmids containing expression cassettes were sequence-confirmed before transformation into *Y. lipolytica*.

Table 8.5 Primers used for Chapter 5

| Primers | |
|---|---|
| LQ379 YLUGA2up | ACTGGGCGCGCC GTCAGATGGCAGCCCTACATGACG |
| LQ380 YLUGA2up | ACTGGCGGCCGC TGTGTGTGAGAAGGTGCTTACAGAG |
| LQ381 YLUGA2do | ACTGGGCCGGCC GCAAAAATGAGTAGTTTCAAGATT |
| LQ382 YLUGA2do | ACTGGTTTAAAC CAAATATAGATAATAATATAATGTCCGTGA |
| LQ361 UGA2 for | ACTGGCGCGCC ATGTTGCGAGCCCTGAATACCGTC |
| LQ362 UGA2 rev | ACT TTAATTAA GATTAAGGCTGAATGTGGGGCTCGAC |
| LQ363 YOX1 for | ACT CCGCGG ATGGATCTGGCGAAAATCACCGA |
| LQ364 YOX1 rev | ACT TTAATTAA TTACCATCGTCCTCCGTTTCGAA |
| LQ365 OSH6 for | ACT GGCGCGCC ATGCACCACCACCTCAACCCCAA |
| LQ366 OSH6 rev | ACT TTAATTAA CTACTGGGCGTCGTGGAACTCGT |

**8.5.4 EMS mutagenesis and high lipid population enrichment**

The EMS mutagenesis procedures were performed following the protocol described by Winston (234). Briefly, an overnight culture was cultivated to OD around 10. Cells were then harvested, washed and suspended with 0.1M sodium phosphate buffer (pH=7). 30 μl of EMS was added and incubated along with an unmutagenized control for 1 hour at 30 ℃, with agitation. The cells were then washed with 5% sodium thiosulfate and prepared for serial transfer experiments to enrich the high lipid population.

The EMS treated cells and unmutagenized cells starting OD approximately equals 5 were first cultured YSC media for 72 hours and then cultured in high glucose media (containing 80 g/L glucose, 0.79 g/L CSM supplement, 6.7 g/L Yeast Nitrogen Base w/ ammonia sulfate w/o amino acid) for 144 hours. High glucose media has been used here to induce lipid accumulation in *Y. lipolytica* (235). The cells were centrifuged down with 100 x g for 2 minutes, the unclear supernatant, which contains enhanced lipogenesis strains, was used as seed for another round of cultivation after pellet down with starting OD approximately equals 0.1. After five rounds of transfer, the cells were plated on Nile Red YSC plate to isolate of high lipid production strains. Individual colonies were picked from the EMS treated cells as well as the unmutagenized but serial transferred cells (spontaneous mutagenesis) for characterization. First round of evolution was performed in 15ml culture tubes with 2ml media with starting OD equals 2.5 and the second round was done in 500ml flask with 100ml media with starting OD equals 0.1.

## 8.5.5 Whole genome sequencing and small nucleotide variation analysis

Next generation sequencing platform Illumina paired ended sequencing PE 2X100 were performed with genomic DNA extracted from strain E26 and E13 by

Genomic Sequencing and Analysis Facility in The University of Texas at Austin.

6,424,381 reads for strain E26 and 6,565,093 reads for strain E13 were collected from

Illumina HiSeq, which lead to a coverage approximately 65X. The illumina reads were

mapped to the CLIB122 genome using BWA (236) and analyzed with Samtools (156)

and BEDTools (157). The SNPs identified were then filtered with SnpSift with

QUAL >= 30 (237). The SNPs identified from PO1f , EMS26 and EMS13 were

compared to extract the authentic SNPs in EMS26 and EMS13. The identified SNPs were

then visualized in the IGV genome visualization software to validate as well as study the

location of the SNPs in the genome due to the high false error rate in SNP calling process

(238).

## 8.5.6 RNA preparation, sequencing and analysis

Samples were taken at the early stationary phase of strain PO1f ura+ leu+ and

E26 (evolved from strain Δpex10, mfe DGA1 ura+ leu+) when growing in with 100ml in

500ml flask (~48 h). Total RNA was extracted by ™ RNA Purification Kit, yeast (Life

technologies) according to the manufacturer's instructions. The RNA quality and quantity

were determined using Agilent 2100 Bioanalyzer (Agilent Technologies, Santa Clara, CA,

USA). The RNA integrity number (RIN) of all RNA samples used for sequencing was

more than 7.0. The RNA samples were then sent to Genomic Sequencing and Analysis

Facility at The University of Texas at Austin for library preparation and sequencing. The

sequencing experiments were performed with using illumina Hiseq single end 100bp

(1X100) platform.

The sequence files in FASTQ format were first groomed with FastQC (239). The RNA-seq single-end reads were analyzed with TopHat and Cufflinks (240). The reads were mapped into transcripts using TopHat by setting the reference genome as *Y. lipolytica* (CLIB122) (65). 18,948,539/19,943,689/18,170,124 reads from triplicates of strain E26 and 18,322,608/20,708,616/18,393,515 reads from triplicates of strain PO1f ura$^+$ leu$^+$ were successfully mapped to the reference sequences. The mapped reads were then analyzed by bedtools (157) and edgeR (192) to identify differentially expressed genes. The differentially expression were further filtered with log2 > 1 (overexpression) or log2 < -1 (downregulation). The gene ontology analysis was performed using DAVID (241) with background setting as *Y. lipolytica*.

## 8.6 Material and Method for Chapter 6

### 8.6.1 Culture media

YSC media was used for starting cultures, consisted of 20 g/L glucose (Fisher Scientific), 0.79 g/L CSM supplement (MP Biomedicals), and 6.7 g/L Yeast Nitrogen Base w/ ammonia sulfate w/o amino acids (Becton, Dickinson, and Company). YSC-LEU media contained 0.69 g/L CSM-Leucine in place of CSM, respectively. Lipid accumulation was promoted by cultivation in media with high glucose, containing 80 g/L glucose, 0.79 g/L CSM supplement, 2 g/L ammonia sulfate and 1.7 g/L Yeast Nitrogen Base w/o ammonia sulfate w/o amino acid for strains with leu$^+$ and ura$^+$ and 160 g/L glucose, 0.79 g/L CSM supplement, 0.2 g/L ammonia sulfate and 1.7 g/L Yeast Nitrogen Base w/o ammonia sulfate w/o amino acid for strains with leu$^+$. YPD media contained 10

g/L yeast extract (Fisher Scientific), 20 g/L peptone (Fisher Scientific) and 20 g/L

glucose, and was often supplemented with 300 μg/ml Hygromycin B (Invitrogen) for

knockout selection. GAA media is the same to YPD media except 50g/L glucose with

5 μM antimycin A (Sigma-Aldrich). The unsaturated fatty acids (UFAs) – oleic (Fisher

Scientific) and palmitoleic acids (Sigma-Aldrich) – were used at a final concentration of

0.5mM each. Minimal media formulations utilized for bioreactor fermentations contained

80 g/L glucose and 3.4 g/L Yeast Nitrogen Base w/o ammonia sulfate w/o amino acids

and 4 g/L $(NH4)_2SO_4$ with another 80g glucose fed at day 3 time point. Solid media for *E.*

*coli* and *Y. lipolytica* were prepared by adding 15 g/L agar (Teknova) to liquid media

formulations. Nile Red plates were made by adding 1mM Nile Red (MP biomedicals)

stock solution dissolved in DMSO (Fisher Scientific) to a final concentration of 1 μM.

## 8.6.2 Plasmid construction

Primer sequences can be found in the **Table 8.6**. *Y.lipolytica* integrative/knockout

related plasmids for DGA1 overexpression and PEX10 knockout were described in (117).

The knockout plasmid for MGA2 was constructed with as described in (117).

Mga2G643R were cloned with primer pair which including 1500 bps upstream to the

start codon to keep its native regulation in plasmids pMCSUAS1B16-TEF as described in

(103) and digested with NdeI/ BamHI to linearized the plasmid for integration. All

plasmids containing expression cassettes were sequence-confirmed before transformation

into *Y. lipolytica*.

Table 8.6 Primers used for Chapter 6

| Primer name | Sequences |
|---|---|
| LQ313 mga2KO upf | ACTGGGCGCGCC gaaaaggaggtggatcgggtatcg |
| LQ314 mga2KO upr | ACTGGCGGCCGC acacgaacaagcggaagaagtctg |
| LQ315 mga2KO downf | ACTGCCCGGG ctgtgttaggtcctggtgctggag |
| LQ316 mga2KO downr | ACTGGTTTAAAC tgaggttgctgtgtatcgcgacc |
| LQ331 ProMga2 f | ATCG CCCGGG atttctcggacgacaagtcgactagc |
| LQ309 Mga2 r | ACTGTTAATTAA tcatgcagcctgggcctgg |

**8.6.3 Whole genome sequencing and small nucleotide variation analysis**

Next generation sequencing platform Illumina paired ended sequencing PE 2X100 were performed with genomic DNA extracted from strain L36 by Genomic Sequencing and Analysis Facility in The University of Texas at Austin. 4,706,014 pair-end reads were collected from Illumina HiSeq, which lead to a coverage approximately 47X. The illumina reads were mapped to the CLIB122 genome using BWA (236) and analyzed with Samtools (156) and BEDTools (157). The SNPs identified were then filtered with SnpSift with QUAL >= 30 (237). The SNPs identified from PO1f (242) and L36 were compared to extract the authentic SNPs in strain L36. The identified SNPs were then visualized in the IGV genome visualization software to validate as well as study the location of the SNPs in the genome due to the high false error rate in SNP calling process (238).

**8.6.4 RNA-Seq and gene differential expression analysis**

Total RNA was extracted from triplicates from strains PO1f leu$^+$ and PO1f Δmga2

MGA2g1927a leu+ using RiboPure™ RNA Purification Kit for yeast (life technologies)

at 36 hour time point with starting OD equals 0.1 in media with 160 g/L glucose, 0.79 g/L

CSM-LEU supplement and 6.7 g/L Yeast Nitrogen Base w/o amino acid. The polyA

mRNA capture and sequential RNA-Seq library construction and next generation

sequencing platform Illumina paired ended sequencing PE 2X100 were performed by

Genomic Sequencing and Analysis Facility in The University of Texas at Austin. The

sequence files in FASTQ format were first groomed with FastQC (239). The reads were

analyzed with TopHat and Cufflinks (240). 8,194,962/13,338,379/14,861,420 reads of the

triplicates from PO1f leu+ and 12,077,107/6,210,940/13,192,029 reads of the triplicates

from PO1fΔmga2 MGA2(g1927a) leu+ were mapped into transcripts using TopHat by

setting the reference genome as *Y. lipolytica* (CLIB122) (65). The transcripts were

assembled and the FPKM (fragments per kilobase of exon per million fragments mapped)

were estimated using Cufflinks with the default parameter settings, followed by

transcripts merge using Cuffmerge. The assembled transcripts between control group and

experimental group were compared using Cuffdiff. The differential gene expressions

were analyzed with bedtools (157) and edgeR (192) for significant expression with output

bam files from TopHat. The differentially expression were further filtered with log2 > 1

(overexpression) or log2 < -1 (downregulation) with p-value and FDR both < 0.05. The

promoter motifs were analysis with SCOPE (243) and the identified motifs were then

compared with transcriptional factor binding sites sequences in YEASTRACT database

(194). The reference sequences and annotation filed were downloaded from Ensembl

Genomes.

# References

1.      Krivoruchko A, Siewers V, Nielsen J. Opportunities for yeast metabolic engineering: Lessons from synthetic biology. Biotechnology Journal. 2011;6(3):262-76.
2.      Siddiqui MS, Thodey K, Trenchard I, Smolke CD. Advancing secondary metabolite biosynthesis in yeast with synthetic biology tools. Fems Yeast Research. 2012;12(2):144-70.
3.      Curran KA, Alper HS. Expanding the chemical palate of cells by combining systems biology and metabolic engineering. Metab Eng. 2012;14(4):289-97.
4.      Peralta-Yahya PP, Zhang F, del Cardayre SB, Keasling JD. Microbial engineering for the production of advanced biofuels. Nature. 2012;488(7411):320-8.
5.      Lee JW, Na D, Park JM, Lee J, Choi S, Lee SY. Systems metabolic engineering of microorganisms for natural and non-natural chemicals. Nat Chem Biol. 2012;8(6):536-46.
6.      Pickens LB, Tang Y, Chooi YH. Metabolic engineering for the production of natural products. Annu Rev Chem Biomol Eng. 2011;2:211-36.
7.      Dunlop M. Engineering microbes for tolerance to next-generation biofuels. Biotechnology for Biofuels. 2011;4(1):32.
8.      Jeffries TW. Engineering yeasts for xylose metabolism. Curr Opin Biotechnol. 2006;17(3):320-6.
9.      Liu L, Redden H, Alper HS. Frontiers of yeast metabolic engineering: diversifying beyond ethanol and Saccharomyces. Current Opinion in Biotechnology. 2013;24(6):1023-30.
10.     Hu B, Lidstrom M. Metabolic engineering of Methylobacterium extorquens AM1 for 1-butanol production. Biotechnology for Biofuels. 2014;7(1):156.
11.     Xu P, Li L, Zhang F, Stephanopoulos G, Koffas M. Improving fatty acids production by engineering dynamic pathway regulation and metabolic control. Proceedings of the National Academy of Sciences. 2014;111(31):11299-304.
12.     Leonard E, Ajikumar PK, Thayer K, Xiao W-H, Mo JD, Tidor B, et al. Combining metabolic and protein engineering of a terpenoid biosynthetic pathway for overproduction and selectivity control. Proceedings of the National Academy of Sciences. 2010;107(31):13654-9.
13.     Thodey K, Galanie S, Smolke CD. A microbial biomanufacturing platform for natural and semisynthetic opioids. Nat Chem Biol. 2014;10(10):837-44.
14.     Ro D-K, Paradise EM, Ouellet M, Fisher KJ, Newman KL, Ndungu JM, et al. Production of the antimalarial drug precursor artemisinic acid in engineered yeast. Nature. 2006;440(7086):940-3.
15.     Blazeck J, Alper HS. Promoter engineering: Recent advances in controlling transcription at the most fundamental level. Biotechnology Journal. 2013;8(1):46-58.
16.     Alper H, Fischer C, Nevoigt E, Stephanopoulos G. Tuning genetic control through promoter engineering. P Natl Acad Sci USA. 2005;102(36):12678-83.

17.     Blazeck J, Garg R, Reed B, Alper HS. Controlling promoter strength and regulation in Saccharomyces cerevisiae using synthetic hybrid promoters. Biotechnology and Bioengineering. 2012;109(11):2884-95.

18.     Curran KA, Crook NC, Karim AS, Gupta A, Wagman AM, Alper HS. Design of synthetic yeast promoters via tuning of nucleosome architecture. Nat Commun. 2014;5.

19.     Karim AS, Curran KA, Alper HS. Characterization of plasmid burden and copy number in Saccharomyces cerevisiae for optimization of metabolic engineering applications. Fems Yeast Research. 2013;13(1):107-16.

20.     Romanos MA, Scorer CA, Clare JJ. Foreign gene expression in yeast: a review. Yeast. 1992;8(6):423-88.

21.     Chen Y, Partow S, Scalcinati G, Siewers V, Nielsen J. Enhancing the copy number of episomal plasmids in Saccharomyces cerevisiae for improved protein production. Fems Yeast Research. 2012;12(5):598-607.

22.     Kim B, Park H, Na D, Lee SY. Metabolic engineering of Escherichia coli for the production of phenol from glucose. Biotechnology Journal. 2014;9(5):621-9.

23.     Tai M, Stephanopoulos G. Engineering the push and pull of lipid biosynthesis in oleaginous yeast Yarrowia lipolytica for biofuel production. Metabolic Engineering. 2013;15(0):1-9.

24.     Xue Z, Sharpe PL, Hong S-P, Yadav NS, Xie D, Short DR, et al. Production of omega-3 eicosapentaenoic acid by metabolic engineering of Yarrowia lipolytica. Nat Biotech. 2013;31(8):734-40.

25.     Guo D, Zhu J, Deng Z, Liu T. Metabolic engineering of Escherichia coli for production of fatty acid short-chain esters through combination of the fatty acid and 2-keto acid pathways. Metabolic Engineering. 2014;22(0):69-75.

26.     Börgel D, van den Berg M, Hüller T, Andrea H, Liebisch G, Boles E, et al. Metabolic engineering of the non-conventional yeast Pichia ciferrii for production of rare sphingoid bases. Metabolic Engineering. 2012;14(4):412-26.

27.     Jiménez A, Santos MA, Pompejus M, Revuelta JL. Metabolic Engineering of the Purine Pathway for Riboflavin Production in Ashbya gossypii. Applied and Environmental Microbiology. 2005;71(10):5743-51.

28.     Scalcinati G, Partow S, Siewers V, Schalk M, Daviet L, Nielsen J. Combined metabolic engineering of precursor and co-factor supply to increase alpha-santalene production by Saccharomyces cerevisiae. Microbial Cell Factories. 2012;11(1):117.

29.     Yao L, Qi F, Tan X, Lu X. Improved production of fatty alcohols in cyanobacteria by metabolic engineering. Biotechnology for Biofuels. 2014;7(1):94.

30.     Scalcinati G, Otero JM, Van Vleet JRH, Jeffries TW, Olsson L, Nielsen J. Evolutionary engineering of Saccharomyces cerevisiae for efficient aerobic xylose consumption. Fems Yeast Research. 2012;12(5):582-97.

31.     Smith KM, Liao JC. An evolutionary strategy for isobutanol production strain development in Escherichia coli. Metabolic Engineering. 2011;13(6):674-81.

32.     Nevoigt E. Progress in Metabolic Engineering of Saccharomyces cerevisiae. Microbiology and Molecular Biology Reviews. 2008;72(3):379-412.

33.      Hong K-K, Nielsen J. Recovery of Phenotypes Obtained by Adaptive Evolution through Inverse Metabolic Engineering. Applied and Environmental Microbiology. 2012;78(21):7579-86.

34.      Zhu X, Tan Z, Xu H, Chen J, Tang J, Zhang X. Metabolic evolution of two reducing equivalent-conserving pathways for high-yield succinate production in Escherichia coli. Metabolic Engineering. 2014;24(0):87-96.

35.      Santos CNS, Xiao W, Stephanopoulos G. Rational, combinatorial, and genomic approaches for engineering L-tyrosine production in Escherichia coli. Proceedings of the National Academy of Sciences. 2012;109(34):13538-43.

36.      Dmytruk KV, Yatsyshyn VY, Sybirna NO, Fedorovych DV, Sibirny AA. Metabolic engineering and classic selection of the yeast Candida famata (Candida flareri) for construction of strains with enhanced riboflavin production. Metabolic Engineering. 2011;13(1):82-8.

37.      Graf A, Dragosits M, Gasser B, Mattanovich D. Yeast systems biotechnology for the production of heterologous proteins. Fems Yeast Research. 2009;9(3):335-48.

38.      Koboldt DC, Steinberg KM, Larson DE, Wilson RK, Mardis ER. The next-generation sequencing revolution and its impact on genomics. Cell. 2013;155(1):27-38. PMCID: 3969849.

39.      Hong K-K, Vongsangnak W, Vemuri GN, Nielsen J. Unravelling evolutionary strategies of yeast for improving galactose utilization through integrated systems level analysis. Proceedings of the National Academy of Sciences. 2011;108(29):12179-84.

40.      Caspeta L, Chen Y, Ghiaci P, Feizi A, Buskov S, Hallström BM, et al. Altered sterol composition renders yeast thermotolerant. Science. 2014;346(6205):75-8.

41.      Eswaran J, Horvath A, Godbole S, Reddy SD, Mudvari P, Ohshiro K, et al. RNA sequencing of cancer reveals novel splicing alterations. Sci Rep. 2013;3.

42.      Trapnell C, Williams BA, Pertea G, Mortazavi A, Kwan G, van Baren MJ, et al. Transcript assembly and quantification by RNA-Seq reveals unannotated transcripts and isoform switching during cell differentiation. Nat Biotech. 2010;28(5):511-5.

43.      Wu JQ, Wang X, Beveridge NJ, Tooney PA, Scott RJ, Carr VJ, et al. Transcriptome Sequencing Revealed Significant Alteration of Cortical Promoter Usage and Splicing in Schizophrenia. PLoS ONE. 2012;7(4):e36351.

44.      Feng X, Zhao H. Investigating host dependence of xylose utilization in recombinant Saccharomyces cerevisiae strains using RNA-seq analysis. Biotechnology for Biofuels. 2013;6(1):96.

45.      Ravin N, Eldarov M, Kadnikov V, Beletsky A, Schneider J, Mardanova E, et al. Genome sequence and analysis of methylotrophic yeast Hansenula polymorpha DL1. BMC Genomics. 2013;14(1):837.

46.      Schirmer A, Rude MA, Li X, Popova E, del Cardayre SB. Microbial Biosynthesis of Alkanes. Science. 2010;329(5991):559-62.

47.      Zhang F, Ouellet M, Batth TS, Adams PD, Petzold CJ, Mukhopadhyay A, et al. Enhancing fatty acid production by the expression of the regulatory transcription factor FadR. Metabolic Engineering. 2012;14(6):653-60.

48.      Lennen RM, Pfleger BF. Microbial production of fatty acid-derived fuels and chemicals. Current Opinion in Biotechnology. 2013;24(6):1044-53.

49.      Beller HR, Goh E-B, Keasling JD. Genes Involved in Long-Chain Alkene Biosynthesis in Micrococcus luteus. Applied and Environmental Microbiology. 2010;76(4):1212-23.

50.      Liu Y, Wang C, Yan J, Zhang W, Guan W, Lu X, et al. Hydrogen peroxide-independent production of alpha-alkenes by OleTJE P450 fatty acid decarboxylase. Biotechnology for Biofuels. 2014;7(1):28.

51.      Steen EJ, Kang Y, Bokinsky G, Hu Z, Schirmer A, McClure A, et al. Microbial production of fatty-acid-derived fuels and chemicals from plant biomass. Nature. 2010;463(7280):559-62.

52.      Hamilton ML, Haslam RP, Napier JA, Sayanova O. Metabolic engineering of Phaeodactylum tricornutum for the enhanced accumulation of omega-3 long chain polyunsaturated fatty acids. Metabolic Engineering. 2014;22(0):3-9.

53.      Rywińska A, Rymowicz W. High-yield production of citric acid by *Yarrowia lipolytica* on glycerol in repeated-batch bioreactors. Journal of Industrial Microbiology & Biotechnology. 2010;37(5):431-5.

54.      Beopoulos A, Chardot T, Nicaud JM. Yarrowia lipolytica: A model and a tool to understand the mechanisms implicated in lipid accumulation. Biochimie. 2009;91(6):692-6.

55.      Beopoulos A, Mrozova Z, Thevenieau F, Le Dall MT, Hapala I, Papanikolaou S, et al. Control of Lipid Accumulation in the Yeast *Yarrowia lipolytica*. Applied and Environmental Microbiology. 2008;74(24):7779-89.

56.      Beopoulos A, Cescut J, Haddouche R, Uribelarrea JL, Molina-Jouve C, Nicaud JM. *Yarrowia lipolytica* as a model for bio-oil production. Progress in Lipid Research. 2009;48(6):375-87.

57.      Papanikolaou S, Muniglia L, Chevalot I, Aggelis G, Marc I. Yarrowia lipolytica as a potential producer of citric acid from raw glycerol. Journal of Applied Microbiology. 2002;92(4):737-44.

58.      Yu Z, Du G, Zhou J, Chen J. Enhanced α-ketoglutaric acid production in Yarrowia lipolytica WSH-Z06 by an improved integrated fed-batch strategy. Bioresource Technology. 2012;114(0):597-602.

59.      Andre A, Chatzifragkou A, Diamantopoulou P, Sarris D, Philippoussis A, Galiotou-Panayotou M, et al. Biotechnological conversions of bio-diesel-derived crude glycerol by Yarrowia lipolytica strains. Eng Life Sci. 2009;9(6):468-78.

60.      Barth G, Gaillardin C. Physiology and genetics of the dimorphic fungus Yarrowia lipolytica. Fems Microbiology Reviews. 1997;19(4):219-37.

61.      Fickers P, Benetti PH, Wache Y, Marty A, Mauersberger S, Smit MS, et al. Hydrophobic substrate utilisation by the yeast Yarrowia lipolytica, and its potential applications. Fems Yeast Research. 2005;5(6-7):527-43.

62.      Muller S, Sandal T, Kamp-Hansen P, Dalboge H. Comparison of expression systems in the yeasts Saccharomyces cerevisiae, Hansenula polymorpha, Klyveromyces

lactis, Schizosaccharomyces pombe and Yarrowia lipolytica. Cloning of two novel promoters from Yarrowia lipolytica. Yeast. 1998;14(14):1267-83.

63.     Madzak C, Gaillardin C, Beckerich JM. Heterologous protein expression and secretion in the non-conventional yeast Yarrowia lipolytica: a review. Journal of Biotechnology. 2004;109(1-2):63-81.

64.     Dominguez A, Ferminan E, Sanchez M, Gonzalez FJ, Perez-Campo FM, Garcia S, et al. Non-conventional yeasts as hosts for heterologous protein production. Int Microbiol. 1998;1(2):131-42.

65.     Dujon B, Sherman D, Fischer G, Durrens P, Casaregola S, Lafontaine I, et al. Genome evolution in yeasts. Nature. 2004;430(6995):35-44.

66.     Sherman D, Durrens P, Iragne F, Beyne E, Nikolski M, Souciet JL. Genolevures complete genomes provide data and tools for comparative genomics of hemiascomycetous yeasts. Nucleic Acids Research. 2006;34:D432-D5.

67.     Davidow LS, Apostolakos D, Odonnell MM, Proctor AR, Ogrydziak DM, Wing RA, et al. INTEGRATIVE TRANSFORMATION OF THE YEAST YARROWIA-LIPOLYTICA. Current Genetics. 1985;10(1):39-48.

68.     Fournier P, Abbas A, Chasles M, Kudla B, Ogrydziak DM, Yaver D, et al. Colocalization of centromeric and replicative functions on autonomously replicating sequences isolated from the yeast Yarrowia lipolytica. Proceedings of the National Academy of Sciences. 1993;90(11):4912-6.

69.     Chen DC, Yang BC, Kuo TT. ONE-STEP TRANSFORMATION OF YEAST IN STATIONARY PHASE. Current Genetics. 1992;21(1):83-4.

70.     Fickers P, Le Dall MT, Gaillardin C, Thonart P, Nicaud JM. New disruption cassettes for rapid gene disruption and marker rescue in the yeast Yarrowia lipolytica. J Microbiol Methods. 2003;55(3):727-37.

71.     Vernis L, Abbas A, Chasles M, Gaillardin CM, Brun C, Huberman JA, et al. An origin of replication and a centromere are both needed to establish a replicative plasmid in the yeast Yarrowia lipolytica. Molecular and Cellular Biology. 1997;17(4):1995-2004.

72.     Vernis L, Poljak L, Chasles M, Uchida K, Casarégola S, Käs E, et al. Only Centromeres Can Supply the Partition System Required for ARS Function in the Yeast Yarrowia lipolytica. J Mol Biol. 2001;305(2):203-17.

73.     Matsuoka M, Matsubara M, Daidoh H, Imanaka T, Uchida K, Aiba S. ANALYSIS OF REGIONS ESSENTIAL FOR THE FUNCTION OF CHROMOSOMAL REPLICATOR SEQUENCES FROM YARROWIA-LIPOLYTICA. Mol Gen Genet. 1993;237(3):327-33.

74.     Juretzek T, Le Dall MT, Mauersberger S, Gaillardin C, Barth G, Nicaud JM. Vectors for gene expression and amplification in the yeast *Yarrowia lipolytica*. Yeast. 2001;18(2):97-113.

75.     Vanheerikhuizen H, Ykema A, Klootwijk J, Gaillardin C, Ballas C, Fournier P. HETEROGENEITY IN THE RIBOSOMAL-RNA GENES OF THE YEAST YARROWIA-LIPOLYTICA - CLONING AND ANALYSIS OF 2 SIZE CLASSES OF REPEATS. Gene. 1985;39(2-3):213-22.

76.     Dulermo T, Nicaud J-M. Involvement of the G3P shuttle and β-oxidation pathway in the control of TAG synthesis and lipid accumulation in Yarrowia lipolytica. Metabolic Engineering. 2011;13(5):482-91.

77.     Nevoigt E, Kohnke J, Fischer CR, Alper H, Stahl U, Stephanopoulos G. Engineering of promoter replacement cassettes for fine-tuning of gene expression in Saccharomyces cerevisiae. Applied and Environmental Microbiology. 2006;72(8):5266-73.

78.     Pfleger BF, Pitera DJ, D Smolke C, Keasling JD. Combinatorial engineering of intergenic regions in operons tunes expression of multiple genes. Nature Biotechnology. 2006;24(8):1027-32.

79.     Deboer HA, Comstock LJ, Vasser M. The Tac Promoter - a Functional Hybrid Derived from the Trp and Lac Promoters. P Natl Acad Sci-Biol. 1983;80(1):21-5.

80.     Rosenberg S, Tekamp-olson P, inventors; Chiron Corporation (Emeryville, CA), assignee. Enhanced yeast transcription employing hybrid GAPDH promoter region constructs. United States. 1992.

81.     Mukai H, Horii H, Tsujikawa M, Kawabe H, Arimura H, Suyama T, inventors; GREEN CROSS CORPORATION (3-3, Imabashi 1-chome Chuo-ku, Osaka-shi, Osaka, JP), assignee. Yeast promoter and process for preparing heterologous protein. Europe. 1992.

82.     Madzak C, Treton B, Blanchin-Roland S. Strong hybrid promoters and integrative expression/secretion vectors for quasi-constitutive expression of heterologous proteins in the yeast Yarrowia lipolytica. J Mol Microb Biotech. 2000;2(2):207-16.

83.     Madzak C, Blanchin-Roland S, Otero RRC, Gaillardin C. Functional analysis of upstream regulating regions from the Yarrowia lipolytica XPR2 promoter. Microbiol-Uk. 1999;145:75-87.

84.     Blanchinroland S, Otero RRC, Gaillardin C. 2 Upstream Activation Sequences Control the Expression of the Xpr2 Gene in the Yeast Yarrowia-Lipolytica. Molecular and Cellular Biology. 1994;14(1):327-38.

85.     Yamane T, Sakai H, Nagahama K, Ogawa T, Matsuoka M. Dissection of centromeric DNA from yeast *Yarrowia lipolytica* and identification of protein-binding site required for plasmid transmission. J Biosci Bioeng. 2008;105(6):571-8.

86.     Gasmi N, Fudalej F, Kallel H, Nicaud J-M. A molecular approach to optimize hIFN α2b expression and secretion in Yarrowia lipolytica. Appl Microbiol Biotechnol. 2011;89(1):109-19.

87.     Haas J, Park EC, Seed B. Codon usage limitation in the expression of HIV-1 envelope glycoprotein. Current Biology. 1996;6(3):315-24.

88.     Nicaud JM, Fabre E, Becherich JM, Fournier P, Gaillardin C. Cloning, sequencing and amplification of the alkaline extracellular protease (XPR2) gene of the yeast Yarrowia lipolytica. Journal of Biotechnology. 1989;12(3-4):285-97.

89.     Damude HGH, DE, US), Gillies, Peter John (Landenberg, PA, US), Macool, Daniel Joseph (Philadelphia, PA, US), Picataggio, Stephen K. (Landenberg, PA, US), Pollak, Dana Walters M. (Media, PA, US), Ragghianti, James John (Bear, DE, US), Xue, Zhixiong (Chadds Ford, PA, US), Yadav, Narendra S. (Chadds Ford, PA, US), Zhang,

Hongxiang (Chadds Ford, PA, US), Zhu, Quinn Qun (West Chester, PA, US), inventor High eicosapentaenoic acid producing strains of Yarrowia lipolytica. United States. 2006.
90.     Sumita T, Iida T, Yamagami S, Horiuchi H, Takagi M, Ohta A. YlALK1 encoding the cytochrome P450ALK1 in *Yarrowia lipolytica* is transcriptionally induced by n-alkane through two distinct cis-elements on its promoter. Biochem Biophys Res Commun. 2002;294(5):1071-8.
91.     Endoh-Yamagami S, Hirakawa K, Morioka D, Fukuda R, Ohta A. Basic helix-loop-helix transcription factor heterocomplex of Yas1p and Yas2p regulates cytochrome P450 expression in response to alkanes in the yeast Yarrowia lipolytica. Eukaryotic Cell. 2007;6(4):734-43.
92.     Yamagami S, Morioka D, Fukuda R, Ohta A. A basic helix-loop-helix transcription factor essential for cytochrome P450 induction in response to alkanes in yeast Yarrowia lipolytica. Journal of Biological Chemistry. 2004;279(21):22183-9.
93.     Miller JH. Experiments in molecular genetics. [Cold Spring Harbor, N.Y.]: Cold Spring Harbor Laboratory; 1972.
94.     Gaillardin C, Ribet AM. LEU2 directed expression of beta-galactosidase activity and phleomycin resistance in Yarrowia lipolytica. Curr Genet. 1987;11(5):369-75.
95.     Young E, Alper H. Synthetic biology: tools to design, build, and optimize cellular processes. J Biomed Biotechnol. 2010;2010:130781. PMCID: 2817555.
96.     Liu L, Reed B, Alper H. From Pathways to Genomes and Beyond: The Metabolic Engineering Toolbox and Its Place in Biofuels Production. Green. 2011;1(1):81-95.
97.     Juretzek T, Wang H, Nicaud JM, Mauersberger S, Barth G. Comparison of Promoters Suitable for Regulated Overexpression of β-Galactosidase in the Alkane-Utilizing Yeast *Yarroiwa lipolytica*. Biotechnol Bioprocess Eng. 2000;5:320-6.
98.     Juretzek T, Wang H-J, Nicaud J-M, Mauersberger S, Barth G. Comparison of promoters suitable for regulated overexpression of β-galactosidase in the alkane-utilizing yeastYarrowia lipolytica. Biotechnology and Bioprocess Engineering. 2000;5(5):320-6.
99.     Le Dall M-T, Nicaud J-M, Gaillardin C. Multiple-copy integration in the yeast Yarrowia lipolytica. Current Genetics. 1994;26(1):38-44.
100.    Ghosh SK, Hajra S, Paek A, Jayaram M. Mechanisms for Chromosome and Plasmid Segregation. Annual Review of Biochemistry. 2006;75(1):211-41.
101.    Chlebowicz-Śledziewska E, Śledziewski AZ. Construction of multicopy yeast plasmids with regulated centromere function. Gene. 1985;39(1):25-31.
102.    Blazeck J, Reed B, Garg R, Gerstner R, Pan A, Agarwala V, et al. Generalizing a hybrid synthetic promoter approach in Yarrowia lipolytica. Appl Microbiol Biotechnol. 2013;97(7):3037-52.
103.    Blazeck J, Liu L, Redden H, Alper H. Tuning Gene Expression in Yarrowia lipolytica by a Hybrid Promoter Approach. Applied and Environmental Microbiology. 2011;77(22):7905-14.
104.    Wittenberg C, Reed SI. Cell cycle-dependent transcription in yeast: promoters, transcription factors, and transcriptomes. Oncogene. 2005;24(17):2746-55.
105.    Spellman PT, Sherlock G, Zhang MQ, Iyer VR, Anders K, Eisen MB, et al. Comprehensive Identification of Cell Cycle–regulated Genes of the Yeast

Saccharomyces cerevisiae by Microarray Hybridization. Molecular Biology of the Cell. 1998;9(12):3273-97.

106.     Cho RJ, Campbell MJ, Winzeler EA, Steinmetz L, Conway A, Wodicka L, et al. A Genome-Wide Transcriptional Analysis of the Mitotic Cell Cycle. Molecular Cell. 1998;2(1):65-73.

107.     Moriya H, Shimizu-Yoshida Y, Kitano H. In Vivo Robustness Analysis of Cell Division Cycle Genes in Saccharomyces cerevisiae. PLoS Genet. 2006;2(7):e111.

108.     Zhang FZ, Carothers JM, Keasling JD. Design of a dynamic sensor-regulator system for production of chemicals and fuels derived from fatty acids. Nature Biotechnology. 2012;30(4):354-60.

109.     Atsumi S, Hanai T, Liao JC. Non-fermentative pathways for synthesis of branched-chain higher alcohols as biofuels. Nature. 2008;451(7174):86-9.

110.     Li Q, Du W, Liu DH. Perspectives of microbial oils for biodiesel production. Appl Microbiol Biotechnol. 2008;80(5):749-56.

111.     Lu XF, Vora H, Khosla C. Overproduction of free fatty acids in *E. coli*: Implications for biodiesel production. Metabolic Engineering. 2008;10(6):333-9.

112.     Rodolfi L, Zittelli GC, Bassi N, Padovani G, Biondi N, Bonini G, et al. Microalgae for Oil: Strain Selection, Induction of Lipid Synthesis and Outdoor Mass Cultivation in a Low-Cost Photobioreactor. Biotechnology and Bioengineering. 2009;102(1):100-12.

113.     Alvarez HM, Mayer F, Fabritius D, Steinbuchel A. Formation of intracytoplasmic lipid inclusions by *Rhodococcus opacus* strain PD630. Archives of Microbiology. 1996;165(6):377-86.

114.     Dellomonaco C, Clomburg JM, Miller EN, Gonzalez R. Engineered reversal of the beta-oxidation cycle for the synthesis of fuels and chemicals. Nature. 2011;476(7360):355-U131.

115.     Makri A, Fakas S, Aggelis G. Metabolic activities of biotechnological interest in *Yarrowia lipolytica* grown on glycerol in repeated batch cultures. Bioresource Technology. 2010;101(7):2351-8.

116.     Fontanille P, Kumar V, Christophe G, Nouaille R, Larroche C. Bioconversion of volatile fatty acids into lipids by the oleaginous yeast *Yarrowia lipolytica*. Bioresource Technology. 2012;114:443-9.

117.     Blazeck J, Liu L, Knight R, Alper HS. Heterologous production of pentane in the oleaginous yeast Yarrowia lipolytica. Journal of Biotechnology. 2013;165(3–4):184-94.

118.     Barth G, Gaillardin C. *Yarrowia lipolytica*. In: Wolf K, editor. Nonconventional Yeasts in Biotechnology: A Handbook: Springer; 1996. p. 313-88.

119.     Zhang H, Zhang L, Chen H, Chen Y, Ratledge C, Song Y, et al. Regulatory properties of malic enzyme in the oleaginous yeast, Yarrowia lipolytica, and its non-involvement in lipid accumulation. Biotechnology Letters. 2013;35(12):2091-8.

120.     Rodríguez-Frómeta RA, Gutiérrez A, Torres-Martínez S, Garre V. Malic enzyme activity is not the only bottleneck for lipid accumulation in the oleaginous fungus *Mucor circinelloides*. Appl Microbiol Biotechnol. 2013;97(7):3063-72.

121.     Vorapreeda T, Thammarongtham C, Cheevadhanarak S, Laoteng K. Alternative routes of acetyl-CoA synthesis identified by comparative genomic analysis: involvement in the lipid production of oleaginous yeast and fungi. Microbiology. 2012;158:217-28.

122.     Caspi R, Altman T, Dreher K, Fulcher CA, Subhraveti P, Keseler IM, et al. The MetaCyc database of metabolic pathways and enzymes and the BioCyc collection of pathway/genome databases. Nucleic Acids Research. 2012;40(D1):D742-D53.

123.     Beopoulos A, Haddouche R, Kabran P, Dulermo T, Chardot T, Nicaud JM. Identification and characterization of DGA2, an acyltransferase of the DGAT1 acyl-CoA:diacylglycerol acyltransferase family in the oleaginous yeast *Yarrowia lipolytica*. New insights into the storage lipid metabolism of oleaginous yeasts. Appl Microbiol Biotechnol. 2012;93(4):1523-37.

124.     Hong S, Sharpe P, Xue Z, Yadav N, Zhu Q, inventors; E. I. du Pont de Nemours and Company (Wilmington, DE), assignee. Peroxisome biogenesis factor protein (pex) disruptions for altering the content of polyunsaturated fatty acids and the total lipid content in oleaginous eukaryotic organisms. 12/244,950 USA. 2008.

125.     Greenspan P, Mayer EP, Fowler SD. Nile red: a selective fluroscent stain for intracelluluar lipid droplets. Journal of Cell Biology. 1985;100(3):965-73.

126.     Ratledge C. Regulation of lipid accumulation in oleaginous micro-organisms. Biochem Soc Trans. 2002;30:1047-50.

127.     Jimenez-Marti E, Zuzuarregui A, Gomar-Alba M, Gutierrez D, Gil C, del Olmo M. Molecular response of *Saccharomyces cerevisiae* wine and laboratory strains to high sugar stress conditions. International Journal of Food Microbiology. 2011;145(1):211-20.

128.     Botham PA, Ratledge C. A biochemical explanation for lipid accumulation in *Candida* 107 and other oleaginous micro-organisms. Journal of General Microbiology. 1979;114(OCT):361-75.

129.     Evans CT, Ratledge C. Biochemical activities during lipid accumulation in *Candida curvata*. Lipids. 1983;18(9):630-5.

130.     Evans CT, Scragg AH, Ratledge C. A comparative study of citrate efflux from mitochondria of oleaginous and non-oleaginous yeasts. Eur J Biochem. 1983;130(1):195-204.

131.     Atkinson BM, F.;. Biochemical Engineering and Biotechnology Handbook: Palgrave Macmillan; 1983.

132.     Hammond EG, Johnson LA, Su C, Wang T, White PJ. Soybean Oil. In: Shahidi F, editor. Bailey's Industrial Oil and Fat Products. 6 ed: John Wiley & Sons, Inc.; 2005. p. 577-653.

133.     Laplante M, Sabatini DM. An Emerging Role of mTOR in Lipid Biosynthesis. Current Biology. 2009;19(22):R1046-R52.

134.     Sancak Y, Peterson TR, Shaul YD, Lindquist RA, Thoreen CC, Bar-Peled L, et al. The Rag GTPases bind raptor and mediate amino acid signaling to mTORC1. Science. 2008;320(5882):1496-501.

135.     Han JM, Jeong SJ, Park MC, Kim G, Kwon NH, Kim HK, et al. Leucyl-tRNA synthetase is an intracellular leucine sensor for the mTORC1-signaling pathway. Cell. 2012;149(2):410-24.

136.    Bonfils G, Jaquenoud M, Bontron S, Ostrowicz C, Ungermann C, De Virgilio C. Leucyl-tRNA synthetase controls TORC1 via the EGO complex. Mol Cell. 2012;46(1):105-10.

137.    Keasling JD. Manufacturing Molecules Through Metabolic Engineering. Science. 2010;330(6009):1355-8.

138.    Trentacoste EM, Shrestha RP, Smith SR, Glé C, Hartmann AC, Hildebrand M, et al. Metabolic engineering of lipid catabolism increases microalgal lipid accumulation without compromising growth. Proceedings of the National Academy of Sciences. 2013.

139.    Blazeck J, Hill A, Liu L, Knight R, Miller J, Pan A, et al. Harnessing Yarrowia lipolytica lipogenesis to create a platform for lipid and biofuel production. Nat Commun. 2014;5.

140.    Tapia V E, Anschau A, Coradini AL, T Franco T, Deckmann A. Optimization of lipid production by the oleaginous yeast Lipomyces starkeyi by random mutagenesis coupled to cerulenin screening. AMB Express. 2012;2(1):64.

141.    Kamisaka Y, Noda N, Tomita N, Kimura K, Kodaki T, Hosaka K. Identification of Genes Affecting Lipid Content Using Transposon Mutagenesis in Saccharomyces cerevisiae. Bioscience, Biotechnology, and Biochemistry. 2006;70(3):646-53.

142.    Shiwa Y, Fukushima-Tanaka S, Kasahara K, Horiuchi T, Yoshikawa H. Whole-Genome Profiling of a Novel Mutagenesis Technique Using Proofreading-Deficient DNA Polymerase delta. Int J Evol Biol. 2012;2012:860797. PMCID: 3364565.

143.    Beopoulos A, Verbeke J, Bordes F, Guicherd M, Bressy M, Marty A, et al. Metabolic engineering for ricinoleic acid production in the oleaginous yeast Yarrowia lipolytica. Appl Microbiol Biotechnol. 2014;98(1):251-62.

144.    Zhang B, Chen H, Li M, Gu Z, Song Y, Ratledge C, et al. Genetic engineering of Yarrowia lipolytica for enhanced production of trans-10, cis-12 conjugated linoleic acid. Microbial Cell Factories. 2013;12(1):70.

145.    De Pourcq K, Vervecken W, Dewerte I, Valevska A, Van Hecke A, Callewaert N. Engineering the yeast Yarrowia lipolytica for the production of therapeutic proteins homogeneously glycosylated with Man8GlcNAc2 and Man5GlcNAc2. Microbial Cell Factories. 2012;11(1):53.

146.    Gasmi N, Ayed A, Nicaud J-M, Kallel H. Design of an efficient medium for heterologous protein production in Yarrowia lipolytica: case of human interferon alpha 2b. Microbial Cell Factories. 2011;10(1):1-13.

147.    Mlíčková K, Roux E, Athenstaedt K, d'Andrea S, Daum G, Chardot T, et al. Lipid Accumulation, Lipid Body Formation, and Acyl Coenzyme A Oxidases of the Yeast Yarrowia lipolytica. Applied and Environmental Microbiology. 2004;70(7):3918-24.

148.    Ruiz-Herrera J, Sentandreu R. Different effectors of dimorphism in Yarrowia lipolytica. Archives of Microbiology. 2002;178(6):477-83.

149.    Casaregola S, Neuvéglise C, Lépingle A, Bon E, Feynerol C, Artiguenave F, et al. Genomic Exploration of the Hemiascomycetous Yeasts: 17. Yarrowia lipolytica. FEBS Letters. 2000;487(1):95-100.

150.    Zerbino DR, Birney E. Velvet: Algorithms for de novo short read assembly using de Bruijn graphs. Genome Research. 2008;18(5):821-9.

151. Tritt A, Eisen JA, Facciotti MT, Darling AE. An Integrated Pipeline for de Novo Assembly of Microbial Genomes. PLoS ONE. 2012;7(9):e42304.

152. Tsai I, Otto T, Berriman M. Improving draft assemblies by iterative mapping and assembly of short reads to eliminate gaps. Genome Biology. 2010;11(4):R41.

153. Assefa S, Keane TM, Otto TD, Newbold C, Berriman M. ABACAS: algorithm-based automatic contiguation of assembled sequences. Bioinformatics. 2009;25(15):1968-9.

154. Stanke M, Waack S. Gene prediction with a hidden Markov model and a new intron submodel. Bioinformatics. 2003;19(suppl 2):ii215-ii25.

155. Conesa A, Götz S, García-Gómez JM, Terol J, Talón M, Robles M. Blast2GO: a universal tool for annotation, visualization and analysis in functional genomics research. Bioinformatics. 2005;21(18):3674-6.

156. Li H, Handsaker B, Wysoker A, Fennell T, Ruan J, Homer N, et al. The Sequence Alignment/Map format and SAMtools. Bioinformatics. 2009;25(16):2078-9.

157. Quinlan AR, Hall IM. BEDTools: a flexible suite of utilities for comparing genomic features. Bioinformatics. 2010;26(6):841-2.

158. Potts PR. The Yin and Yang of the MMS21–SMC5/6 SUMO ligase complex in homologous recombination. DNA Repair. 2009;8(4):499-506.

159. Robinson JT, Thorvaldsdottir H, Winckler W, Guttman M, Lander ES, Getz G, et al. Integrative genomics viewer. Nat Biotech. 2011;29(1):24-6.

160. Gebre S, Connor R, Xia Y, Jawed S, Bush JM, Bard M, et al. Osh6 overexpression extends the lifespan of yeast by increasing vacuole fusion. Cell Cycle. 2012;11(11):2176-88.

161. Ramos F, El Guezzar M, Grenson M, Wiame J-M. Mutations affecting the enzymes involved in the utilization of 4-aminobutyric acid as nitrogen source by the yeast Saccharomyces cerevisiae. Eur J Biochem. 1985;149(2):401-4.

162. Bach B, Meudec E, Lepoutre J-P, Rossignol T, Blondin B, Dequin S, et al. New Insights into γ-Aminobutyric Acid Catabolism: Evidence for γ-Hydroxybutyric Acid and Polyhydroxybutyrate Synthesis in Saccharomyces cerevisiae. Applied and Environmental Microbiology. 2009;75(13):4231-9.

163. Roy A, Kucukural A, Zhang Y. I-TASSER: a unified platform for automated protein structure and function prediction. Nat Protocols. 2010;5(4):725-38.

164. Yuan Z, Yin B, Wei D, Yuan YA. Structural basis for cofactor and substrate selection by cyanobacterium succinic semialdehyde dehydrogenase. Journal of Structural Biology. 2013;182(2):125-35.

165. Fong SS, Burgard AP, Herring CD, Knight EM, Blattner FR, Maranas CD, et al. In silico design and adaptive evolution of Escherichia coli for production of lactic acid. Biotechnology and Bioengineering. 2005;91(5):643-8.

166. Jiang L-Y, Chen S-G, Zhang Y-Y, Liu J-Z. Metabolic evolution of Corynebacterium glutamicum for increased production of L-ornithine. BMC Biotechnology. 2013;13(1):47.

167. Evans CT, Ratledge C. Effect of Nitrogen Source on Lipid Accumulation in Oleaginous Yeasts. Journal of General Microbiology. 1984;130(7):1693-704.

168. Cao J, Barbosa JM, Singh NK, Locy RD. GABA shunt mediates thermotolerance in Saccharomyces cerevisiae by reducing reactive oxygen production. Yeast. 2013;30(4):129-44.

169. Kamei Y, Tamura T, Yoshida R, Ohta S, Fukusaki E, Mukai Y. GABA metabolism pathway genes, UGA1 and GAD1, regulate replicative lifespan in Saccharomyces cerevisiae. Biochemical and Biophysical Research Communications. 2011;407(1):185-90.

170. Fendt S-M, Bell EL, Keibler MA, Olenchock BA, Mayers JR, Wasylenko TM, et al. Reductive glutamine metabolism is a function of the α-ketoglutarate to citrate ratio in cells. Nat Commun. 2013;4.

171. Coleman ST, Fang TK, Rovinsky SA, Turano FJ, Moye-Rowley WS. Expression of a Glutamate Decarboxylase Homologue Is Required for Normal Oxidative Stress Tolerance in Saccharomyces cerevisiae. Journal of Biological Chemistry. 2001;276(1):244-50.

172. Cardenas ME, Cutler NS, Lorenz MC, Di Como CJ, Heitman J. The TOR signaling cascade regulates gene expression in response to nutrients. Gene Dev. 1999;13(24):3271-9.

173. Staschke KA, Dey S, Zaborske JM, Palam LR, McClintick JN, Pan T, et al. Integration of General Amino Acid Control and Target of Rapamycin (TOR) Regulatory Pathways in Nitrogen Assimilation in Yeast. Journal of Biological Chemistry. 2010;285(22):16893-911.

174. Alper H, Miyaoku K, Stephanopoulos G. Construction of lycopene-overproducing E. coli strains by combining systematic and combinatorial gene knockout targets. Nat Biotech. 2005;23(5):612-6.

175. Zhang F, Carothers JM, Keasling JD. Design of a dynamic sensor-regulator system for production of chemicals and fuels derived from fatty acids. Nat Biotech. 2012;30(4):354-9.

176. Alper H, Stephanopoulos G. Global transcription machinery engineering: a new approach for improving cellular phenotype. Metab Eng. 2007;9(3):258-67.

177. Alper H, Moxley J, Nevoigt E, Fink GR, Stephanopoulos G. Engineering yeast transcription machinery for improved ethanol tolerance and production. Science. 2006;314(5805):1565-8.

178. Henry SA, Kohlwein SD, Carman GM. Metabolism and Regulation of Glycerolipids in the Yeast Saccharomyces cerevisiae. Genetics. 2012;190(2):317-49.

179. Seip J, Jackson R, He H, Zhu Q, Hong S-P. Snf1 Is a Regulator of Lipid Accumulation in Yarrowia lipolytica. Applied and Environmental Microbiology. 2013;79(23):7360-70.

180. Wang C-W, Lee S-C. The ubiquitin-like (UBX)-domain-containing protein Ubx2/Ubxd8 regulates lipid droplet homeostasis. Journal of Cell Science. 2012;125(12):2930-9.

181. Wang Z-P, Xu H-M, Wang G-Y, Chi Z, Chi Z-M. Disruption of the MIG1 gene enhances lipid biosynthesis in the oleaginous yeast Yarrowia lipolytica ACA-DC 50109.

Biochimica et Biophysica Acta (BBA) - Molecular and Cell Biology of Lipids. 2013;1831(4):675-82.

182.    Kandasamy P, Vemula M, Oh C-S, Chellappa R, Martin CE. Regulation of Unsaturated Fatty Acid Biosynthesis in Saccharomyces: THE ENDOPLASMIC RETICULUM MEMBRANE PROTEIN, Mga2p, A TRANSCRIPTION ACTIVATOR OF THE OLE1 GENE, REGULATES THE STABILITY OF THE OLE1 mRNA THROUGH EXOSOME-MEDIATED MECHANISMS. Journal of Biological Chemistry. 2004;279(35):36586-92.

183.    Hoppe T, Matuschewski K, Rape M, Schlenker S, Ulrich HD, Jentsch S. Activation of a Membrane-Bound Transcription Factor by Regulated Ubiquitin/Proteasome-Dependent Processing. Cell. 2000;102(5):577-86.

184.    Shi X, Li J, Zou X, Greggain J, Rødkær SV, Færgeman NJ, et al. Regulation of lipid droplet size and phospholipid composition by stearoyl-CoA desaturase. Journal of Lipid Research. 2013;54(9):2504-14.

185.    Zhang S, Skalsky Y, Garfinkel DJ. MGA2 or SPT23 Is Required for Transcription of the Δ9 Fatty Acid Desaturase Gene, OLE1, and Nuclear Membrane Integrity in Saccharomyces cerevisiae. Genetics. 1999;151(2):473-83.

186.    Zhang S, Burkett TJ, Yamashita I, Garfinkel DJ. Genetic redundancy between SPT23 and MGA2: regulators of Ty-induced mutations and Ty1 transcription in Saccharomyces cerevisiae. Molecular and Cellular Biology. 1997;17(8):4718-29.

187.    Jiang Y, Vasconcelles MJ, Wretzel S, Light A, Martin CE, Goldberg MA. MGA2 Is Involved in the Low-Oxygen Response Element-Dependent Hypoxic Induction of Genes inSaccharomyces cerevisiae. Molecular and Cellular Biology. 2001;21(18):6161-9.

188.    Micolonghi C, Ottaviano D, Di Silvio E, Damato G, Heipieper HJ, Bianchi MM. A dual signalling pathway for the hypoxic expression of lipid genes, dependent on the glucose sensor Rag4, is revealed by the analysis of the KlMGA2 gene in Kluyveromyces lactis. Microbiology. 2012;158(Pt 7):1734-44.

189.    Kaliszewski P, Szkopińska A, Ferreira T, Świezewska E, Berges T, Zołądek T. Rsp5p ubiquitin ligase and the transcriptional activators Spt23p and Mga2p are involved in co-regulation of biosynthesis of end products of the mevalonate pathway and triacylglycerol in yeast Saccharomyces cerevisiae. Biochimica et Biophysica Acta (BBA) - Molecular and Cell Biology of Lipids. 2008;1781(10):627-34.

190.    Letunic I, Doerks T, Bork P. SMART 7: recent updates to the protein domain annotation resource. Nucleic Acids Research. 2012;40(D1):D302-D5.

191.    Wesolowski-Louvel M, Goffrini P, Ferrero I, Fukuhara H. Glucose transport in the yeast Kluyveromyces lactis. I. Properties of an inducible low-affinity glucose transporter gene. Mol Gen Genet. 1992;233(1-2):89-96.

192.    Robinson MD, McCarthy DJ, Smyth GK. edgeR: a Bioconductor package for differential expression analysis of digital gene expression data. Bioinformatics. 2010;26(1):139-40.

193.    Castegna A, Scarcia P, Agrimi G, Palmieri L, Rottensteiner H, Spera I, et al. Identification and Functional Characterization of a Novel Mitochondrial Carrier for

Citrate and Oxoglutarate in Saccharomyces cerevisiae. Journal of Biological Chemistry. 2010;285(23):17359-70.

194.    Teixeira MC, Monteiro PT, Guerreiro JF, Gonçalves JP, Mira NP, dos Santos SC, et al. The YEASTRACT database: an upgraded information system for the analysis of gene and genomic transcription regulation in Saccharomyces cerevisiae. Nucleic Acids Research. 2014;42(D1):D161-D6.

195.    Chellappa R, Kandasamy P, Oh C-S, Jiang Y, Vemula M, Martin CE. The Membrane Proteins, Spt23p and Mga2p, Play Distinct Roles in the Activation of Saccharomyces cerevisiae OLE1 Gene Expression: FATTY ACID-MEDIATED REGULATION OF Mga2p ACTIVITY IS INDEPENDENT OF ITS PROTEOLYTIC PROCESSING INTO A SOLUBLE TRANSCRIPTION ACTIVATOR. Journal of Biological Chemistry. 2001;276(47):43548-56.

196.    Jeffries TW, Grigoriev IV, Grimwood J, Laplaza JM, Aerts A, Salamov A, et al. Genome sequence of the lignocellulose-bioconverting and xylose-fermenting yeast Pichia stipitis. Nat Biotech. 2007;25(3):319-26.

197.    Swaney DL, Beltrao P, Starita L, Guo A, Rush J, Fields S, et al. Global analysis of phosphorylation and ubiquitylation cross-talk in protein degradation. Nat Meth. 2013;10(7):676-82.

198.    Piwko W, Jentsch S. Proteasome-mediated protein processing by bidirectional degradation initiated from an internal site. Nat Struct Mol Biol. 2006;13(8):691-7.

199.    Xiao G, Harhaj EW, Sun S-C. NF-κB-Inducing Kinase Regulates the Processing of NF-κB2 p100. Molecular Cell.7(2):401-9.

200.    Zhu Z, Zhang S, Liu H, Shen H, Lin X, Yang F, et al. A multi-omic map of the lipid-producing yeast Rhodosporidium toruloides. Nat Commun. 2012;3:1112.

201.    Paul D, Magbanua Z, Arick M, French T, Bridges SM, Burgess SC, et al. Genome Sequence of the Oleaginous Yeast Rhodotorula glutinis ATCC 204091. Genome Announcements. 2014;2(1).

202.    Bhattacharya S, Shcherbik N, Vasilescu J, Smith JC, Figeys D, Haines DS. Identification of Lysines within Membrane-Anchored Mga2p120 that Are Targets of Rsp5p Ubiquitination and Mediate Mobilization of Tethered Mga2p90. J Mol Biol. 2009;385(3):718-25.

203.    Lin L, DeMartino GN, Greene WC. Cotranslational dimerization of the Rel homology domain of NF‐κB1 generates p50‐p105 heterodimers and is required for effective p50 production2000.

204.    Nehlin JO, Carlberg M, Ronne H. Yeast SKO1 gene encodes a bZIP protein that binds to the CRE motif and acts as a repressor of transcription. Nucleic Acids Research. 1992;20(20):5271-8.

205.    Alonso-Monge R, Román E, Arana DM, Prieto D, Urrialde V, Nombela C, et al. The Sko1 protein represses the yeast-to-hypha transition and regulates the oxidative stress response in Candida albicans. Fungal Genetics and Biology. 2010;47(7):587-601.

206.    Boer VM, Daran J-M, Almering MJH, de Winde JH, Pronk JT. Contribution of the Saccharomyces cerevisiae transcriptional regulator Leu3p to physiology and gene

expression in nitrogen- and carbon-limited chemostat cultures. FEMS Yeast Research. 2005;5(10):885-97.

207.     Slattery MG, Liko D, Heideman W. The Function and Properties of the Azf1 Transcriptional Regulator Change with Growth Conditions in Saccharomyces cerevisiae. Eukaryotic Cell. 2006;5(2):313-20.

208.     Nguyen LN, Nosanchuk JD. Lipid droplet formation protects against gluco/lipotoxicity in Candida parapsilosis: An essential role of fatty acid desaturase Ole1. Cell Cycle. 2011;10(18):3159-67.

209.     Listenberger LL, Han X, Lewis SE, Cases S, Farese RV, Ory DS, et al. Triglyceride accumulation protects against fatty acid-induced lipotoxicity. Proceedings of the National Academy of Sciences. 2003;100(6):3077-82.

210.     Subramaniam R, Dufreche S, Zappi M, Bajpai R. Microbial lipids from renewable resources: production and characterization. Journal of Industrial Microbiology & Biotechnology. 2010;37(12):1271-87.

211.     Lin J, Li S, Sun M, Zhang C, Yang W, Zhang Z, et al. Microbial lipid production by oleaginous yeast in d-xylose solution using a two-stage culture mode. RSC Advances. 2014;4(66):34944-9.

212.     Klose J, Kronstad JW. The Multifunctional β-Oxidation Enzyme Is Required for Full Symptom Development by the Biotrophic Maize Pathogen Ustilago maydis. Eukaryotic Cell. 2006;5(12):2047-61.

213.     Crespo JL, Hall MN. Elucidating TOR Signaling and Rapamycin Action: Lessons from Saccharomyces cerevisiae. Microbiology and Molecular Biology Reviews. 2002;66(4):579-91.

214.     Courchesne WE, Magasanik B. Regulation of nitrogen assimilation in Saccharomyces cerevisiae: roles of the URE2 and GLN3 genes. Journal of Bacteriology. 1988;170(2):708-13.

215.     Xu S, Falvey DA, Brandriss MC. Roles of URE2 and GLN3 in the proline utilization pathway in Saccharomyces cerevisiae. Molecular and Cellular Biology. 1995;15(4):2321-30.

216.     Papini M, Nookaew I, Uhlen M, Nielsen J. Scheffersomyces stipitis: a comparative systems biology study with the Crabtree positive yeast Saccharomyces cerevisiae. Microbial Cell Factories. 2012;11(1):136.

217.     Lee S-M, Jellison T, Alper HS. Directed Evolution of Xylose Isomerase for Improved Xylose Catabolism and Fermentation in the Yeast Saccharomyces cerevisiae. Applied and Environmental Microbiology. 2012;78(16):5708-16.

218.     Franz AK, Danielewicz MA, Wong DM, Anderson LA, Boothe JR. Phenotypic Screening with Oleaginous Microalgae Reveals Modulators of Lipid Productivity. ACS Chemical Biology. 2013;8(5):1053-62.

219.     Song L, Qin JG, Su S, Xu J, Clarke S, Shan Y. Micronutrient Requirements for Growth and Hydrocarbon Production in the Oil Producing Green Alga Botryococcus braunii (Chlorophyta). PLoS ONE. 2012;7(7):e41459.

220.     Zhao X, Kong X, Hua Y, Feng B, Zhao Z. Medium optimization for lipid production through co-fermentation of glucose and xylose by the oleaginous yeast

Lipomyces starkeyi. European Journal of Lipid Science and Technology. 2008;110(5):405-12.

221.    Galvagno MA, Iannone LJ, Bianchi J, Kronberg F, Rost E, Carstens MR, et al. Optimization of biomass production of a mutant of Yarrowia lipolytica with an increased lipase activity using raw glycerol. Revista argentina de microbiolog á. 2011;43:218-25.

222.    Tomaszewska L, Rymowicz W, Rywińska A. Mineral Supplementation Increases Erythrose Reductase Activity in Erythritol Biosynthesis from Glycerol by Yarrowia lipolytica. Appl Biochem Biotechnol. 2014;172(6):3069-78.

223.    Sambrook J, Russell DW. Molecular cloning : a laboratory manual. 3rd ed. Cold Spring Harbor, N.Y.: Cold Spring Harbor Laboratory Press; 2001.

224.    Folch J, Lees M, Stanley GHS. A simple method for the isolation and purification of total lipids from animal tissues. Journal of Biological Chemistry. 1957;226(1):497-509.

225.    Schneiter R, Daum G. Extraction of Yeast Lipids. In: Xiao W, editor. Yeast Protocol: Humana Press; 2006. p. 41-5.

226.    Puigbo P, Bravo IG, Garcia-Vallve S. CAIcal: A combined set of tools to assess codon usage adaptation. Biology Direct. 2008;3.

227.    Nakamura Y, Gojobori T, Ikemura T. Codon usage tabulated from international DNA sequence databases: status for the year 2000. Nucleic Acids Research. 2000;28(1):292-.

228.    Mumberg D, Muller R, Funk M. Yeast vectors for the controlled expression of heterologous proteins in different genetic backgrounds. Gene. 1995;156(1):119-22.

229.    Sheff MA, Thorn KS. Optimized cassettes for fluorescent protein tagging in Saccharomyces cerevisiae. Yeast. 2004;21(8):661-70.

230.    Kalnins A, Otto K, Ruther U, Muller-Hill B. Sequence of the lacZ gene of Escherichia coli. EMBO J. 1983;2(4):593-7. PMCID: 555066.

231.    Schneiter R, Daum G. Extraction of yeast lipids. Methods in Molecular Biology. 2006;313:41-5.

232.    Liu B, Zhao Z. Biodiesel production by direct methanolysis of oleaginous microbial biomass. Journal of Chemical Technology and Biotechnology. 2007;82(8):775-80.

233.    Gaillardin C, Ribet AM, Heslot H. Integrative transformation of the yeast Yarrowia lipolytica. Current Genetics. 1985;10(1):49-58.

234.    Winston F. EMS and UV Mutagenesis in Yeast.  Current Protocols in Molecular Biology: John Wiley & Sons, Inc.; 2001.

235.    Papanikolaou S, Chatzifragkou A, Fakas S, Galiotou-Panayotou M, Komaitis M, Nicaud J-M, et al. Biosynthesis of lipids and organic acids by Yarrowia lipolytica strains cultivated on glucose. European Journal of Lipid Science and Technology. 2009;111(12):1221-32.

236.    Li H, Durbin R. Fast and accurate short read alignment with Burrows–Wheeler transform. Bioinformatics. 2009;25(14):1754-60.

237.    Pablo C, Viral MP, Melissa C, Tung N, Susan JL, Douglas MR, et al. Using Drosophila melanogaster as a Model for Genotoxic Chemical Mutational Studies with a New Program, SnpSift. Frontiers in Genetics. 2012;3.

238.    Liu Q, Guo Y, Li J, Long J, Zhang B, Shyr Y. Steps to ensure accuracy in genotype and SNP calling from Illumina sequencing data. BMC Genomics. 2012;13(Suppl 8):S8.
239.    Andrews S. FastQC a quality-control tool for high-throughput sequence data. http://wwwbioinformaticsbabrahamacuk/projects/fastqc/.
240.    Trapnell C, Roberts A, Goff L, Pertea G, Kim D, Kelley DR, et al. Differential gene and transcript expression analysis of RNA-seq experiments with TopHat and Cufflinks. Nat Protocols. 2012;7(3):562-78.
241.    Huang DW, Sherman BT, Lempicki RA. Systematic and integrative analysis of large gene lists using DAVID bioinformatics resources. Nat Protocols. 2008;4(1):44-57.
242.    Liu L, Alper HS. Draft Genome Sequence of the Oleaginous Yeast Yarrowia lipolytica PO1f, a Commonly Used Metabolic Engineering Host. Genome Announcements. 2014;2(4).
243.    Carlson JM, Chakravarty A, DeZiel CE, Gross RH. SCOPE: a web server for practical de novo motif discovery. Nucleic Acids Research. 2007;35(suppl 2):W259-W64.